ESTIMATION OF GEOPOTENTIAL FROM SATELLITE-TO-SATELLITE RANGE RATE DATA: NUMERICAL RESULTS

Glenn E. Thobe
Sam C. Bose
APPLIED SCIENCE ANALYTICS, INC.
7049 Owensmouth Avenue
Canoga Park, CA 91303

March 1987

Final Report for Period August 1983-January 1987

Prepared for

NASA
GODDARD SPACE FLIGHT CENTER
Greenbelt, Maryland 20771

Contents

List of Figures

List of Tables

Symbols

a	semi-major axis Keplerian element
$\vec{a}$	acceleration vector
a_e	earth radius
A_{lm}	complex form of geopotential harmonic coefficients
$(a)_n$	Pochhammer symbol or generalized factorial, equal to $a(a+1)\cdots(a+n-1)$
$\operatorname{argmin}_x\{f(x) \mid y\}$	value of x which minimizes $f(x)$ with fixed y
C_{lm}	cosine geopotential harmonic coefficient
E	total energy
e	orbit eccentricity Keplerian element
f	true anomaly
$\mathcal{F}[\, f(\psi) \mid k \,]$	Fourier coefficient operator, yields function of k
$F_{lmp}(\iota)$	inclination function in Keplerian element expansion of geopotential
${}_2\mathrm{F}_1(\alpha, \beta; \gamma; z)$	Gaussian hypergeometric function or polynomial
gcd	greatest common divisor function
$G_{lpq}(e)$	eccentricity function in Keplerian element expansion of geopotential
H	observation matrix
i	$\sqrt{-1}$
Im	imaginary part operator
k	frequency or wave number index in Fourier analysis
l	harmonic degree
$l_{\max}$	maximum value of degree in truncated harmonic expansion
m	harmonic order
M	mean anomaly Keplerian element
M_0	value of M at time t_0
N_d	integral number of sidereal days in mission period
N_r	integral number of orbit revolutions in mission period
n	Keplerian mean motion
p	summation index for harmonic expansion in orbital coordinates
$\vec{p}$	momentum vector
p_r	radial conjugate momentum
p_u	angular conjugate momentum
q	summation index for harmonic expansion in orbital coordinates
r	radial distance from geocenter
R	range between satellites
$\dot{R}$	range rate between satellites
Re	real part operator
$r^{(k)}$	unitary (Euclidean) norm of 2-vector $(h_{il}^{(k)},\ h_{jl}^{(k)})$
s	auxiliary index in F_{lmp} formula

$\dot{s}$	speed
$S_{lmpq}(\omega, M, \Omega, \theta)$	function in orbital coordinate expansion of geopotential
S_{lm}	sine geopotential harmonic coefficient
T	kinetic energy
t_0	time at start of mission period
U	Givens unitary (orthogonal) transformation matrix
u	orbit-plane polar angle coordinate $u = \omega + f$
$U^{(k)}$	k-th elementary Givens unitary (orthogonal) transformation matrix
V	gravitational potential, sign follows physics convention
v	noise vector in observation equation
V_{lm}	individual term in harmonic expansion of V
x	state vector in linear observation equation
$\hat{x}$	optimal estimate of x
$\vec{x}$	position vector
y	vector observation
$\alpha_{ij}^{(k)}$	element of $U^{(k)}$ at i-th row and j-th column
$\Delta\dot{R}$	perturbed SST range rate
$\Delta\dot{R}(k)$	perturbed SST range rate in Fourier domain
$\Delta\dot{R}_{lmpq}$	perturbed SST range rate harmonic
$\Delta\dot{R}_{lmpq}(k)$	perturbed SST range rate harmonic in Fourier domain
$\Delta\dot{s}_{lmpq}$	speed perturbation harmonic
ΔT_{lmpq}	kinetic energy perturbation harmonic
Δ	perturbation operator
δ	difference operator comparing like quantities for two satellites
δ_n	Kronecker delta, equals 1 for $n = 0$, equals 0 otherwise
θ	Greenwich sidereal radian time, angle of earth's axial rotation
θ_0	value of θ at time t_0
ι	orbit plane inclination Keplerian element
λ	longitude
μ	product of universal gravitation constant G and earth mass M_e
σ^2	variance
Φ_{col}	diagonal matrix of column dependent factors of observation matrix
Φ_{row}	diagonal matrix of row dependent factors of observation matrix
ϕ	latitude
ψ	"angle" which varies linearly from 0 to 2π over a mission period, not to be confused with ψ_{lmpq}
ψ_{lmpq}	argument of exponential in definition of S_{lmpq}
Ω	longitude of ascending node Keplerian element
ω	argument of perigee Keplerian element
ω_e	Earth rotation rate

∇	gradient
$\|n\|_m$	n mod m
$\|\|v\|\|$	unitary (Euclidean) norm of vector v
$\bar{v}$	complex conjugate of v
v^*	adjoint (transpose) of vector v
$\langle\cdot\rangle$	averaging operator

TECHNICAL REPORT STANDARD TITLE PAGE

1. Report No.	2. Government Accession No.	3. Recipient's Catalog No.

4. Title and Subtitle	5. Report Date
Estimation of Geopotential from Satellite-to-Satellite Range Rate Data: Numerical Results	March 1987
	6. Performing Organization Code
7. Author(s)	8. Performing Organization Report No.
Glenn E. Thobe, Sam C. Bose	ASA-TR-87-1
9. Performing Organization Name and Address	10. Work Unit No.
Applied Science Analytics, Inc. 7049 Owensmouth Avenue, Canoga Park, California 91303	11. Contract or Grant No. NAS5-27743
12. Sponsoring Agency Name and Address	13. Type of Report and Period Covered
National Aeronautics & Space Administration Goddard Space Flight Center Greenbelt, Maryland 20771	Final Report Aug 1983-Jan 1987
	14. Sponsoring Agency Code

15. Supplementary Notes

16. Abstract

A technique for high-resolution geopotential field estimation by recovering the harmonic coefficients from satellite-to-satellite range rate data is presented and tested against both a controlled analytical simulation of a one-day satellite mission (maximum degree and order 8) and then against a Cowell method simulation of a 32-day mission (maximum degree and order 180). Innovations include: (1) a new frequency-domain observation equation based upon kinetic energy perturbations which avoids much of the complication of the usual Keplerian element perturbation approaches; (2) a new method of computing the normalized inclination functions which unlike previous methods is both efficient and numerically stable even for large harmonic degrees and orders; (3) the application of a mass storage FFT to the entire mission range rate history; (4) the exploitation of newly discovered symmetries in the block diagonal observation matrix which reduce each block to the product of (a) a real diagonal matrix factor, (b) a real trapezoidal factor with half the number of rows as before, and (c) a complex diagonal factor; (5) a block-by-block least-squares solution of the observation equation by means of a custom-designed Givens orthogonal rotation method which is both numerically stable and tailored to the trapezoidal matrix structure for fast execution.

17. Key words (Selected by Author(s))	18. Distribution Statement
satellite geodesy, gravity, range-rate, satellite-to-satellite tracking, harmonic analysis, Fourier analysis	Unlimited

19. Security Classif. (of this report)	20. Security Classif. (of this page)	21. No. of Pages	22. Price*
Unclassified	Unclassified	105	

*For sale by the Clearinghouse for Federal Scientific and Technical Information, Springfield, Virginia 22151.

1 Introduction

1.1 Background

Since the early days of artificial satellites it has been recognized that one could map variations in the Earth's gravitational field by accurately tracking the perturbations in satellite trajectories. Unfortunately, however, the accuracy limitations of conventional absolute tracking methods make these single satellite methods inadequate for high resolution mapping. A way out of the impasse is to use the so-called satellite-to-satellite (SST) tracking methods. The first of these is the *high-low* system in which a test satellite orbits in low earth orbit where its trajectory is most affected by the disturbing geopotential and use one or more satellites in well known orbits at higher altitudes to track it. The method which we are studying here is the *low-low*, interferometric, or differential method. In the ideal configuration, a pair of satellites orbit in identical low polar circular orbits, one trailing the other at a "fixed" distance. Millimeter or optical electromagnetic waves are transmitted from one to the other and back so that the relative speed of the two satellites can be detected as a doppler shift in the wave frequency. Our area of interest lies in developing the methods by which one processes this relative range rate data to map the geopotential field.

Important work in this area has been done by Colombo [4], who proposed a method based on random fields on a sphere. See also our own work, Bose et al. [1], in which the advantages of treating the global geopotential as a homogeneous and isotropic random field on the sphere and sampling it on a uniform global grid are analyzed in detail. In a later work, Colombo [6] presented the theory and results of a variational method motivated by G. W. Hill's lunar theory. One of the conditions for Colombo's methods is that the satellite pair execute synchronous orbits, i.e. that the number of sidereal days and the number of revolutions be relatively prime causing the trajectory to close on itself and the ground track to repeat.

The reader is also referred to Wagner [16], who presents spectral analyses based on the simplistic signal equation of Wolff [17], and performs a low degree and order 4×4 recovery based on a more elaborate signal equation derived from conventional Keplerian element perturbations.

Most important as a basis for the present work is Kaula's paper [10] and the subsequent work of Bose and Thobe [2] in which an observation equation in the frequency domain was developed starting with a harmonic expansion of the geopotential in terms of modified Keplerian elements of the satellites. Fourier analysis of the harmonic expansion leads to an approximate uncoupling of the signal equation according to the harmonic order and parity of degree. Included in [10] are Kaula's results of numerical recovery experiments for an 8×8 degree and order harmonic geopotential. In Thobe et Bose [14], we applied Colombo's condition of a synchronous orbit to the method of Kaula [10], rigorously demonstrating the uncoupling of the signal equation and the resulting mathematical simplification.

1.2 Purpose and Scope

The purpose of this research is to develop techniques of recovering the spherical harmonic coefficients of the geopotential field from SST range rate data, and to demonstrate their effectiveness by numerical experiments. A key objective is to improve the resolution of gravity models, which implies recovering harmonics of high degree and order. At the same time, adequate numerical accuracy and reasonable computational efficiency must be maintained. Care had to be taken at all stages of development to insure that our software would be able to deal with much larger models than most previous efforts, nominally 180×180 and potentially still larger. The analysis had to be rigorously correct yet simple and elegant so that exploitable regularities would be apparent, and the equations could be reduced to their simplest form. Data storage requirements had to be minimized. Efficient methods of computing special functions had to be devised. Observation matrix structure had to be exploited to reduce computational complexity to a manageable minumum. Numerically stable solution techniques had to be selected so that mathematically correct solutions would not be swamped by numerical errors.

1.3 Technical Approach

The first step toward achieving the objectives set out above was to rederive the signal and observation equations from fundamental physical principles. The rotating earth gives rise to a time dependent gravitational potential, which in turn means that the mechanical system of a free particle, i.e. a satellite uninfluenced by drag or other external forces, can be characterized by a time-dependent hamiltonian. By using the basic variational calculus energy conservation laws as they apply to a time varying hamiltonian, and applying the elementary relationship between speed and kinetic energy, we were able to derive a simple yet correct signal and observation equation. We thereby avoided the complicated constructions from perturbations of individual Keplerian elements characteristic of previous signal equation developments.

The next step was to impose the condition of a tuned synchronous orbit of N_r revolutions in N_d days where these are relatively prime integers. Geometrically, this means that the spacecraft covers the earth's surface in a set of evenly spaced north-south and south-north traverses and repeats the same trajectory relative to an earth-fixed frame once in each mission period. Mathematically, it means we are dealing with a periodic process and so can apply old fashioned Fourier series.

After applying the Fourier coefficient operator to the time domain signal equation to obtain the SST range rate spectrum, we find that all observation matrix elements vanish except at the zeros of an integer relation connecting the frequency k, and the harmonic indices l, m, p, and q. This gives rise to a sparse structure — in fact, it uncouples the signal equation into smaller independent sub-equations. With such a sparse structure, the previously massive computational requirements are reduced by several orders of magnitude to become manageable on a modest computer, such as the DEC VAX 11/750. By factoring

the observation matrix into the product of a diagonal matrix factor, a real matrix factor, and another diagonal matrix factor, and employing an inclination function identity, we reduced the observation matrix to a real one with half the number of rows as the former complex observation matrix. Remarkably, the reduced matrix is simply an array of inclination functions.

As to software, we set it up to perform the Fourier analysis on the entire mission range rate history at one time using a public domain mass storage Fast Fourier Transform (FFT) package adapted by us to handle double precision computer arithmetic. We then use sorting to group elements of the spectrum into their respective blocks. Thereafter each block is processed separately: the matrix elements are computed and the observation equation is solved. In order to demonstrate the essentials of the method, we made certain interim simplifications: we took the reference orbit to be circular, neglecting linear and higher order terms in the eccentricity. Also we limited ourselves to a single iteration in the solution of the observation equations.

Key to being able to compute the range rate spectrum and matrix elements, was the invention of an efficient, numerically stable, partially recursive technique for computing the inclination functions. Naive application of published analytical formulas led to problems of poor efficiency or instability.

The experimental phase of the study began with the development of software to perform the Fourier analysis, to compute the inclination functions, to construct the observation vector and observation matrix block by block, and to solve the observation equation. Careful testing and validation of each element of the software was a necessity. An analytical simulation totally under our control was developed for debugging and preliminary validation of the software. Finally, we tested the method and software on foreign simulation data from the University of Texas Encke method numerical integration of a 32 sidereal day, 525 revolution synchronous orbit mission.

1.4 Summary of Results

We analytically simulated a one-day, 16-orbit mission, producing artificial range rate data from which we successfully recovered the geopotential coefficients to an accuracy of approximately one part in 10^4. We then tested our method and software on data produced at the University of Texas by Schutz et al. [13]. Using the SST range rate signal from their much larger scale 32-day 525-revolution simulated mission, we computed the complex fourier coefficients of the range rate signal, evaluated the observation matrix elements, and numerically solved the observation equation for several of the lower degree blocks to order 180. For instance, for order $m = 1$ and even degrees $l \leq 40$, errors in the recovered coefficients were typically as low as 10%. The error figures deteriorated rapidly for higher orders, unfortunately. We ascribe this in part to fact that we assumed a very simple circular reference orbit, neglected linear and higher terms in the geopotential harmonic expansion, and did not iterate our solution. On the other hand, the spectra predicted by

our signal equation show good qualitative agreement with the spectra we extracted from the Texas data. This can be seen by visually comparing the spectral magnitude plots in the Appendix A. It is possible that errors in the Texas simulation contributed in part to the discrepancies; in fact, the spectra of the Texas data show unnatural regularities at wave numbers greater than 50000 (half the presumed bandwidth), tending toward constant amplitude and phase.

A gratifying conclusion to be drawn from these experiments is that high resolution recovery can be performed on modest sized computers. Each block takes approximately 5 minutes on a DEC VAX 11/750. Further work is needed however to improve the quality of the recovered coefficients.

1.5 Overview of Report

In this report we present both the theory and validating numerical experiments of our own system of geopotential coefficient recovery, as it has evolved from the seminal work of Kaula. In Section 2 we derive our new signal model starting from fundamental physical principles. We first obtain a spherical harmonic expansion of the kinetic energy of a single satellite, then its speed, and then the relative speed of two satellites. This is in constrast to previous methods, which either simplistically relate the relative range rate to potential energy differences between the two satellites, or employ complicated constructions based on perturbations in individual Keplerian elements. In Section 3 we develop the signal model into an observation equation which can be solved to recover the coefficients. The sparse structure of the frequency domain observation matrix is exploited to drastically reduce the cost of obtaining a solution. We take advantage of additional, newly discovered symmetries to reduce the observation matrix still further, finally obtaining a block diagonal matrix of real trapezoidal blocks. In Section 4 we present certain numerical techniques crucial to generating the matrix elements and solving the observation equation. In particular, we present our partially recursive, summation free method of computing the inclination functions $F_{lmp}(\iota)$. Also we outline the use of numerically stable Givens orthogonal rotations to obtain the optimal solution of the over-determined linear observation equation. In Section 5 we describe our validation methods, especially the analytical simulation which we used to produce test data. Then we detail the results of large scale (maximum degree and order 180) coefficient recovery experiments from the University of Texas 32-day, 525-revolution Cowell simulation. Section 6 presents our conclusions and recommendations. In Appendix A we have reproduced tables and spectral plots showing partial quantitative results of our recovery experiments from the Texas data.

2 Signal Model

2.1 Single Satellite Motion

The geopotential is given in Kaula [9,10] as the spherical harmonic expansion

$$V = -\frac{\mu}{r} + \sum_{l=2}^{\infty} \sum_{m=0}^{l} V_{lm} \tag{1}$$

where in terms of the geocentric latitude ϕ and longitude λ, an individual harmonic may be expressed as

$$V_{lm} = -\frac{\mu a_e^l}{r^{l+1}} P_{lm}(\sin\phi)(C_{lm}\cos m\lambda + S_{lm}\sin m\lambda) = \sum_{p=0}^{l} \sum_{q=-\infty}^{\infty} V_{lmpq} \tag{2}$$

In terms of the Keplerian elements of an orbiting satellite, and the sidereal time θ expressed in radians, the potential is expressed as

$$V_{lmpq} = -\frac{\mu a_e^l}{a^{l+1}} F_{lmp}(\iota) G_{lpq}(e) \operatorname{Re} S_{lmpq}(\omega, M, \Omega, \theta) \tag{3}$$

Note that the physics sign convention is used for the potential energy V, whereby $\vec{a} = -\nabla V$. Here $\vec{a}$ denotes specific force or acceleration. Other symbols in Equation 3 are given by

$$S_{lmpq} = A_{lm} \exp i\psi_{lmpq} \tag{4}$$

$$\psi_{lmpq} = (l-2p)\omega + (l-2p+q)M + m(\Omega - \theta) \tag{5}$$

$$A_{lm} = (-i)^{|l-m|_2}[C_{lm} - iS_{lm}] \tag{6}$$

The notation $|l-m|_2$ is equivalent to $l - m \bmod 2$. The cosine and sine harmonic coefficients C_{lm} and S_{lm}, respectively, are a set of empirically determined numbers which quantitatively describe the disturbing potential. The objective of this study is to develop effective techniques for estimating these coefficients from experimental data, namely the satellite-to-satellite (SST) range rate $\Delta\dot{R}$. In the following, we shall estimate the complex coefficients A_{lm} and then solve Equation 6 to obtain

$$C_{lm} = \operatorname{Re} \overline{i^{|l-m|_2} A_{lm}} \tag{7}$$

$$S_{lm} = \operatorname{Im} \overline{i^{|l-m|_2} A_{lm}} \tag{8}$$

In addition, the special functions of orbital mechanics, the *inclination* function F_{lmp} and the *eccentricity* function G_{lpq}, have more complicated definitions for which the reader is referred to Kaula [9]. Techniques for computing these functions are discussed in Section 4.1.

We introduce the total energy E, the kinetic energy T, the potential energy V, the speed or path rate $\dot{s}$, the partial time derivative $\partial/\partial t$, and the total time derivative d/dt

or overdot ($\dot{}$). The hamiltonian H is an explicit function of the position $\vec{x}$, the momentum $\vec{p}$, and the time t:

$$E = T + V = \tfrac{1}{2}\dot{s}^2 + V = H(\vec{x}, \vec{p}, t) \tag{9}$$

From the fundamental variational theory of classical mechanics we have:

$$\dot{E} = \frac{\partial H}{\partial t} \tag{10}$$

From Equation 9, we have

$$\frac{\partial H}{\partial t} = \frac{\partial V}{\partial t} \tag{11}$$

By definition,

$$\dot{V} = \frac{dV}{dt} \tag{12}$$

so that

$$\dot{T} = \dot{E} - \dot{V} = \frac{\partial V}{\partial t} - \frac{dV}{dt} \tag{13}$$

Integrating Equation 13 and applying the perturbation operator Δ to Equation 9 we get a general expression for the perturbed speed of a satellite.

$$\Delta\dot{s} = \frac{1}{\dot{s}} \int \left[\frac{\partial \Delta V}{\partial t} - \frac{d\Delta V}{dt} \right] dt \tag{14}$$

We observe that of all the dependent variables in Equation 3, only θ is explicitly a function of time. The others collectively represent the position $\vec{x}$ and momentum $\vec{p}$ of the restricted phase space. We need not be working in a canonical coordinate system for our derivation to be valid; we only require that the time dimension be distinct from the position and momentum. To compute $\dot{T}$ using Equations 3 and 13, we need the time derivatives

$$\frac{\partial \operatorname{Re} S_{lmpq}}{\partial t}(\omega, M, \Omega, \omega_e[t - t_0] + \theta_0) \tag{15}$$

$$\frac{d \operatorname{Re} S_{lmpq}}{dt}(\omega, n[t - t_0] + M_0, \Omega, \omega_e[t - t_0] + \theta_0) \tag{16}$$

There is a degree of approximation in Equation 16 because ω, n, M_0, and Ω have been treated as constants. A better approximation would incorporate at least the linear terms in t due to secular perturbations. Continuing:

$$\frac{\partial S_{lmpq}}{\partial t} = A_{lm} i \frac{\partial \psi_{lmpq}}{\partial t} = -im\omega_e S_{lmpq} \tag{17}$$

$$\frac{dS_{lmpq}}{dt} = A_{lm} i \frac{d\psi_{lmpq}}{dt} = i[(l - 2p + q)n - m\omega_e] S_{lmpq} \tag{18}$$

$$\frac{\partial \operatorname{Re} S_{lmpq}}{\partial t} - \frac{d \operatorname{Re} S_{lmpq}}{dt} = -\operatorname{Re} i(l-2p+q)nS_{lmpq} \quad (19)$$

$$= (l-2p+q)n \operatorname{Im} S_{lmpq} \quad (20)$$

Substituting into Equation 5 the relations

$$M = M_0 + \dot{M}[t-t_0] \quad (21)$$

$$\theta = \theta_0 + \dot{\theta}[t-t_0] \quad (22)$$

$$\dot{M} = N_{\mathrm{r}}\dot{\psi} \quad (23)$$

$$\dot{\theta} = \omega_{\mathrm{e}} = N_{\mathrm{d}}\dot{\psi} \quad (24)$$

$$\psi_{lmpq}(0) = (l-2p)\omega + (l-2p+q)M_0 + m(\Omega - \theta_0) \quad (25)$$

$$\psi(t) = \dot{\psi}[t-t_0] \quad (26)$$

we get an expression for ψ_{lmpq} which is linear in time:

$$\psi_{lmpq}(t) = \psi_{lmpq}(0) + [(l-2p+q)N_{\mathrm{r}} - mN_{\mathrm{d}}]\psi(t) \quad (27)$$

Finally, we get the kinetic energy perturbation:

$$\Delta T_{lmpq} = \int \Delta \dot{T}_{lmpq} dt = \frac{\mu a_{\mathrm{e}}^l}{a^{l+1}} F_{lmp} G_{lpq} \frac{[l-2p+q]N_{\mathrm{r}} \operatorname{Re} S_{lmpq}}{[l-2p+q]N_{\mathrm{r}} - mN_{\mathrm{d}}} \quad (28)$$

The kinetic energy perturbation is related to the velocity perturbation as follows:

$$\Delta T = \Delta\left(\tfrac{1}{2}\vec{v}\cdot\vec{v}\right) = \vec{v}\cdot\Delta\vec{v} \quad (29)$$

which is to say that ΔT is proportional to the along track component of the perturbation in velocity. Applying $\dot{s} \approx na$ for a circular orbit, we get:

$$\Delta \dot{s}_{lmpq} = \frac{\mu a_{\mathrm{e}}^l}{na^{l+2}} F_{lmp} G_{lpq} \frac{[l-2p+q]\dot{M} \operatorname{Re} S_{lmpq}}{[l-2p+q]\dot{M} - m\dot{\theta}} \quad (30)$$

Thus we have expressions for the perturbed kinetic energy and speed of a single satellite in a circular orbit.

We note that for a circular orbit the angle between the satellite-to-satellite relative range vector $\vec{R}$ and the velocity vector $\vec{v}$ is $\frac{1}{2}\delta u$, which is rather a small angle. For computing the range rate perturbation, we are interested in the component of $\Delta\vec{v}$ on $\vec{R}$. It is not quite accurate to substitute the one component of $\Delta\vec{v}$ for the other, but this is what we have done, and the results of this approximation are reflected in the observation Equation 43 and in the numerical experiments reported in this document. A more rigorous observation equation derivation, which does not make this approximation is carried out in Section 2.3.

2.2 Relative Motion

In this section we apply the results of the previous section to compute the perturbed relative speed, a.k.a. the perturbed SST range rate, of the two satellites. We introduce the difference operator $\delta(\cdot) = (\cdot)_1 - (\cdot)_2$, i.e. the value of some quantity for the number 1 (lead) satellite minus that for the number 2 (trailing) satellite. Since the orbits are coplanar we have:

$$\begin{aligned} \delta S_{lmpq} &= A_{lm} \exp i[(l-2p)\omega + m(\Omega - \theta)] \times \qquad (31) \\ &\quad \times \{\exp i(l-2p+q)(M + \frac{\delta M}{2}) - \exp i(l-2p+q)(M - \frac{\delta M}{2})\} \\ &= 2iS_{lmpq}(M) \cdot \sin(l-2p+q)\frac{\delta M}{2} \qquad (32) \end{aligned}$$

and

$$\delta \operatorname{Re} S_{lmpq} = -2\sin(l-2p+q)\frac{\delta M}{2} \cdot \operatorname{Im} S_{lmpq} \qquad (33)$$

From the geometry of the circular orbit we obtain the SST range rate perturbation in the time domain:

$$\begin{aligned} \Delta \dot{R}_{lmpq} &= \delta \Delta \dot{s}_{lmpq} \cos\frac{\delta M}{2} \qquad (34) \\ &= -2\cos\frac{\delta M}{2}\sin(l-2p+q)\frac{\delta M}{2}\operatorname{Im} S_{lmpq} \times \qquad (35) \\ &\quad \times \frac{\mu a_e^l}{n a^{l+2}} F_{lmp} G_{lpq} \frac{[l-2p+q]\dot{M}}{[l-2p+q]\dot{M} - m\dot{\theta}} \end{aligned}$$

Here $M = (M_1 + M_2)/2$ is the mean anomaly of a fictitious *mean* satellite. Next, we compute the fourier coefficients of the SST range rate Equation 35. Applying Equations 4 and 27 we get

$$S_{lmpq}(\psi) = \underbrace{S_{lmpq}(0)}_{\equiv v} \exp i \underbrace{[(l-2p+q)N_r - mN_d]}_{\equiv w} \psi \qquad (36)$$

Applying the fourier coefficient operator $\mathcal{F}$, defined as

$$\mathcal{F}[\, f(\psi) \mid k \,] \equiv \frac{1}{2\pi}\int_0^{2\pi} \exp(-ik\psi) f(\psi)\, d\psi \qquad (37)$$

we have in general

$$\mathcal{F}[\operatorname{Im}(v \exp iw\psi) \mid k\,] = \frac{1}{2i}\{\delta_{w-k}v - \delta_{w+k}\overline{v}\} \qquad (38)$$

where $\delta_n = 1$ if $n = 0$ and $\delta_n = 0$ otherwise. In particular,

$$\mathcal{F}[\operatorname{Im} S_{lmpq}(\psi) \mid k\,] = \frac{1}{2i}\{\delta_{(l-2p+q)N_r - mN_d - k} S_{lmpq}(0) - \delta_{(l-2p+q)N_r - mN_d + k}\overline{S_{lmpq}(0)}\} \qquad (39)$$

from which we obtain the frequency domain expression for the SST range rate:

$$\Delta\dot{R}_{lmpq}(k) = \frac{\mu a_{\rm e}^{l}}{na^{l+2}} F_{lmp} G_{lpq} \cos\frac{\delta M}{2} \sin(l-2p+q)\frac{\delta M}{2} \cdot \frac{[l-2p+q]N_{\rm r}}{[l-2p+q]N_{\rm r} - mN_{\rm d}} \times \quad (40)$$
$$\times \{\delta_{(l-2p+q)N_{\rm r}-mN_{\rm d}-k} S_{lmpq}(0) - \delta_{(l-2p+q)N_{\rm r}-mN_{\rm d}+k} \overline{S_{lmpq}(0)}\}$$

For the sake of simplicity, let us consider only the case $m \neq 0$. Furthermore, let us consider $l \leq l_{\rm max}$ where $l_{\rm max}$ is a suitably chosen function of $N_{\rm r}$ and $N_{\rm d}$. Then, because of redundancy, we need only consider the possibility

$$k = (l-2p+q)N_{\rm r} - mN_{\rm d} \quad (41)$$

This allows us to drop the terms corresponding to

$$-k = (l-2p+q)N_{\rm r} - mN_{\rm d} \quad (42)$$

to produce the simpler SST range rate equation:

$$\Delta\dot{R}_{lmpq}(k) = i\frac{\mu a_{\rm e}^{l}}{na^{l+2}} F_{lmp} G_{lpq} \cos(N_{\rm r}\frac{\delta\psi}{2}) \sin\left([l-2p+q]N_{\rm r}\frac{\delta\psi}{2}\right) \frac{[l-2p+q]N_{\rm r}\, S_{lmpq}(0)}{[l-2p+q]N_{\rm r} - mN_{\rm d}} \quad (43)$$

We arbitrarily exclude the case $k = 0$ because of the vanishing denominator. We have reached our goal of a signal equation in the fourier domain.

2.3 Extended Signal Model

In the previous section, we derived an SST range rate perturbation signal model based on the kinetic energy perturbation of each of a pair of satellites. The kinetic energy perturbation is easily converted to a speed perturbation which is essentially the horizontal component of the velocity perturbation. This is projected onto the satellite-to-satellite range vector. What is neglected in this procedure is the vertical component of individual satellite's velocity perturbation which also has a non-zero projection on the range vector. If we pass to the limit as the satellite separation distance approaches zero, clearly projection of this vertical component on the range vector approaches zero as well. However, numerical experiments reported by Colombo [], indicate that for reasonable separations, the vertical components can contribute significantly to the overall SST range rate spectrum.

In this section we present an extended range rate signal model which includes the vertical components. The perturbation of the vector velocity of a satellite cannot be obtained from consideration of a scalar kinetic energy, so the approach will be different. However, the result is essentially in agreement with what we have already derived except for the addition of a term proportional to the sine of half the angle separating the two satellites.

Following Bose and Thobe [2, sec. 4] we compute the inter-satellite range

$$R = \|\vec{R}\| \tag{44}$$

the range rate

$$\dot{R} = \vec{R} \cdot \dot{\vec{R}}/R \tag{45}$$

and the range rate perturbation

$$\Delta\dot{R} = R^{-1}\left\{\vec{R}\cdot\Delta\dot{\vec{R}} + \dot{\vec{R}}\cdot\left[\mathbf{1} - R^{-2}\vec{R}\otimes\vec{R}\right]\cdot\Delta\vec{R}\right\} \tag{46}$$

Neglecting the term containing the projection operator $\mathbf{1} - R^{-2}\vec{R}\otimes\vec{R}$ and converting to the polar coordinates r and u in the orbit plane, we get

$$\Delta\dot{R} \approx \sin\frac{\delta u}{2}(\Delta\dot{r}_1 + \Delta\dot{r}_2) + r\cos\frac{\delta u}{2}(\Delta\dot{u}_1 - \Delta\dot{u}_2) \tag{47}$$

or in terms of the operators Σ and δ defined by

$$\delta(\cdot) = (\cdot)_1 - (\cdot)_2 \tag{48}$$

and

$$\Sigma(\cdot) = (\cdot)_1 + (\cdot)_2 \tag{49}$$

where 1 and 2 represent the leading and trailing satellites, respectively, we get

$$\Delta\dot{R} \approx \sin\frac{\delta u}{2}\Sigma(\Delta\dot{r}) + r\cos\frac{\delta u}{2}\delta(\Delta\dot{u}) \tag{50}$$

We again use the physics sign convention for the potential

$$V = -\frac{\mu}{r} + V_{lm} \tag{51}$$

where the (l, m)-th spherical harmonic of the geopotential is given in plane polar coordinates by Kaula [9, eq. 3.61]:

$$V_{lm}(r,u) = -\mu a_e^l r^{-l-1} \sum_{p=0}^{l} F_{lmp} \operatorname{Re}(A_{lm} \exp i[(l-2p)u + m(\Omega - \theta)]) \tag{52}$$

where $u = \omega + f$ and where again we have used the complex A_{lm} of Equation 6 to streamline the notation. In the plane polar coordinates the Lagrangian of an orbiting satellite is given by

$$L = T - V = \tfrac{1}{2}\dot{r}^2 + \tfrac{1}{2}r^2\dot{u}^2 - V \tag{53}$$

from which we obtain the conjugate momenta

$$p_r = \frac{\partial L}{\partial \dot{r}} = \dot{r} \tag{54}$$

$$p_u = \frac{\partial L}{\partial \dot{u}} = r^2\dot{u} \tag{55}$$

and the Hamiltonian

$$H = T + V = \tfrac{1}{2}p_r^2 + \tfrac{1}{2}r^{-2}p_u^2 - \mu r^{-1} + V_{lm} \tag{56}$$

Hamilton's equations yield the equations of motion

$$\dot{p}_r = -\frac{\partial H}{\partial r} = r^{-3}p_u^2 - \mu r^{-2} - \frac{\partial V_{lm}}{\partial r} \tag{57}$$

$$\dot{r} = \frac{\partial H}{\partial p_r} = p_r \tag{58}$$

$$\dot{p}_u = -\frac{\partial H}{\partial u} = -\frac{\partial V_{lm}}{\partial u} \tag{59}$$

$$\dot{u} = \frac{\partial H}{\partial p_u} = r^{-2}p_u \tag{60}$$

which are linearized to give the perturbation differential equations

$$\Delta\dot{p}_r = \left\langle -2r^{-3} - 3r^{-4}p_u^2 \right\rangle \Delta r + \left\langle 2r^{-3}p_u \right\rangle \Delta p_u - \frac{\partial V_{lm}}{\partial r} \tag{61}$$

$$\Delta\dot{r} = \Delta p_r \tag{62}$$

$$\Delta\dot{p}_u = -\frac{\partial V_{lm}}{\partial u} \tag{63}$$

$$\Delta\dot{u} = \left\langle -2r^{-3}p_u \right\rangle \Delta r + r^{-2}\Delta p_u \tag{64}$$

Here the unperturbed or referenced system is determined by the Keplerian potential $V = -\mu r^{-1}$. The brackets "$\langle\cdot\rangle$" indicate time averaging, so that the bracketed expressions may be treated as constants. Equation 64 is superfluous. Since the perturbations are given in terms of the conjugate momenta instead of the velocities, the observation Equation 50 is restated as follows

$$\Delta\dot{R} \approx \sin\frac{\delta u}{2}\Sigma(\Delta p_r) + r^{-1}\cos\frac{\delta u}{2}\delta(\Delta p_u) \tag{65}$$

We now compute the generalized disturbing force in (r, u)-coordinates.

$$\frac{\partial V_{lm}}{\partial r} = (k+1)\mu a_e^l r^{-l-2}\sum_{p=0}^{l} F_{lmp}\,\mathrm{Re}(A_{lm}\exp i[(l-2p)u + m(\Omega-\theta)]) \tag{66}$$

$$\frac{\partial V_{lm}}{\partial u} = \mu a_e^l r^{-l-1}\sum_{p=0}^{l}(l-2p)F_{lmp}\,\mathrm{Im}(A_{lm}\exp i[(l-2p)u + m(\Omega-\theta)]) \tag{67}$$

In anticipation of performing a Fourier analysis, we use Hansen's expansion to remove r and f, which are complicated functions of time, replacing them by a, which is constant, and M, which is linear in time.

$$\left(\frac{r}{a}\right)^{-l-1}\exp i(l-2p)f = \sum_q G_{lpq}\exp i(l-2p+q)M \tag{68}$$

$$\left(\frac{r}{a}\right)^{-l-2}\exp i(l-2p)f = \sum_q G_{l+1,p+\frac{1}{2},q}\exp i(l-2p+q)M \tag{69}$$

Note that for small e

$$G_{lpq}(e) \sim e^{|q|} \tag{70}$$

The same holds for $G_{l+1,p+\frac{1}{2},q}$, of course. Substituting, we get:

$$\frac{\partial V_{lm}}{\partial r} = (k+1)\mu a_e^l a^{-l-2}\sum_{p=0}^{l} F_{lmp}\sum_q G_{l+1,p+\frac{1}{2},q}\,\mathrm{Re}\,S_{lmpq} \tag{71}$$

$$\frac{\partial V_{lm}}{\partial u} = \mu a_e^l a^{-l-1}\sum_{p=0}^{l}(l-2p)F_{lmp}\sum_q G_{lpq}\,\mathrm{Im}\,S_{lmpq} \tag{72}$$

where S_{lmpq} is given by Equation 4. Note that ω, M, Ω, and θ are all linear in time for a Keplerian reference orbit. For polar orbits $\dot{\Omega} = 0$. The "frozen orbit" condition $\dot{\omega} = 0$ of Colombo [5, p.117] would require some small expenditure of fuel. We now perform the Fourier analysis over a mission period, assuming an N_d-day and N_r-revolution stationary orbit. Let ψ vary from 0 to 2π over this period.

We now obtain some needed Fourier coefficient formulas. In addition to Equation 38, we have

$$\mathcal{F}\left[\mathrm{Re}(v \exp iw\psi) \mid k\right] = \tfrac{1}{2}\{\delta_{w-k}v + \delta_{w+k}\bar{v}\} \tag{73}$$

By requiring $m \neq 0$, $l_{\max} < N_{\mathrm{r}}/2$, and $\gcd(N_{\mathrm{r}}, N_{\mathrm{d}}) = 1$, the δ_{w+k} terms vanish leaving

$$\mathcal{F}\left[\mathrm{Im}\, S_{lmpq}(\psi) \mid k\right] = \frac{1}{2i}\delta_{(l-2p+q)N_{\mathrm{r}}-mN_{\mathrm{d}}-k} S_{lmpq}(0) \tag{74}$$

and

$$\mathcal{F}\left[\mathrm{Re}\, S_{lmpq}(\psi) \mid k\right] = \frac{1}{2}\delta_{(l-2p+q)N_{\mathrm{r}}-mN_{\mathrm{d}}-k} S_{lmpq}(0) \tag{75}$$

These result in the Fourier coefficients of the generalized forces:

$$\mathcal{F}\left[\frac{\partial V_{lm}}{\partial r} \mid k\right] = (l+1)\mu a_{\mathrm{e}}^{l} a^{-l-2} \sum_{p=0}^{l} F_{lmp} \sum_{q} G_{l+1,p+\frac{1}{2},q} \frac{1}{2} \delta_{(l-2p+q)N_{\mathrm{r}}-mN_{\mathrm{d}}-k} S_{lmpq}(0) \tag{76}$$

$$\mathcal{F}\left[\frac{\partial V_{lm}}{\partial u} \mid k\right] = \mu a_{\mathrm{e}}^{l} a^{-l-1} \sum_{p=0}^{l} (l-2p) F_{lmp} \sum_{q} G_{lpq} \frac{1}{2i} \delta_{(l-2p+q)N_{\mathrm{r}}-mN_{\mathrm{d}}-k} S_{lmpq}(0) \tag{77}$$

We are now in a position to Fourier analyze the perturbation equations.

$$ik\dot{\psi}\Delta p_{\mathrm{r}}(k) = \left\langle 2\mu r^{-3} - 3r^{-4}p_u^2 \right\rangle \Delta r(k) + \left\langle 2r^{-3}p_u \right\rangle \Delta p_u(k) - \frac{\partial V_{lm}}{\partial r}(k) \tag{78}$$

$$ik\dot{\psi}\Delta r(k) = \Delta p_{\mathrm{r}}(k) \tag{79}$$

$$ik\dot{\psi}\Delta p_u(k) = -\frac{\partial V_{lm}}{\partial u}(k) \tag{80}$$

$$ik\dot{\psi}\Delta u(k) = \left\langle -2r^{-3}p_u \right\rangle \Delta r(k) + r^{-2}\Delta p_u(k) \tag{81}$$

Averaging the feedback coefficients, we can solve this system of algebraic equations for the spectra of the momentum perturbations.

$$\Delta p_r(k) = \frac{-k\dot{\psi}}{k^2\dot{\psi}^2 + \langle 2\mu r^{-3} - 3r^{-4}p_u^2 \rangle} \left\{ \left\langle 2r^{-3}p_u \right\rangle \Delta p_u(k) - \frac{\partial V_{lm}}{\partial r}(k) \right\} \tag{82}$$

$$\Delta p_u(k) = \frac{-1}{ik\dot{\psi}} \frac{\partial V_{lm}}{\partial u}(k) \tag{83}$$

This completes the consideration of the single satellite. The sum and difference identities

$$\Sigma S_{lmpq} = 2\cos\frac{(l-2p+q)\delta M}{2} S_{lmpq} \tag{84}$$

$$\delta S_{lmpq} = 2i\sin\frac{(l-2p+q)\delta M}{2} S_{lmpq} \tag{85}$$

are employed to obtain a final expression for the range rate spectrum:

$$\begin{aligned}\Delta\dot{R}(k) = &\sum_{lmpq} \delta_{(l-2p+q)N_r - mN_d - k} F_{lmp} S_{lmpq}(0) \\ &\times \mu a_e^l a^{-l-2} \left\{ \sin\frac{\delta u}{2} \cos\frac{(l-2p+q)\delta M}{2} \frac{-ik\dot{\psi}}{k^2\dot{\psi}^2 + \langle 2\mu r^{-3} - 3r^{-4}p_u^2 \rangle} \right. \\ &\times \left[\left\langle 2r^{-3}p_u \right\rangle \frac{a(l-2p)}{k\dot{\psi}} G_{lpq} - (l+1) G_{l+1,p+\frac{1}{2},q} \right] \\ &\left. + i\cos\frac{\delta u}{2} \sin\frac{(l-2p+q)\delta M}{2} \frac{l-2p}{r} \frac{G_{lpq}}{k\dot{\psi}} \right\} \end{aligned} \tag{86}$$

This can be compared to the kinetic energy result Equation 43 by neglecting the terms proportional to $\sin\frac{\delta u}{2}$ and applying the substitutions:

$$r = a \tag{87}$$

$$\delta u = \delta M = N_r \delta\psi \tag{88}$$

$$\dot{\psi} = n/N_r \tag{89}$$

$$p_u = a^2 n \tag{90}$$

A minor discrepancy remains, namely the factor of $l - 2p$ appearing here in place of the factor $l - 2p + q$ of the kinetic energy derivation. The consequences on observation matrix structure of using Equation 86 in place of Equation 43 are not severe, inasmuch as the non-zero elements are determined by the solution of the integer Equation 41 in either case.

3 Observation Equation

3.1 Matrix Formulation

The signal Equation 43 is linear in the unknown coefficients A_{lm}. This is easily seen by considering Equation 4. Note well that A_{lm} is merely a complex representation of the pair (C_{lm}, S_{lm}) according to Equations 6, 7, and 8; so that when we estimate A_{lm}, we will for all practical purposes be estimating C_{lm} and S_{lm}. The signal equation thus becomes a linear observation:

$$\Delta\dot{R}_{lmpq}(k) = \frac{\partial\Delta\dot{R}_{lmpq}(k)}{\partial A_{lm}} A_{lm} + \text{noise} \tag{91}$$

We shall not at this time dwell on the nature of this noise term. For now we may consider it to be zero-mean gaussian with covariance $\sigma^2 I$, where I is the identity matrix. Equation 91 may be rewritten as

$$\Delta\dot{R}(k) = \sum_{lmpq} \frac{\partial\Delta\dot{R}_{lmpq}(k)}{\partial A_{lm}} A_{lm} + \text{noise} \tag{92}$$

where the summation indices are subject — at least in the case of $m = 0$ — to the constraint of Equation 41. Isolating the summations over l and m, we have:

$$\Delta\dot{R}(k) = \sum_{lm} \frac{\partial\sum_{pq}\Delta\dot{R}_{lmpq}(k)}{\partial A_{lm}} A_{lm} + \text{noise} \tag{93}$$

Since Equation 41 implies the mapping:

$$k \mapsto l - 2p + q, m \tag{94}$$

we can set

$$\frac{\partial\Delta\dot{R}(k)}{\partial A_{lm}} = \frac{\partial\sum_{pq}\Delta\dot{R}_{lmpq}(k)}{\partial A_{lm}} \tag{95}$$

where p and q are constrained by the fixed value of the expression $l - 2p + q$. In the special case of $q \equiv 0$ considered below, we have p unique, making the summation over p and q a trivial one. The observation equation is now in matrix form and may be formally represented as

$$y = Hx + v \tag{96}$$

or

$$y_k = \sum_{lm} H_{k,lm} x_{lm} + v_k \tag{97}$$

where

$$y_k = \Delta\dot{R}(k) \tag{98}$$

$$H_{k,lm} = \frac{\partial\Delta\dot{R}(k)}{\partial A_{lm}} \tag{99}$$

$$x_{lm} = A_{lm} \tag{100}$$

$$v_{lm} = \text{noise} \tag{101}$$

3.2 Block Structure

In this section we indicate how the observation matrix, i.e. $\partial \Delta \dot{R}(k)/\partial A_{lm}$, decouples into independent blocks, and how these blocks factor into three matrix factors. Two of the factors, the row-dependent and column-dependent ones, are diagonal and the third (middle) factor is real, in fact consisting of only F_{lmp} values. Finally, because of an additional symmetry, the number of rows of each block can be reduced by half.

For simplicity, in this development we restrict the problem by requiring $q = 0$ and $m \neq 0$. Additional constraints are required by the method:

$$\gcd(N_{\mathrm{r}}, N_{\mathrm{d}}) = 1 \tag{102}$$

$$2 \leq l \leq N_{\mathrm{r}}/2 \tag{103}$$

$$|k| \leq l_{\max} \cdot (N_{\mathrm{r}} + N_{\mathrm{d}}) \tag{104}$$

Given these constraints, it has been shown in Thobe and Bose [14] that the linear diophantine equation

$$k = (l - 2p)N_{\mathrm{r}} - mN_{\mathrm{d}} \tag{105}$$

will have a unique solution for the unknowns $l - 2p$ and m, though such a solution may not be guaranteed to exist. A generalized Euclid's algorithm is used in our software to solve Equation 105 for m and the set of l which satisfy it and the constraints. Since the rows of the observation matrix are indexed by k, this means that $l - 2p$ and m are constant throughout any row. In fact, the matrix elements corresponding to a given order m and parity of degree $|l|_2 = |l - 2p|_2$ form, after a suitable permutation of rows and columns, a block which is independent of all other orders and parities. Thus the solution of the observation equation may be carried out block by block, with massive computational savings.

Given the above, an observation matrix element (see RHS of Equation 43) factors into three parts.

$$\frac{\partial \Delta \dot{R}(k)}{\partial A_{lm}} = \Phi_{\mathrm{row}}(k) F_{lmp} \Phi_{\mathrm{col}}(l) \tag{106}$$

The first is dependent only upon the row index k.

$$\Phi_{\mathrm{row}}(k) = \cos N_{\mathrm{r}} \frac{\delta\psi}{2} \cdot \sin[l - 2p] N_{\mathrm{r}} \frac{\delta\psi}{2} \cdot \frac{[l - 2p]N_{\mathrm{r}}}{k} i \exp i\psi_{lmp0}(0) \tag{107}$$

The second is simply the inclination function, which is real, and the the third is dependent only on the column multi-index (l, m).

$$\Phi_{\mathrm{col}}(l) = \frac{\mu}{na^2} \left(\frac{a_e}{a}\right)^l \tag{108}$$

Thus (each block of) the observation matrix is factored into the product of a diagonal matrix, a rectangular matrix, and another diagonal matrix.

Figure 1 shows the bounding non-zero elements of the observation matrix block $m = 45$, $|l|_2$=0. All even-even points on and inside the isosceles trapezoid are non-zero and all those outside are zero. For blocks such that $|l|_2 = 1$, the odd-odd elements are, of course, selected. The lowest and highest values of l are, respectively:

$$\min\{l\} = \max\{m, 2\} + |\max\{m, 2\} + |l|_2|_2 \tag{109}$$

$$\max\{l\} = l_{\max} - |l_{\max} + |l|_2|_2 \tag{110}$$

Since the oblique upper and lower boundaries of observation matrix block satisfy $l-2p = \pm l$, it is a simple matter to obtain the indices of the vertices.

Having reduced the observation matrix essentially to a real isosceles trapezoid, we now explain the additional symmetry which allows the number of rows to be reduced by half. Consider what happens to the factors of Equation 106 as $l-2p \rightarrow -(l-2p)$ or, equivalently, as $p \rightarrow l - p$. As can be seen from Figure 1, this constitutes a reflection of the matrix about the horizontal axis $l - 2p = 0$. We use the identity

$$F_{lm[l-p]}(90°) \equiv (-1)^{|l-2p|_2} F_{lmp}(90°) \tag{111}$$

Defining $k' = (-l + 2p)N_r - mN_d$ and restricting $l - 2p \geq 0$, we have k representing rows in the top half of Figure 1 and k' representing their images in the bottom half. We then define the reduced measurement or observation vector to be:

$$y(k) = \frac{1}{2}\left\{\frac{\Delta\dot{R}(k)}{\Phi_{\text{row}}(k)} + (-1)^{|l-m|_2}\frac{\Delta\dot{R}(k')}{\Phi_{\text{row}}(k')}\right\} \tag{112}$$

Then solve the overdetermined linear system

$$y(k) = \sum_{l,m} F_{lmp} z(l, m) \tag{113}$$

for $z(l, m)$ and compute

$$A_{lm} = z(l, m)/\Phi_{\text{col}}(l, m) \tag{114}$$

Note that the only significant computational effort is in solving Equation 113. This effort is an order of magnitude less than solving the original observation equation

$$\Delta\dot{R}(k) = \sum_{l,m} \frac{\partial\Delta\dot{R}(k)}{\partial A_{lm}} A_{lm} \tag{115}$$

which has twice the number of rows and is complex as well.

The reduction of the observation equation just described can be rigorously proved using elementary properties of the pseudo-inverse. The reduced observation matrix for the block has the form of a right trapezoid. The computation of the reduced observation matrix elements F_{lmp} and the least squares solution of the reduced observation equation is discussed in Section 4.

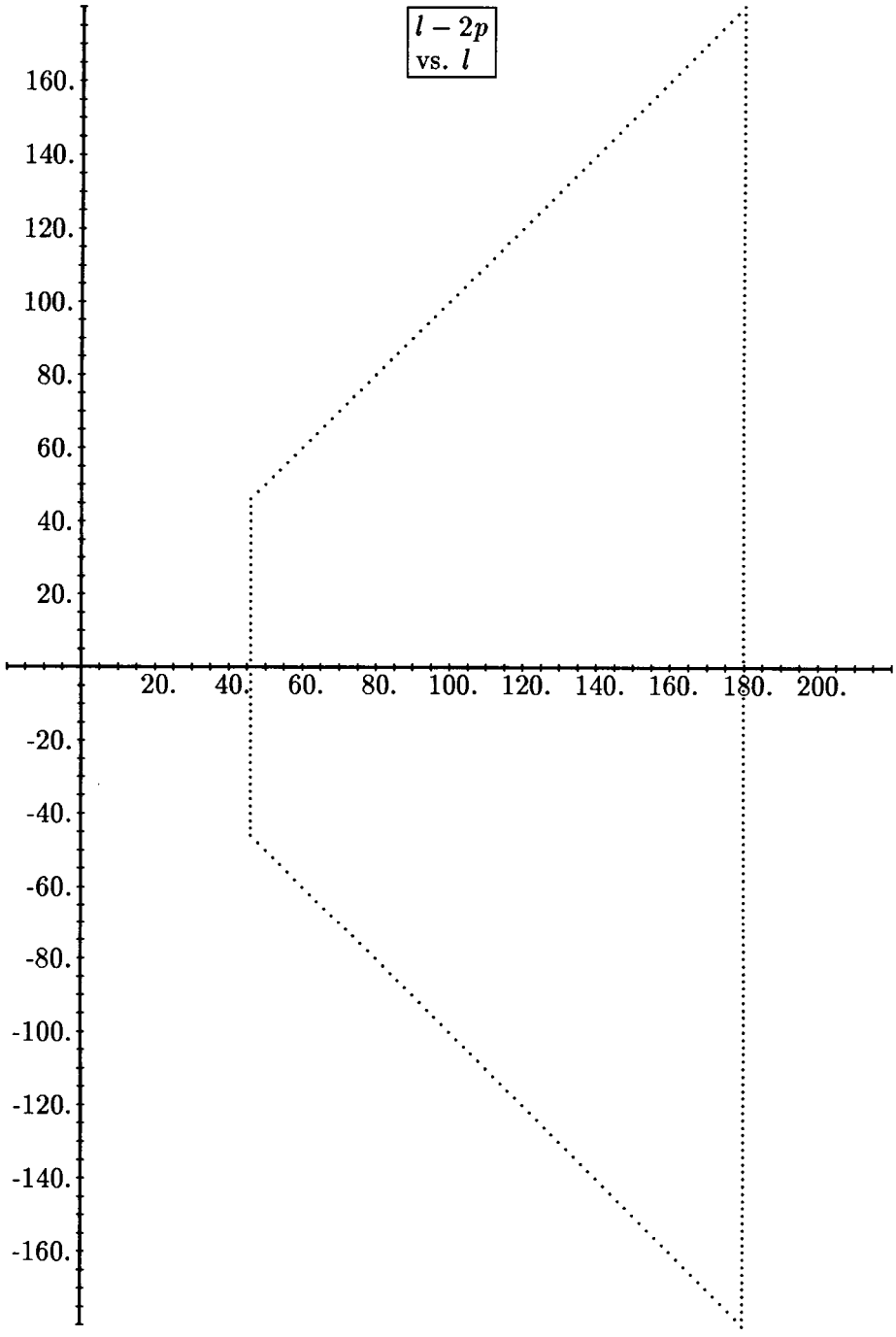

Figure 1: Non-Zero Observation Matrix Elements for Block: $m = 45$, $|l|_2 = 0$

4 Numerical Techniques

4.1 Inclination Function Computation

A stable, efficient, reliable method of computing the inclination functions $F_{lmp}(\iota)$ is an essential and nontrivial element in the coefficient recovery process, as well as orbit prediction and simulation in a perturbed geopotential environment. We considered a number of existing techniques, all of which were unsatisfactory for our purposes for different reasons.

Previously, we have not concerned ourselves with the question of normalization. We bring it up here because the use of the normalizing factor [9, formula (1.34)]:

$$\sqrt{\frac{(l+m)!}{(l-m)!(2l+1)(2-\delta_m)}} \tag{116}$$

sharply reduces numerical problems associated with excessive dynamic range in the values of the harmonics and harmonic coefficients. While the other equations in this report are transparent with respect to whether normalized or unnormalized harmonics and harmonic equations are employed, actual expressions for the inclination functions F_{lmp} and the associated Legendre polynomials P_{lm} must be divided by Equation 116. The recovered harmonic coefficients will then be multiplied by the normalization factor. The expressions below are given in *unnormalized* form. The reader may apply the conversion himself.

The first approach to computing F_{lmp} was by direct application of Kaula [9, formula (3.62)]

$$\begin{aligned} F_{lmp}(\iota) \;=\; & \sum_{t=0}^{\min\{p,k\}} \frac{(2l-2t)!}{t!(l-t)!(l-m-2t)!2^{2l-2t}} sin^{l-m-2t}\iota \\ & \times \sum_{s=0}^{m} \binom{m}{s} \cos^s \iota \sum_{c=\max\{0,p-t-m+s\}}^{\min\{p-t,l-m-2t+s\}} \binom{l-m-2t+s}{c} \binom{m-s}{p-t-c} (-1)^{c-k} \end{aligned} \tag{117}$$

where $k = \lfloor (l-m)/2 \rfloor$ (greatest integer or floor function). When specialized to $\iota = 90°$, the dummy index s can only have the value zero and the number of summations is reduced from three to two.

$$\begin{aligned} F_{lmp}(90°) \;=\; & \sum_{t=0}^{\min\{p,k\}} \frac{(2l-2t)!}{t!(l-t)!(l-m-2t)!2^{2l-2t}} \\ & \times \sum_{c=\max\{0,p-t-m\}}^{\min\{p-t,l-m-2t\}} \binom{l-m-2t}{c} \binom{m}{p-t-c} (-1)^{c-k} \end{aligned} \tag{118}$$

Even Equation 118 is computationally too slow for larger values of the indices l, m, p when large numbers of the coefficients are required, and we used it only for producing comparison values when testing our own method.

A second method which we attempted to use consists in part of evaluating P_{lm} at equally spaced intervals on an inclined circular orbit and employing an FFT to obtain the corresponding F_{lmp}. While interesting and accurate for small index values, say ≤ 20; we found the implementation to be unstable for larger values, at least at the 90° inclination of interest. A further difficulty with the method is that the order in which the coefficients are produced: straight lexicographic ordering according to l, m, p (i.e. 200, 201, 202, 210, 211, etc.). This would entail precomputing large numbers of coefficients, sorting them into blocks and rows according to the our observation matrix block structure, and storing them in a data base for recall during evaluation of the matrix elements. Our tests of this method were performed using a program kindly supplied by Clyde Goad of the Ohio State University Department of Geodetic Science. A description of this method is to be found in Wagner [15].

To overcome these problems, we developed our own recursive method based on the analytical representation of Brumberg [3]. This new method is accurate, stable, and efficient to high index values. The inclination need not be restricted to 90°. Values are produced in a convenient order so that they can be computed on the fly, rather than precomputed, sorted, and stored. We have

$$F_{lmp}(\iota) = \lambda_{lmp} \cdot (\sin\frac{\iota}{2})^{|l-2p-m|}(\cos\frac{\iota}{2})^{|l-2p+m|} \cdot {}_2\mathrm{F}_1\left(\begin{matrix} -s, 2l-s+1 \\ 1+|l-2p-m| \end{matrix} \middle| \sin^2\frac{\iota}{2} \right) \quad (119)$$

where

$$s = l - (|l-2p-m| + |l-2p+m|)/2 \quad (120)$$

and

$$\lambda_{lmp} = (-1)^{\lfloor\frac{l-m}{2}\rfloor+\max\{0,l-2p-m\}} \cdot \frac{(1)_{l+m}(-2l+2p)_{\max\{0,l-2p-m\}}(-2p)_{\max\{0,-l+2p+m\}}}{2^l(1)_p(1)_{l-2p}(1)_{|l-2p-m|}} \quad (121)$$

We derived Equation 121 ourselves from a formula of Izsak [8] according to Brumberg's instructions when his own unnumbered formula preceding [3, eq. 22], gave incorrect values, probably due to a misprint.

The notation $(a)_n = a(a+1)\cdots(a+n-1)$ denotes the Pochhammer symbol or generalized factorial, and ${}_2\mathrm{F}_1$ denotes the gaussian hypergeometric polynomial:

$${}_2\mathrm{F}_1\left(\begin{matrix} -a, b \\ c \end{matrix} \middle| x \right) = \sum_{n=0}^{a} \frac{(-a)_n(b)_n}{(c)_n}\frac{x^n}{n!} \quad (122)$$

It turns out that direct application of Equation 122 leads to gross numerical difficulties, making it useless for all except calculations in a very small number of terms. If the evaluation is carried out by simple evaluation and summing of the terms, then the method fails because the terms are very large, alternate in sign, and have a very small sum. If the evaluation is carried out by a simple recursion using Horner's rule, then the method fails

because the resulting difference equation becomes unstable after a small number of iterations. According to Wagner [16], "fully recursive formulations in the literature ... appear to be unstable at high degree."

Our contribution lies in inventing a recursive technique for evaluating ${}_2\mathrm{F}_1$, which is stable and efficiently produces accurate values for even large index values. Consider Equation 119. The hypergeometric polynomial can be abbreviated as

$$ {}_2\mathrm{F}_1\left(\begin{array}{c} -s, 2l-s+1 \\ 1+|l-2p-m| \end{array} \middle| \sin^2\frac{\iota}{2} \right) = {}_2\mathrm{F}_1\left(\begin{array}{c} \alpha, \beta \\ \gamma \end{array} \middle| x \right) = \mathrm{F}(\alpha, \beta) \tag{123} $$

We apply two of the so-called gaussian contiguous relations

$$ (\alpha-\beta)\mathrm{F}(\alpha,\beta) - \alpha\mathrm{F}(\alpha+1,\beta) + \beta\mathrm{F}(\alpha,\beta+1) = 0 \tag{124} $$

and

$$ (\alpha-\beta)(1-x)\mathrm{F}(\alpha,\beta) + (\gamma-\alpha)\mathrm{F}(\alpha-1,\beta) - (\gamma-\beta)\mathrm{F}(\alpha,\beta-1) = 0 \tag{125} $$

which may be found in Lebedev [11, p.242, eqs. 9.2.10-11]. In matrix form, these two second-order linear difference equations become:

$$ \begin{bmatrix} \mathrm{F}(\alpha,\beta+1) \\ \mathrm{F}(\alpha,\beta) \end{bmatrix} = \begin{bmatrix} \frac{\beta-\alpha}{\beta} & \frac{\alpha}{\beta} \\ 1 & 0 \end{bmatrix} \begin{bmatrix} \mathrm{F}(\alpha,\beta) \\ \mathrm{F}(\alpha+1,\beta) \end{bmatrix} \tag{126} $$

and

$$ \begin{bmatrix} \mathrm{F}(\alpha-1,\beta+1) \\ \mathrm{F}(\alpha,\beta+1) \end{bmatrix} = \begin{bmatrix} \frac{\beta+1-\alpha}{\beta}(1-x) & \frac{\beta+1-\gamma}{\gamma-\alpha} \\ 1 & 0 \end{bmatrix} \begin{bmatrix} \mathrm{F}(\alpha,\beta+1) \\ \mathrm{F}(\alpha,\beta) \end{bmatrix} \tag{127} $$

Combining, we find that given $\mathrm{F}(\alpha,\beta)$ and $\mathrm{F}(\alpha+1,\beta)$, we can by successively applying Equations 126 and 127, compute $\mathrm{F}(\alpha-1,\beta+1)$ and $\mathrm{F}(\alpha,\beta+1)$. Note that the transition

$$ (\alpha,\beta) \rightarrow (\alpha-1,\beta+1) \tag{128} $$

occurs when $s \rightarrow s+1$, which in turn occurs when $l \rightarrow l+2$ and $p \rightarrow p+1$ simultaneously as m and $l-2p$ remain constant; in other words, as we take one step to the right along any row of the matrix block of Figure 1. Equations 126, 127, and 128 constitute a recursion, so that once starting values are computed using Equation 122, ${}_2\mathrm{F}_1$ can be efficiently computed for an entire row.

The best news is that this recursion turns out to be a stable one. This method has been used to evaluate the inclination function for index values up to one thousand. We used it to compute our observation matrix elements and also in our analytical trajectory simulation.

4.2 Observation Equation Solution

Since the observation equation has been shown to have a block diagonal structure, it can be treated as a collection of uncoupled observation equations. Each block of the large observation matrix becomes the observation matrix for a smaller least squares estimation problem. Formally, let us write the (smaller) observation equation as

$$y = Hx + v \tag{129}$$

For generality, regard all quantities as complex in the definitions:

$$\begin{array}{rcl} x & = & \text{zero-mean } n\text{-vector of unknown coefficients} \\ y & = & \text{zero-mean } m\text{-vector of measurements, } m \geq n \\ v & = & \text{zero-mean } n\text{-vector of measurement noises} \\ H & = & m \times n \text{ observation matrix of rank } m \end{array}$$

Since v is a unit-covariance complex white noise vector, it obeys the equations:

$$\mathbf{E}v = 0 \tag{130}$$

$$\mathbf{E}vv^* = \sigma^2 I \tag{131}$$

$$\mathbf{E}v\bar{v}^* = 0 \tag{132}$$

That is to say, the real and imaginary parts of all components of v are mutually independent, and each has mean zero and variance $\sigma^2/2$.

The "best" solution of Equation 129 in the conditional mean sense, i.e. $\hat{x} = \mathbf{E}\{x \mid y\}$, is the one which conditionally minimizes the vector norm of the error:

$$\hat{x} = \underset{x}{\operatorname{argmin}} \left\{ \|y - Hx\|^2 \mid y \right\} \tag{133}$$

If U is a unitary (orthogonal in the real case) matrix, i.e. $U^{-1} = U^*$, then Equation 133 is equivalent to:

$$\hat{x} = \underset{x}{\operatorname{argmin}} \left\{ \|\tilde{y} - \tilde{H}x\|^2 \mid \tilde{y} \right\} \tag{134}$$

where $\tilde{y} = Uy$ and $\tilde{H} = UH$. Thus we have changed the problem but not the solution by multiplying both y and H by a unitary (or orthogonal) matrix U.

To simplify bookkeeping, let us define the augmented matrix $[H \mid y]$. Then by judiciously selecting U, we can put $[\tilde{H} \mid \tilde{y}]$ into the form:

$$U[H \mid y] = [UH \mid Uy] = [\tilde{H} \mid \tilde{y}] = \left[\begin{array}{c|c} \tilde{H}_1 & \tilde{y}_1 \\ \tilde{H}_2 & \tilde{y}_2 \end{array}\right] = \begin{array}{|c|c|} \hline \tilde{H}_1 \diagdown & \tilde{y}_1 \\ \hline 0 \diagup & \\ \hline 0 & \tilde{y}_2 \\ \hline \end{array} \tag{135}$$

where $\tilde{H}_1$ is a full-rank upper triangular matrix and $\tilde{H}_2$ is a zero matrix.

From Equations 135 and 134 we have:

$$\hat{x} = \underset{x}{\operatorname{argmin}} \left\{ \|\tilde{y}_1 - \tilde{H}_1 x\|^2 + \|\tilde{y}_2\|^2 \mid \tilde{y}_1, \tilde{y}_2 \right\} \tag{136}$$

Now $\tilde{H}_1$ is invertible so that

$$\hat{x} = \tilde{H}_1^{-1} \tilde{y}_1 \tag{137}$$

since

$$\|\tilde{y}_1 - \tilde{H}_1 \hat{x}\|^2 + \|\tilde{y}_2\|^2 = 0 + \|\tilde{y}_2\|^2 \tag{138}$$

which is clearly the minumum value.

In practice, a finite sequence of unitary transformations is used:

$$U = U^{(K)} U^{(K-1)} \dots U^{(k)} \dots U^{(1)} \tag{139}$$

where

$$U^{(k)} [H^{(k)} | y^{(k)}] = [H^{(k+1)} | y^{(k+1)}] \tag{140}$$

For the Givens or rotation method, the elementary transformations are of the form:

$$U^{(k)} = \begin{bmatrix} 1 & & & & & & & & & \\ & \ddots & & & & & & & 0 & \\ & & 1 & & & & & & & \\ & & & \alpha_{ii}^{(k)} & & & \alpha_{ij}^{(k)} & & & \\ & & & & 1 & & & & & \\ & & & & & \ddots & & & & \\ & & & & & & 1 & & & \\ & & & \alpha_{ji}^{(k)} & & & \alpha_{jj}^{(k)} & & & \\ & & & & & & & 1 & & \\ & 0 & & & & & & & \ddots & \\ & & & & & & & & & 1 \end{bmatrix} \tag{141}$$

where the k-dependent indices i and j indicate the two rows of $[H^{(k)} \mid y^{(k)}]$ affected by the transformation. Assuming that for some $l \geq 1$, the first $l-1$ columns of $H^{(k)}$ are zero, and that for $h_{il}^{(k)}$ and $h_{jl}^{(k)}$ are not both zero, then Equation 140 becomes:

$$\begin{aligned} \begin{bmatrix} \alpha_{ii}^{(k)} & \alpha_{ij}^{(k)} \\ \alpha_{ji}^{(k)} & \alpha_{jj}^{(k)} \end{bmatrix} & \left[\begin{array}{ccccccc|c} 0 & \cdots & 0 & h_{il}^{(k)} & h_{i[l+1]}^{(k)} & \cdots & h_{in}^{(k)} & y_i^{(k)} \\ 0 & \cdots & 0 & h_{jl}^{(k)} & h_{j[l+1]}^{(k)} & \cdots & h_{jn}^{(k)} & y_j^{(k)} \end{array}\right] \\ &= \left[\begin{array}{ccccccc|c} 0 & \cdots & 0 & r^{(k)} & h_{i[l+1]}^{(k+1)} & \cdots & h_{in}^{(k+1)} & y_i^{(k+1)} \\ 0 & \cdots & 0 & 0 & h_{j[l+1]}^{(k+1)} & \cdots & h_{jn}^{(k+1)} & y_j^{(k+1)} \end{array}\right] \end{aligned} \tag{142}$$

where

$$r^{(k)} = \sqrt{|h_{il}^{(k)}|^2 + |h_{jl}^{(k)}|^2} \neq 0 \tag{143}$$

Note that $h_{il}^{(k+1)} = r^{(k)}$ and $h_{jl}^{(k+1)} = 0$. The reader may check for himself that this is true when for $U^{(k)}$ one selects the unitary matrix:

$$\begin{bmatrix} \alpha_{ii}^{(k)} & \alpha_{ij}^{(k)} \\ \alpha_{ji}^{(k)} & \alpha_{jj}^{(k)} \end{bmatrix} = \begin{bmatrix} \bar{h}_{il}^{(k)}/r^{(k)} & \bar{h}_{jl}^{(k)}/r^{(k)} \\ -h_{jl}^{(k)}/r^{(k)} & h_{il}^{(k)}/r^{(k)} \end{bmatrix} \tag{144}$$

The algorithm proceeds by selecting pairs of columns and rows to systematically zero out elements column by column from left to right, and row by row from the first subdiagonal downward, until the pattern of Equation 135 is obtained. Then the solution $\hat{x}$ of Equation 137 is obtained by an efficient back substitution. So far we have described the standard method for solving least squares estimation problems by means of unitary Givens rotational transformations. For our problem, the augmented matrix has the special sparseness profile of a right trapezoid. For extra efficiency, one only need stop the downward scan when the bottom boundary of the profile is reached. It takes very little additional programming logic to accomplish this, which is one reason why the Givens method was selected. Furthermore, it is straightforward to include *a priori* estimates and covariances as well as correlated measurement noise. The main reason for selecting Givens rotations, however, is the excellent numerical stability of the method.

5 Simulation Results

After having designed a spectral model for the satellite-to-satellite range rate, and after constructing software to recover the geopotential coefficients from the range rate data, it was necessary to exercise the software on simulation-produced data. That is the objective of this section. We will mainly concentrate on describing the tests and their results including mention of simplifying assumptions. Detailed descriptions of the math models and of the software algorithms are to be found in previous sections.

The test article being subjected to validation testing is the recovery software itself. It is divided into parts according to the functions:

- Obtaining the range rate spectrum from the data and classifying the spectrum into blocks according to order m and parity of degree $|l|_2$;
- Generating the observation matrix for each block;
- Constructing the observation vector and solving for the estimated geopotential harmonic coefficients.

In order to exercise these functions and test the recovery software, we developed a one-sidereal day analytical simulation, restricting the maximum degree and order to eight. This allowed us to precisely control the test parameters so that discrepancies could be easily traced. Upon completion of this debugging and validation phase, we were able to proceed with confidence to tests involving foreign data, obtained from the much larger University of Texas simulation data set. Discrepancies at that stage could still be due to either our own modelling assumptions or to the Texas simulation, but not likely to errors in our software. We should point out that in accordance with good software engineering practice, detailed module testing of our software was performed prior to system level testing with *any* simulation data.

5.1 Analytical Validation

A one day, 16-orbit trajectory of a satellite pair was simulated. The harmonic coefficients used are those of Rapp [12]. The perturbation included only tesseral terms, i.e. $m \neq 0$. As an additional check, the SST range rate was computed in two ways with identical results:

- by a time domain computation followed by an FFT;
- and by a direct frequency domain computation.

The orbital parameters used in the simulation are given in Table 1.

N_r	16	number of revolutions
N_d	1	number of days
a	6 640 419m	semi-major axis
e	0	eccentricity
ι	90°	inclination
ω	7.292158×10^{-5}	perigee
Ω	90°	ascending node
M_0	0	initial mean anomaly
R	300km	satellite separation
a_e	6 378 155m	earth radius
n	$1.66745368 \times 10^{-3}$	mean motion

Table 1: Orbit Parameters for One-day Simulation

The general time domain signal model equation is given by

$$\Delta\dot{R}_{lmpq}(t) = -2\frac{\mu a_e^l}{na^{l+2}} F_{lmp} G_{lpq} \cos\frac{\delta M}{2} \sin[(l-2p+q)\frac{\delta M}{2}] \times \\ \times \frac{[l-2p+q]\dot{M}}{[l-2p+q]\dot{M} - m\dot{\theta}} \operatorname{Im} S_{lmpq}(t) \tag{145}$$

Here we take $\dot{M} = N_r\dot{\psi}$ and $\dot{\theta} = N_d\dot{\psi}$ based on the assumption of a synchronized orbit and neglecting any secular motion. The frequency domain counterpart to Equation 145 with the noted assumptions is given by

$$\Delta\dot{R}_{lmpq}(k) = i\frac{\mu a_e^l}{na^{l+2}} F_{lmp} G_{lpq} \cos\frac{\delta M}{2} \sin[(l-2p+q)\frac{\delta M}{2}] \times \\ \times \frac{[l-2p+q]\dot{M}}{[l-2p+q]\dot{M} - m\dot{\theta}} S_{lmpq}(0) \tag{146}$$

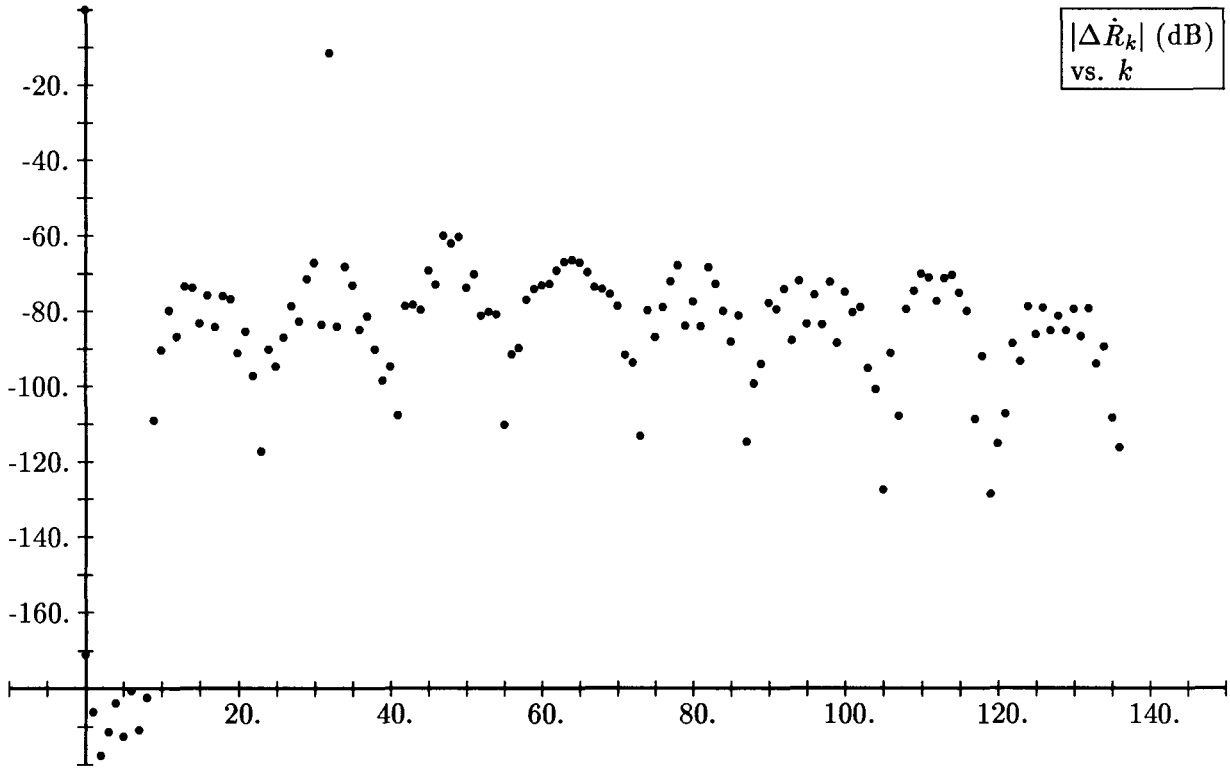

Figure 2: One-day SST Range Rate Perturbation Spectral Amplitude

Summation in Equations 145 and 146 is performed over l, m, p, and q with the restrictions $q = 0$ and $k = (l - 2p + q)N_{\mathrm{r}} - mN_{\mathrm{d}}$.

Since this is the same model assumed by the recovery software, we expected the assumed coefficients to be recovered more or less exactly, which is precisely what occurred. As can be seen from Table 2, the difference between the model coefficients and the those recovered is seldom more than one or two in the fourth decimal place. The log amplitude (dB) of the magnitude of the spectrum of $\Delta\dot{R}$ as a function of positive wave numbers k is given in Figure 2.

Note that the structure of the spectrum is only clear when individual blocks are viewed.

		estimate		truth	
l	m	C_{lm}	S_{lm}	C_{lm}	S_{lm}
2	1	-0.6762×10^{-09}	-0.1535×10^{-08}	-0.6763×10^{-09}	-0.1535×10^{-08}
4	1	-0.5364×10^{-06}	-0.4744×10^{-06}	-0.5363×10^{-06}	-0.4743×10^{-06}
6	1	-0.7151×10^{-07}	0.2120×10^{-07}	-0.7149×10^{-07}	0.2120×10^{-07}
8	1	0.1393×10^{-07}	0.4834×10^{-07}	0.1393×10^{-07}	0.4833×10^{-07}
3	1	0.2029×10^{-05}	0.2494×10^{-06}	0.2029×10^{-05}	0.2493×10^{-06}
5	1	-0.5193×10^{-07}	-0.1032×10^{-06}	-0.5191×10^{-07}	-0.1032×10^{-06}
7	1	0.2696×10^{-06}	0.8782×10^{-07}	0.2696×10^{-06}	0.8780×10^{-07}
2	2	0.2437×10^{-05}	-0.1401×10^{-05}	0.2436×10^{-05}	-0.1400×10^{-05}
4	2	0.3502×10^{-06}	0.6604×10^{-06}	0.3501×10^{-06}	0.6602×10^{-06}
6	2	0.5102×10^{-07}	-0.3618×10^{-06}	0.5101×10^{-07}	-0.3617×10^{-06}
8	2	0.9864×10^{-07}	0.6648×10^{-07}	0.9861×10^{-07}	0.6646×10^{-07}
3	2	0.9030×10^{-06}	-0.6155×10^{-06}	0.9027×10^{-06}	-0.6153×10^{-06}
5	2	0.6422×10^{-06}	-0.3294×10^{-06}	0.6420×10^{-06}	-0.3293×10^{-06}
7	2	0.3665×10^{-06}	0.1151×10^{-06}	0.3664×10^{-06}	0.1151×10^{-06}
4	3	0.9944×10^{-06}	-0.2023×10^{-06}	0.9942×10^{-06}	-0.2022×10^{-06}
6	3	0.5621×10^{-07}	0.1751×10^{-08}	0.5620×10^{-07}	0.1750×10^{-08}
8	3	-0.1625×10^{-07}	-0.6826×10^{-07}	-0.1624×10^{-07}	-0.6824×10^{-07}
3	3	0.7187×10^{-06}	0.1417×10^{-05}	0.7186×10^{-06}	0.1417×10^{-05}
5	3	-0.4562×10^{-06}	-0.2176×10^{-06}	-0.4561×10^{-06}	-0.2175×10^{-06}
7	3	0.2414×10^{-06}	-0.2067×10^{-06}	0.2413×10^{-06}	-0.2066×10^{-06}
4	4	-0.1923×10^{-06}	0.3056×10^{-06}	-0.1923×10^{-06}	0.3056×10^{-06}
6	4	-0.9177×10^{-07}	-0.4688×10^{-06}	-0.9175×10^{-07}	-0.4687×10^{-06}
8	4	-0.2438×10^{-06}	0.7623×10^{-07}	-0.2438×10^{-06}	0.7621×10^{-07}
5	4	-0.2900×10^{-06}	0.4980×10^{-07}	-0.2899×10^{-06}	0.4979×10^{-07}
7	4	-0.2721×10^{-06}	-0.1282×10^{-06}	-0.2721×10^{-06}	-0.1281×10^{-06}
6	5	-0.2639×10^{-06}	-0.5363×10^{-06}	-0.2638×10^{-06}	-0.5362×10^{-06}
8	5	-0.1945×10^{-07}	0.8331×10^{-07}	-0.1945×10^{-07}	0.8329×10^{-07}
5	5	0.1733×10^{-06}	-0.6612×10^{-06}	0.1733×10^{-06}	-0.6610×10^{-06}
7	5	0.1254×10^{-07}	0.1899×10^{-07}	0.1253×10^{-07}	0.1899×10^{-07}
6	6	0.6874×10^{-08}	-0.2372×10^{-06}	0.6872×10^{-08}	-0.2371×10^{-06}
8	6	-0.6644×10^{-07}	0.3111×10^{-06}	-0.6642×10^{-07}	0.3110×10^{-06}
7	6	-0.3608×10^{-06}	0.1518×10^{-06}	-0.3607×10^{-06}	0.1518×10^{-06}
8	7	0.6964×10^{-07}	0.7325×10^{-07}	0.6962×10^{-07}	0.7323×10^{-07}
7	7	0.5054×10^{-08}	0.2150×10^{-07}	0.5054×10^{-08}	0.2149×10^{-07}

Table 2: Recovered Coefficients for One-Day Analytically Simulated Mission

5.2 Texas Tape Recovery

Our recovery software was exercised on SST range rate data produced at the University of Texas by Schutz et al. [13]. They simulated a 32-sidereal day mission of 525 near circular polar orbits. As required by our software, the orbit is synchronous — tuned to close on itself and repeat the same ground track each thirty two-day period. Table 3 gives the orbit characteristics.

N_r	525	number of revolutions
N_d	32	number of days
a	6 538 155m	semi-major axis
e	0.00114	eccentricity
ι	90°	inclination
ω	90°	perigee
Ω	90°	ascending node
M_0	0	initial mean anomaly
R	300km	satellite separation
a_e	6 378 155m	earth radius
n	1.1963697×10^{-3}	mean motion

Table 3: Orbit Parameters for University of Texas Simulation

The data were supplied in ASCII in the form of a full 6250-bpi, 1800-ft magnetic tape. We converted this data to binary and extracted the SST range rate signal. The 5-sec sampling interval was converted to 5.25903854 sec using linear interpolation so that precisely $2^{19} = 524288$ sampling intervals would equal one mission period. Due to the great length of the sample vector, we computed the complex spectrum of the range rate using the mass storage FFT of Fraser [7]. To assure ourselves of accurate numerical results, we carried out a simple analytical error analysis — converting the mass FFT software to double precision, comparing the results to those obtained with single precision, and applying the inverse FFT to obtain the original sampled signal.

The spectrum was then permuted into blocks according to order m and parity of degree $|l|_2$ using a merge sort. Eack block was stored in a separate record of a direct-access file for easy retrieval. The recovery software computed each observation matrix block and solved the observation equation for that block thereby recovering the geopotential harmonic coefficients assumed by the University of Texas simulation. The equation solver had been tested on a 100×100 matrix of pseudo random numbers on the unit interval (0, 1]. When computing each block of the observation matrix, we also compute a predicted spectrum for that block using the assumed coefficients. This prediction should compare well with the spectrum extracted from the simulation data. We think it does, in particularly considering

that so far certain important considerations have been omitted from the analysis:

- The whole range rate signal was used instead of the residual (perturbation) after removal of the reference orbit range rate. In effect an ideal circular reference orbit was used.
- Secular perturbations of the orbit elements have not been included. This omission is justified by Kaula [9, eqs. 3.75, p. 40], in which the perturbation of $\dot{\Omega} \approx 0$ for an inclination of 90° and the perturbation of $\dot{M} + \dot{\omega} \approx 6.9°$ per day.
- Terms in our signal model Equation 146 for which $q \neq 0$ have to date not been incorporated into the recovery software.

Plots of the amplitude and phase of the SST range rate spectra are given in Figures 26, 27, 5, and 6. The predicted spectra are those computed by us using the above described simplified kinetic energy model which is built into the recovery software. The observed spectra were computed by us from the University of Texas simulation data using the previously mentioned mass storage FFT and block permutation.

It is interesting to note that the observed spectra degenerate into an approximately constant magnitude of -130 dB and phase of $\pm 60°$ beyond a wave number of approximately 60 000 or 60% of bandwith of 100 260. We presume this reflects a limit to the fidelity of the U. of T. simulation. Our spectral model shows a definite and interesting structure in the outer 40% of the band, which is completely obscured in the simulation data.

In the inner 60% of the band, the magnitudes agree fairly well, quantitatively as well as qualitatively. The main discrepancy in comparing both the magnitudes and phases is in the weakest points of the spectra. The phases agree best the closer one approaches $k = 0$. Out to about $k = 20000$ the discrepancy seldom exceeds 20°.

It is likely that by including $q = \pm 1$ in the model, making improvements in the reference trajectory, considering secular motion, and iterating, that agreement would improve. The results so far are promising, indeed.

Table 6 shows recovered values of the harmonic coefficients for $m = 2$ and $l \leq 60$ and even. Except for $l = 2$, which would be heavily influenced by the uncorrected-for eccentricity in the reference orbit, the agreement between prediction and experiment is good. Also, no attempt was made to exclude the apparently erroneous data at extreme wave numbers. The computation was actually carried out to recover C_{lm} and S_{lm} for values of l up to 180, but the higher l values were excluded for brevity. For values ≥ 100 the agreement is poor, since these values depend upon the extreme wave numbers. The software is general enough to be applied to any given block. The various refinements in modeling the signal spectrum would be expected to improve the agreement between predicted and estimated values.

6 Summary

6.1 Conclusions

We have described the analytical basis for our approach to the recovery of the harmonic coefficients of the geopotential field from satellite-to-satellite range rate data. We then presented the results of numerical experiments with the objective of validating the approach, as well as demonstrating our ability to process the data on the scale required.

The general basis of the method is that presented in Kaula [10]. However, the observation equation has been freshly derived by us based upon much simpler expressions for the perturbation in the satellite kinetic energy, and the close relationship between variations in kinetic energy and variations in satellite speed. This avoids much of the intricate dealings with perturbations of individual Keplerian elements. In addition, we borrowed from Colombo [5] the assumption of a synchronous orbit in which the ground track of each satellite repeats after N_r revolutions and N_d days, these being a mutually prime pair of integers. This makes the spectrum discrete and allows one to employ fourier analysis to uncouple the observation equation into manageable-sized blocks.

In the frequency domain, the observation matrix assumes a block diagonal structure. Without such a structure, the computational resources required to perform coefficient recovery would be truly massive. When q is restricted to zero as with circular polar orbits, there is one block for each combination of the harmonic order m and parity of degree $|l|_2$. In addition, each block is further reduced to a real, right trapezoidal structure, which makes both its computation and solution even easier.

On the numerical analysis front, we have developed a method, based on the mass-storage FFT of Fraser [7] and resampling of data, of obtaining the fourier coefficients of the sampled range rate over the entire mission period. A contribution which others in the orbit prediction field will find useful is the stable and efficient method of computing the inclination function F_{lmp} based on the analytical formulas of Brumberg [3] and the recursive generation of the hypergeometric polynomials using the contiguous relations of Gauss. We have employed the method of unitary Givens rotational transformations to solve the reduced and uncoupled frequency domain observation equations, while efficiently exploiting trapezoidal sparseness pattern of the blocks.

We have demonstrated the low computational cost of the method. For a maximum degree of 180, each block can be set up and solved in a time less than or equal to approximately five minutes on a DEC VAX 11/750. While we have not yet reached the limits of accuracy of the recovered coefficients, we feel that the results achieved thus far on the University of Texas simulation data are highly encouraging. Experimental recovery of data generated by our own low degree and order analytical simulation shows excellent agreement between known and recovered coefficients, leading us to believe that considerable improvements in results of the Texas data experiments can be expected as well.

6.2 Recommendations

It is recommended that the progress made this far be followed up and extended. A major priority is to improve the quality of the recovered coefficients. This can be done by:

- improving spectrum modelling fidelity by:
  - employing the extended signal model of Section 2.3;
  - including the neglected $q \neq 0$ terms in the signal equation;
  - computing an eccentric reference orbit;
  - including secular perturbation effects.
- employing iterative solution techniques including:
  - constructing intermediary reference orbits from modified Keplerian element perturbations;
  - adding $q \neq 0$ terms to the observation matrix and employing operator perturbation methods;
- extending preprocessing of recorded trajectory data using orbit determination techniques, filtering, and smoothing, to estimate mission period and other orbit characteristics.

Our newly derived signal equation opens up the immediate possibility of investigating the following extensions of the method:

- recovering the zonal ($m = 0$) coefficients;
- using of common ground track trajectories rather than coplanar orbits;
- using SST *range* rather than, or in conjunction with, the SST range rate as the physical measurement of choice.
- performing parametric studies, e.g. varying the satellite-to-satellite separation angle;
- tilting the orbit plane off of 90° inclination;
- admitting non-zero eccentricities.

We believe that additional simulation and validation will prove valuable. In particular we recommend:

- perform our own Cowell method trajectory simulation;
- use only small numbers of harmonics to limit simulation costs;

- use our efficient and stable computation of the inclination functions;
- rule out possible errors in the University of Texas simulation data.

In conclusion, we wish to stress the crucial role of effective data processing techniques in high resolution gravity mapping by satellite.

References

[1] S.C. Bose, G.E.Thobe, J.T.Kouba, and R.E.Mortensen. *Optimal Global Gravity Field Estimation.* Proc. IAG Symposia, Hamburg, 1983. vol. 1, pp. 449-482.

[2] S.C. Bose and G.E. Thobe. *Gravity Field Recovery by Fourier Analysis of Satellite-to-Satellite Range Rate.* Applied Science Analytics, Inc., report No. ASA-TR-84-4, August 1984.

[3] V.A. Brumberg. *Razozhlenie perturbatsionnoi funktsii v sputnikovykh zadachakh.* Biulleten' Instituta Teoreticheskoi Astronomii. vol. XI, No. 2(125), 1967.

[4] O.L. Colombo. *Numerical Methods for Harmonic Analysis on the Sphere.* The Ohio State University, Dept. of Geodetic Science. Report No. 310, 1981.

[5] O.L. Colombo. *Global Geopotential Modelling from Satellite-to-Satellite Tracking.* The Ohio State University, Dept. of Geodetic Science. Report No. 317, 1981.

[6] O.L. Colombo. *The Global Mapping of Gravity with Two Satellites.* Netherlands Geodetic Commission, Publications on Geodesy, New Series, vol.7, No. 3. Delft, The Netherlands. 1984.

[7] Donald Fraser. *Optimized Mass Storage FFT Program* in *Programs for Digital Signal Processing.* IEEE Press. 1979.

[8] I.G. Izsák. *Tesseral Harmonics of the Geopotential and Corrections to Station Coordinates.* JGR. vol. 69, p.2621. 1964.

[9] William M. Kaula. *Theory of Satellite Geodesy.* Blaisdell. 1966.

[10] William M. Kaula. *Inference of Variations in the Gravity Field From Satellite-to-Satellite Range Rate.* JGR, vol.88, no.B10, pp.8345-8349. October 19, 1983.

[11] N.N. Lebedev. *Special Functions and their Applications.* Translated by Richard A. Silverman. Dover Publications, New York. 1972.

[12] Richard H. Rapp. *The Earth's Gravity Field to Degree and Order 180 Using Seasat Altimeter Data, Terrestrial Gravity Data, And Other Data.* AFGL-TR-82-0019 and NTIS AD-A113098. December, 1981.

[13] B.E.Schutz, B.D.Tapley, J.B.Lundberg and P.Halamek. *Simulation of a Geopotential Research Mission for Gravity Studies.* Center for Space Research, U. of Texas, Austin, Texas. 1986.

[14] G.E. Thobe and S.C. Bose. *Uncoupling of Satellite-to-Satellite Range Rate Observation Equation for Higher Degree and Order Gravity Models.* presented at the American Geophysical Union Spring Meeting, Baltimore, Maryland, 27-31 May, 1985.

[15] C.A. Wagner. *The Accuracy of Goddard Earth Models.* NASA Report x-921-76-187, Appendix B. 1976.

[16] C.A. Wagner. *Direct Determination of Gravitational Harmonics from Low-Low GRAVSAT Data.* JGR, vol.88, No. B12, pp. 10309-10321, Dec., 1983.

[17] M. Wolff. *Direct Measurements of the Earth's Gravity Potential Using a Satellite Pair.* JGR, vol.14, pp. 5295-5300, 1979.

A Coefficients and Spectra

This appendix contains

- tables of known and recovered geopotential harmonic coefficients for degrees 2 through 10 and orders 1 through 10;
- magnitude plots of observed SST range rate spectra for degrees 2 through 10 and orders 1 through 10;
- magnitude plots of predicted SST range rate spectra for degrees 2 through 10 and orders 1 through 10;
- phase plots of observed and predicted SST range rate spectra for order 2 and even degree.

The recovered data were obtained by processing the simulated range rate samples produced at the University of Texas by Schutz et al. [13].

		estimate		truth	
l	m	C_{lm}	S_{lm}	C_{lm}	S_{lm}
2	1	0.1444×10^{-06}	0.1128×10^{-06}	-0.6763×10^{-09}	-0.1535×10^{-08}
4	1	-0.4121×10^{-06}	-0.3739×10^{-06}	-0.5363×10^{-06}	-0.4743×10^{-06}
6	1	-0.6507×10^{-07}	0.1868×10^{-07}	-0.7149×10^{-07}	0.2120×10^{-07}
8	1	0.1453×10^{-07}	0.4659×10^{-07}	0.1393×10^{-07}	0.4833×10^{-07}
10	1	0.8760×10^{-07}	-0.9714×10^{-07}	0.9224×10^{-07}	-0.1084×10^{-06}
12	1	-0.4906×10^{-07}	-0.4822×10^{-07}	-0.5404×10^{-07}	-0.5187×10^{-07}
14	1	-0.5574×10^{-08}	0.1671×10^{-07}	-0.4713×10^{-08}	0.1738×10^{-07}
16	1	0.1717×10^{-07}	0.2547×10^{-07}	0.1752×10^{-07}	0.2689×10^{-07}
18	1	-0.1333×10^{-07}	-0.2578×10^{-07}	-0.1322×10^{-07}	-0.2658×10^{-07}
20	1	-0.3281×10^{-08}	-0.1052×10^{-07}	-0.2899×10^{-08}	-0.1087×10^{-07}
22	1	0.3895×10^{-08}	0.2388×10^{-08}	0.5177×10^{-08}	0.1781×10^{-08}
24	1	-0.5822×10^{-08}	0.9940×10^{-09}	-0.6499×10^{-08}	-0.1834×10^{-09}
26	1	-0.1507×10^{-08}	-0.7800×10^{-08}	-0.1452×10^{-08}	-0.8250×10^{-08}
28	1	-0.1700×10^{-08}	0.4712×10^{-08}	-0.1839×10^{-08}	0.5243×10^{-08}
30	1	0.9224×10^{-09}	0.3825×10^{-08}	0.1356×10^{-08}	0.4000×10^{-08}
32	1	-0.1302×10^{-08}	0.4120×10^{-08}	-0.2123×10^{-08}	0.4917×10^{-08}
34	1	-0.1409×10^{-08}	0.4356×10^{-09}	-0.1342×10^{-08}	0.3466×10^{-09}
36	1	0.2026×10^{-08}	0.2300×10^{-08}	0.2431×10^{-08}	0.3313×10^{-08}
38	1	0.4043×10^{-08}	0.1863×10^{-08}	0.4255×10^{-08}	0.2295×10^{-08}
40	1	0.6782×10^{-09}	0.1311×10^{-08}	0.6140×10^{-09}	0.6692×10^{-09}
42	1	-0.4086×10^{-08}	0.6461×10^{-09}	-0.4274×10^{-08}	0.1452×10^{-08}
44	1	0.5148×10^{-08}	-0.1039×10^{-08}	0.5799×10^{-08}	-0.1478×10^{-08}
46	1	0.7982×10^{-09}	0.1198×10^{-08}	-0.1142×10^{-09}	0.1749×10^{-08}
48	1	0.3715×10^{-09}	-0.6214×10^{-09}	0.1079×10^{-08}	-0.3868×10^{-09}
50	1	0.1521×10^{-08}	-0.2816×10^{-08}	0.1295×10^{-08}	-0.2786×10^{-08}
52	1	-0.1021×10^{-09}	-0.2293×10^{-08}	-0.2642×10^{-09}	-0.3123×10^{-08}
54	1	-0.2173×10^{-08}	0.3152×10^{-08}	-0.2520×10^{-08}	0.3036×10^{-08}
56	1	0.1907×10^{-08}	0.3869×10^{-08}	0.2692×10^{-08}	0.3798×10^{-08}
58	1	0.1050×10^{-08}	-0.4803×10^{-09}	0.4218×10^{-09}	-0.2446×10^{-09}
60	1	-0.2743×10^{-09}	-0.2411×10^{-09}	0.3801×10^{-09}	-0.7171×10^{-11}

Table 4: Recovered Coefficients for Block $m = 1$, $|l|_2 = 0$

		estimate		truth	
l	m	C_{lm}	S_{lm}	C_{lm}	S_{lm}
3	1	0.1533×10^{-05}	0.5114×10^{-06}	0.2029×10^{-05}	0.2493×10^{-06}
5	1	-0.5652×10^{-07}	-0.5324×10^{-07}	-0.5191×10^{-07}	-0.1032×10^{-06}
7	1	0.2333×10^{-06}	0.8872×10^{-07}	0.2696×10^{-06}	0.8780×10^{-07}
9	1	0.1497×10^{-06}	0.3023×10^{-07}	0.1652×10^{-06}	0.2544×10^{-07}
11	1	0.3551×10^{-08}	-0.2303×10^{-08}	-0.4969×10^{-09}	-0.3546×10^{-08}
13	1	-0.3275×10^{-07}	0.1891×10^{-07}	-0.3460×10^{-07}	0.2038×10^{-07}
15	1	0.9368×10^{-08}	0.1150×10^{-08}	0.1013×10^{-07}	-0.1564×10^{-09}
17	1	-0.2890×10^{-07}	-0.1663×10^{-07}	-0.3198×10^{-07}	-0.1995×10^{-07}
19	1	-0.1785×10^{-07}	0.4028×10^{-08}	-0.1839×10^{-07}	0.4721×10^{-08}
21	1	-0.1643×10^{-07}	0.2230×10^{-07}	-0.1717×10^{-07}	0.2369×10^{-07}
23	1	0.5693×10^{-08}	0.2124×10^{-07}	0.5657×10^{-08}	0.2192×10^{-07}
25	1	-0.1692×10^{-08}	-0.1142×10^{-08}	-0.1478×10^{-08}	-0.1733×10^{-08}
27	1	0.3783×10^{-09}	-0.4727×10^{-08}	0.4540×10^{-09}	-0.4560×10^{-08}
29	1	-0.1739×10^{-08}	-0.2564×10^{-08}	-0.1741×10^{-08}	-0.3093×10^{-08}
31	1	0.8449×10^{-08}	-0.7747×10^{-08}	0.8799×10^{-08}	-0.8503×10^{-08}
33	1	-0.2872×10^{-08}	-0.2495×10^{-08}	-0.2939×10^{-08}	-0.3018×10^{-08}
35	1	-0.3241×10^{-08}	-0.1036×10^{-07}	-0.3242×10^{-08}	-0.1101×10^{-07}
37	1	0.5872×10^{-09}	-0.1581×10^{-08}	0.5488×10^{-09}	-0.1970×10^{-08}
39	1	0.1054×10^{-08}	0.4739×10^{-08}	0.7538×10^{-09}	0.4863×10^{-08}
41	1	-0.1244×10^{-08}	-0.6224×10^{-08}	-0.1540×10^{-08}	-0.6808×10^{-08}
43	1	-0.5495×10^{-09}	0.1426×10^{-08}	0.1653×10^{-10}	0.1368×10^{-08}
45	1	0.6479×10^{-08}	-0.4578×10^{-08}	0.6386×10^{-08}	-0.4770×10^{-08}
47	1	-0.4427×10^{-08}	-0.2029×10^{-08}	-0.4816×10^{-08}	-0.2427×10^{-08}
49	1	0.3104×10^{-08}	0.1926×10^{-09}	0.3324×10^{-08}	0.5027×10^{-10}
51	1	0.1355×10^{-08}	0.5262×10^{-08}	0.1287×10^{-08}	0.5867×10^{-08}
53	1	-0.1829×10^{-09}	0.3123×10^{-08}	-0.2536×10^{-09}	0.3811×10^{-08}
55	1	-0.3162×10^{-08}	0.2393×10^{-08}	-0.3048×10^{-08}	0.2357×10^{-08}
57	1	0.3347×10^{-08}	-0.2054×10^{-08}	0.3466×10^{-08}	-0.2877×10^{-08}
59	1	-0.3589×10^{-08}	-0.9398×10^{-09}	-0.4108×10^{-08}	-0.1050×10^{-08}

Table 5: Recovered Coefficients for Block $m = 1$, $|l|_2 = 1$

		estimate		truth	
l	m	C_{lm}	S_{lm}	C_{lm}	S_{lm}
2	2	0.1872×10^{-05}	-0.8803×10^{-06}	0.2436×10^{-05}	-0.1400×10^{-05}
4	2	0.2783×10^{-06}	0.5191×10^{-06}	0.3501×10^{-06}	0.6602×10^{-06}
6	2	0.4816×10^{-07}	-0.3117×10^{-06}	0.5101×10^{-07}	-0.3617×10^{-06}
8	2	0.9533×10^{-07}	0.6114×10^{-07}	0.9861×10^{-07}	0.6646×10^{-07}
10	2	-0.6886×10^{-07}	-0.5066×10^{-07}	-0.7968×10^{-07}	-0.5588×10^{-07}
12	2	-0.1107×10^{-07}	0.3879×10^{-08}	-0.1426×10^{-07}	0.6699×10^{-08}
14	2	-0.3366×10^{-07}	-0.6479×10^{-08}	-0.3911×10^{-07}	-0.3987×10^{-08}
16	2	-0.1526×10^{-07}	0.3188×10^{-07}	-0.1750×10^{-07}	0.3526×10^{-07}
18	2	-0.5517×10^{-08}	0.1175×10^{-07}	-0.5740×10^{-08}	0.1213×10^{-07}
20	2	0.1344×10^{-07}	0.7026×10^{-08}	0.1247×10^{-07}	0.7729×10^{-08}
22	2	-0.8773×10^{-08}	-0.1057×10^{-07}	-0.1036×10^{-07}	-0.1124×10^{-07}
24	2	0.1625×10^{-08}	0.1223×10^{-07}	0.1379×10^{-08}	0.1386×10^{-07}
26	2	-0.5094×10^{-08}	0.1153×10^{-07}	-0.6698×10^{-08}	0.1189×10^{-07}
28	2	-0.1322×10^{-07}	-0.9856×10^{-08}	-0.1452×10^{-07}	-0.1033×10^{-07}
30	2	-0.1211×10^{-07}	0.2679×10^{-09}	-0.1307×10^{-07}	0.6876×10^{-09}
32	2	0.4168×10^{-08}	-0.3034×10^{-08}	0.3524×10^{-08}	-0.3278×10^{-08}
34	2	0.7397×10^{-09}	0.1307×10^{-08}	0.3590×10^{-09}	0.1509×10^{-08}
36	2	-0.7337×10^{-08}	-0.4118×10^{-09}	-0.7192×10^{-08}	-0.8300×10^{-09}
38	2	0.6144×10^{-08}	0.2582×10^{-08}	0.6316×10^{-08}	0.4104×10^{-08}
40	2	-0.3477×10^{-08}	0.3275×10^{-08}	-0.4274×10^{-08}	0.2938×10^{-08}
42	2	-0.2654×10^{-08}	-0.2853×10^{-08}	-0.3842×10^{-08}	-0.3374×10^{-08}
44	2	0.8150×10^{-09}	0.4283×10^{-08}	0.1645×10^{-08}	0.4861×10^{-08}
46	2	0.6489×10^{-08}	0.2263×10^{-08}	0.7099×10^{-08}	0.2783×10^{-08}
48	2	0.6447×10^{-08}	0.1009×10^{-08}	0.6258×10^{-08}	0.1205×10^{-08}
50	2	-0.4983×10^{-08}	-0.5469×10^{-08}	-0.6227×10^{-08}	-0.6425×10^{-08}
52	2	0.1358×10^{-08}	-0.1646×10^{-08}	0.2101×10^{-08}	-0.1145×10^{-08}
54	2	-0.3422×10^{-09}	-0.9696×10^{-10}	-0.1451×10^{-08}	-0.2208×10^{-09}
56	2	-0.4565×10^{-08}	0.2627×10^{-08}	-0.5034×10^{-08}	0.3383×10^{-08}
58	2	0.5005×10^{-09}	0.2964×10^{-08}	0.8286×10^{-09}	0.3406×10^{-08}
60	2	0.3091×10^{-08}	-0.1886×10^{-08}	0.2667×10^{-08}	-0.2332×10^{-08}

Table 6: Recovered Coefficients for Block $m = 2$, $|l|_2 = 0$

		estimate		truth	
l	m	C_{lm}	S_{lm}	C_{lm}	S_{lm}
3	2	0.8017×10^{-06}	-0.1662×10^{-06}	0.9027×10^{-06}	-0.6153×10^{-06}
5	2	0.4713×10^{-06}	-0.6898×10^{-07}	0.6420×10^{-06}	-0.3293×10^{-06}
7	2	0.2683×10^{-06}	0.2325×10^{-06}	0.3664×10^{-06}	0.1151×10^{-06}
9	2	-0.3634×10^{-08}	0.7449×10^{-07}	0.3687×10^{-07}	-0.3407×10^{-07}
11	2	-0.1816×10^{-07}	-0.1124×10^{-07}	0.1644×10^{-07}	-0.1000×10^{-06}
13	2	0.2794×10^{-08}	-0.5879×10^{-08}	0.3141×10^{-07}	-0.7884×10^{-07}
15	2	-0.3252×10^{-07}	0.4657×10^{-07}	-0.9468×10^{-08}	-0.1029×10^{-07}
17	2	-0.4000×10^{-07}	0.6687×10^{-07}	-0.2073×10^{-07}	0.1717×10^{-07}
19	2	0.1326×10^{-08}	0.4616×10^{-07}	0.2100×10^{-07}	0.1465×10^{-08}
21	2	-0.1196×10^{-07}	0.4226×10^{-07}	0.3745×10^{-08}	0.1671×10^{-08}
23	2	-0.1576×10^{-07}	0.2733×10^{-07}	-0.3115×10^{-09}	-0.9216×10^{-08}
25	2	-0.1129×10^{-08}	0.4263×10^{-07}	0.1332×10^{-07}	0.8387×10^{-08}
27	2	-0.1168×10^{-07}	0.3314×10^{-07}	0.1510×10^{-08}	0.1559×10^{-09}
29	2	-0.1302×10^{-07}	0.2850×10^{-07}	-0.6303×10^{-10}	-0.1084×10^{-08}
31	2	-0.7414×10^{-08}	0.3154×10^{-07}	0.5693×10^{-08}	0.2865×10^{-08}
33	2	-0.1391×10^{-07}	0.2816×10^{-07}	-0.3023×10^{-08}	0.1033×10^{-08}
35	2	-0.2122×10^{-07}	0.2803×10^{-07}	-0.1125×10^{-07}	0.1704×10^{-08}
37	2	-0.1022×10^{-07}	0.1478×10^{-07}	0.1144×10^{-08}	-0.1125×10^{-07}
39	2	-0.6168×10^{-08}	0.3219×10^{-07}	0.3519×10^{-08}	0.7746×10^{-08}
41	2	-0.7113×10^{-08}	0.2675×10^{-07}	0.3365×10^{-08}	0.2446×10^{-08}
43	2	-0.2024×10^{-07}	0.2083×10^{-07}	-0.1085×10^{-07}	-0.2325×10^{-08}
45	2	-0.1174×10^{-07}	0.2107×10^{-07}	-0.2293×10^{-08}	-0.2528×10^{-08}
47	2	-0.4169×10^{-08}	0.2402×10^{-07}	0.5032×10^{-08}	0.1200×10^{-08}
49	2	-0.6067×10^{-08}	0.2555×10^{-07}	0.2439×10^{-08}	0.3160×10^{-08}
51	2	-0.1340×10^{-07}	0.1773×10^{-07}	-0.3924×10^{-08}	-0.3983×10^{-08}
53	2	-0.3291×10^{-08}	0.2158×10^{-07}	0.6056×10^{-08}	-0.2101×10^{-10}
55	2	-0.1085×10^{-07}	0.1830×10^{-07}	-0.2157×10^{-08}	-0.3524×10^{-08}
57	2	-0.1125×10^{-07}	0.2149×10^{-07}	-0.1878×10^{-08}	-0.3267×10^{-09}
59	2	-0.5292×10^{-08}	0.2250×10^{-07}	0.4060×10^{-08}	0.5905×10^{-09}

Table 7: Recovered Coefficients for Block $m = 2$, $|l|_2 = 1$

		estimate		truth	
l	m	C_{lm}	S_{lm}	C_{lm}	S_{lm}
4	3	0.1533×10^{-06}	0.4716×10^{-07}	0.9942×10^{-06}	-0.2022×10^{-06}
6	3	-0.1983×10^{-06}	0.9548×10^{-07}	0.5620×10^{-07}	0.1750×10^{-08}
8	3	-0.1347×10^{-06}	-0.5858×10^{-08}	-0.1624×10^{-07}	-0.6824×10^{-07}
10	3	-0.9960×10^{-07}	-0.9940×10^{-07}	-0.2184×10^{-07}	-0.1500×10^{-06}
12	3	0.7885×10^{-09}	0.4635×10^{-07}	0.5914×10^{-07}	0.2832×10^{-07}
14	3	0.4717×10^{-08}	0.1526×10^{-07}	0.4714×10^{-07}	-0.4331×10^{-08}
16	3	-0.5001×10^{-07}	-0.1725×10^{-08}	-0.2484×10^{-07}	-0.1647×10^{-07}
18	3	-0.2268×10^{-07}	0.4357×10^{-08}	-0.6219×10^{-09}	-0.6738×10^{-08}
20	3	-0.2409×10^{-07}	0.2070×10^{-07}	-0.5467×10^{-08}	0.1412×10^{-07}
22	3	-0.6422×10^{-08}	0.1650×10^{-07}	0.8121×10^{-08}	0.9310×10^{-08}
24	3	-0.1897×10^{-07}	0.5718×10^{-08}	-0.6055×10^{-08}	0.7817×10^{-09}
26	3	-0.9953×10^{-08}	0.8732×10^{-08}	0.2038×10^{-08}	0.3983×10^{-08}
28	3	-0.9259×10^{-08}	0.1307×10^{-07}	0.2488×10^{-09}	0.9066×10^{-08}
30	3	-0.9180×10^{-08}	-0.1011×10^{-07}	-0.8652×10^{-09}	-0.1456×10^{-07}
32	3	-0.1255×10^{-07}	0.5310×10^{-08}	-0.5179×10^{-08}	0.2764×10^{-08}
34	3	0.4211×10^{-08}	0.9458×10^{-08}	0.1227×10^{-07}	0.6631×10^{-08}
36	3	-0.4421×10^{-08}	-0.6014×10^{-08}	0.1311×10^{-08}	-0.9415×10^{-08}
38	3	-0.1700×10^{-08}	0.3068×10^{-08}	0.4206×10^{-08}	0.7150×10^{-09}
40	3	-0.5889×10^{-08}	0.3516×10^{-08}	-0.4008×10^{-09}	0.7041×10^{-09}
42	3	-0.3014×10^{-08}	0.1044×10^{-07}	0.1826×10^{-08}	0.8389×10^{-08}
44	3	-0.7043×10^{-10}	-0.6512×10^{-08}	0.4865×10^{-08}	-0.9264×10^{-08}
46	3	-0.5420×10^{-08}	0.1444×10^{-08}	-0.9530×10^{-09}	0.1723×10^{-09}
48	3	-0.4603×10^{-08}	0.7096×10^{-09}	-0.7420×10^{-09}	-0.1397×10^{-08}
50	3	-0.4063×10^{-08}	0.2287×10^{-08}	-0.9008×10^{-10}	-0.6754×10^{-10}
52	3	-0.2204×10^{-08}	-0.1738×10^{-08}	0.2020×10^{-08}	-0.2870×10^{-08}
54	3	-0.3967×10^{-09}	0.3214×10^{-08}	0.4001×10^{-08}	0.1551×10^{-08}
56	3	-0.5718×10^{-08}	0.3769×10^{-08}	-0.3507×10^{-08}	0.2631×10^{-08}
58	3	-0.6050×10^{-08}	-0.2390×10^{-08}	-0.2602×10^{-08}	-0.5124×10^{-08}
60	3	0.4281×10^{-09}	0.1946×10^{-08}	0.3904×10^{-08}	0.1673×10^{-08}

Table 8: Recovered Coefficients for Block $m = 3$, $|l|_2 = 0$

		estimate		truth	
l	m	C_{lm}	S_{lm}	C_{lm}	S_{lm}
3	3	0.6979×10^{-06}	0.1167×10^{-05}	0.7186×10^{-06}	0.1417×10^{-05}
5	3	-0.2431×10^{-06}	-0.4817×10^{-07}	-0.4561×10^{-06}	-0.2175×10^{-06}
7	3	0.2714×10^{-06}	-0.1019×10^{-06}	0.2413×10^{-06}	-0.2066×10^{-06}
9	3	-0.1122×10^{-06}	0.1455×10^{-08}	-0.1696×10^{-06}	-0.4890×10^{-07}
11	3	-0.2274×10^{-07}	-0.8263×10^{-07}	-0.5211×10^{-07}	-0.1181×10^{-06}
13	3	-0.5361×10^{-08}	0.8903×10^{-07}	-0.2617×10^{-07}	0.7483×10^{-07}
15	3	0.5755×10^{-07}	0.3770×10^{-07}	0.4578×10^{-07}	0.2490×10^{-07}
17	3	0.1247×10^{-07}	0.1914×10^{-07}	0.3229×10^{-08}	0.9191×10^{-08}
19	3	-0.3787×10^{-08}	-0.2998×10^{-08}	-0.1299×10^{-07}	-0.1209×10^{-07}
21	3	0.2096×10^{-07}	0.2011×10^{-07}	0.1550×10^{-07}	0.1320×10^{-07}
23	3	-0.7860×10^{-08}	-0.7228×10^{-08}	-0.1499×10^{-07}	-0.1462×10^{-07}
25	3	-0.8604×10^{-08}	0.5417×10^{-08}	-0.1387×10^{-07}	0.3318×10^{-09}
27	3	0.6637×10^{-08}	0.6051×10^{-08}	0.2441×10^{-08}	0.1593×10^{-08}
29	3	0.4905×10^{-08}	-0.1179×10^{-08}	0.1166×10^{-08}	-0.6380×10^{-08}
31	3	0.4518×10^{-09}	-0.5663×10^{-08}	-0.3106×10^{-08}	-0.8561×10^{-08}
33	3	-0.1281×10^{-08}	0.5220×10^{-08}	-0.3819×10^{-08}	0.2197×10^{-08}
35	3	0.9278×10^{-08}	0.3788×10^{-08}	0.6000×10^{-08}	0.1159×10^{-09}
37	3	0.2585×10^{-08}	0.2392×10^{-08}	0.8462×10^{-10}	0.5645×10^{-09}
39	3	0.5326×10^{-09}	0.8049×10^{-08}	-0.2278×10^{-08}	0.5925×10^{-08}
41	3	0.3345×10^{-08}	0.6215×10^{-08}	0.1445×10^{-08}	0.4432×10^{-08}
43	3	0.1228×10^{-08}	0.1442×10^{-08}	-0.8106×10^{-09}	-0.1860×10^{-08}
45	3	0.2292×10^{-09}	-0.3070×10^{-08}	-0.2299×10^{-08}	-0.4414×10^{-08}
47	3	0.2280×10^{-08}	0.4549×10^{-08}	0.7248×10^{-09}	0.2860×10^{-08}
49	3	-0.9555×10^{-09}	0.5253×10^{-08}	-0.2684×10^{-08}	0.4022×10^{-08}
51	3	-0.2587×10^{-08}	-0.3772×10^{-08}	-0.4379×10^{-08}	-0.6072×10^{-08}
53	3	-0.7821×10^{-09}	0.3073×10^{-08}	-0.2601×10^{-08}	0.2135×10^{-08}
55	3	0.6751×10^{-08}	0.2234×10^{-08}	0.5257×10^{-08}	0.6296×10^{-09}
57	3	-0.2258×10^{-08}	0.5332×10^{-08}	-0.3694×10^{-08}	0.3792×10^{-08}
59	3	0.1287×10^{-08}	-0.4196×10^{-08}	0.5700×10^{-09}	-0.5525×10^{-08}

Table 9: Recovered Coefficients for Block $m = 3$, $|l|_2 = 1$

		estimate		truth	
l	m	C_{lm}	S_{lm}	C_{lm}	S_{lm}
4	4	-0.1701×10^{-06}	-0.2678×10^{-06}	-0.1923×10^{-06}	0.3056×10^{-06}
6	4	-0.8381×10^{-08}	-0.4253×10^{-06}	-0.9175×10^{-07}	-0.4687×10^{-06}
8	4	-0.1603×10^{-06}	0.5026×10^{-07}	-0.2438×10^{-06}	0.7621×10^{-07}
10	4	-0.5495×10^{-07}	-0.8789×10^{-07}	-0.1013×10^{-06}	-0.9117×10^{-07}
12	4	-0.5193×10^{-07}	-0.7567×10^{-08}	-0.7965×10^{-07}	0.6760×10^{-09}
14	4	0.1721×10^{-07}	-0.2953×10^{-07}	0.3440×10^{-08}	-0.2587×10^{-07}
16	4	0.4307×10^{-07}	0.5396×10^{-07}	0.3724×10^{-07}	0.6272×10^{-07}
18	4	0.3578×10^{-07}	0.7285×10^{-08}	0.3180×10^{-07}	0.1073×10^{-07}
20	4	0.7858×10^{-08}	-0.2046×10^{-07}	0.2339×10^{-08}	-0.1833×10^{-07}
22	4	0.1001×10^{-07}	0.2736×10^{-07}	0.6285×10^{-08}	0.3154×10^{-07}
24	4	0.8392×10^{-08}	0.2735×10^{-08}	0.6034×10^{-08}	0.4618×10^{-08}
26	4	0.1145×10^{-07}	-0.7205×10^{-08}	0.9073×10^{-08}	-0.5606×10^{-08}
28	4	0.4827×10^{-08}	0.3404×10^{-08}	0.2244×10^{-08}	0.4970×10^{-08}
30	4	-0.1563×10^{-08}	-0.3982×10^{-09}	-0.1821×10^{-08}	0.8802×10^{-09}
32	4	0.2723×10^{-08}	-0.1024×10^{-07}	0.3081×10^{-09}	-0.9114×10^{-08}
34	4	-0.8392×10^{-09}	-0.1329×10^{-08}	-0.2465×10^{-08}	-0.2254×10^{-09}
36	4	0.2712×10^{-08}	-0.1896×10^{-08}	0.1652×10^{-08}	-0.1150×10^{-08}
38	4	0.4448×10^{-08}	-0.1371×10^{-08}	0.2565×10^{-08}	-0.5651×10^{-09}
40	4	0.2511×10^{-08}	-0.8719×10^{-08}	0.1973×10^{-08}	-0.7505×10^{-08}
42	4	0.2387×10^{-08}	0.8158×10^{-09}	0.1846×10^{-08}	0.1485×10^{-08}
44	4	0.4612×10^{-08}	-0.8832×10^{-09}	0.3702×10^{-08}	-0.2616×10^{-09}
46	4	0.2954×10^{-08}	-0.6171×10^{-08}	0.1743×10^{-08}	-0.5470×10^{-08}
48	4	-0.7957×10^{-09}	-0.3980×10^{-09}	-0.1717×10^{-08}	0.2607×10^{-09}
50	4	-0.1026×10^{-07}	0.2690×10^{-08}	-0.1191×10^{-07}	0.2552×10^{-08}
52	4	0.3199×10^{-08}	0.1057×10^{-08}	0.2909×10^{-08}	0.1443×10^{-08}
54	4	0.5895×10^{-09}	-0.2972×10^{-08}	-0.6773×10^{-09}	-0.2658×10^{-08}
56	4	0.8456×10^{-09}	0.3098×10^{-08}	-0.8299×10^{-10}	0.3959×10^{-08}
58	4	-0.1509×10^{-08}	-0.2837×10^{-08}	-0.1607×10^{-08}	-0.1826×10^{-08}
60	4	0.7255×10^{-08}	0.1546×10^{-08}	0.7021×10^{-08}	0.2241×10^{-08}

Table 10: Recovered Coefficients for Block $m = 4$, $|l|_2 = 0$

		estimate		truth	
l	m	C_{lm}	S_{lm}	C_{lm}	S_{lm}
5	4	-0.2435×10^{-06}	0.1821×10^{-06}	-0.2899×10^{-06}	0.4979×10^{-07}
7	4	-0.2488×10^{-06}	0.1012×10^{-07}	-0.2721×10^{-06}	-0.1281×10^{-06}
9	4	-0.4188×10^{-07}	0.1279×10^{-06}	-0.1425×10^{-07}	0.3122×10^{-07}
11	4	-0.7311×10^{-07}	-0.1180×10^{-07}	-0.4948×10^{-07}	-0.9853×10^{-07}
13	4	-0.3162×10^{-07}	0.4863×10^{-07}	-0.3766×10^{-08}	-0.1850×10^{-07}
15	4	-0.5069×10^{-07}	0.5675×10^{-07}	-0.2786×10^{-07}	0.3129×10^{-08}
17	4	-0.3419×10^{-07}	0.6640×10^{-07}	-0.1306×10^{-07}	0.1698×10^{-07}
19	4	-0.9324×10^{-08}	0.3870×10^{-07}	0.1146×10^{-07}	-0.5676×10^{-08}
21	4	-0.2108×10^{-07}	0.4319×10^{-07}	-0.1167×10^{-08}	0.5677×10^{-08}
23	4	-0.2917×10^{-07}	0.4405×10^{-07}	-0.1119×10^{-07}	0.6884×10^{-08}
25	4	-0.1704×10^{-07}	0.3248×10^{-07}	0.7004×10^{-09}	-0.1541×10^{-08}
27	4	-0.1946×10^{-07}	0.3490×10^{-07}	-0.3016×10^{-08}	0.4139×10^{-08}
29	4	-0.3953×10^{-07}	0.3034×10^{-07}	-0.2486×10^{-07}	0.3877×10^{-09}
31	4	-0.7787×10^{-08}	0.2302×10^{-07}	0.8584×10^{-08}	-0.5909×10^{-08}
33	4	-0.1676×10^{-07}	0.2725×10^{-07}	-0.1881×10^{-08}	0.8881×10^{-09}
35	4	-0.1634×10^{-07}	0.2751×10^{-07}	-0.1558×10^{-08}	0.1530×10^{-08}
37	4	-0.8961×10^{-08}	0.2379×10^{-07}	0.5658×10^{-08}	-0.1382×10^{-08}
39	4	-0.2107×10^{-07}	0.1652×10^{-07}	-0.7801×10^{-08}	-0.8662×10^{-08}
41	4	-0.1737×10^{-07}	0.2564×10^{-07}	-0.4081×10^{-08}	0.2775×10^{-08}
43	4	-0.1111×10^{-07}	0.2383×10^{-07}	0.2402×10^{-08}	0.3607×10^{-09}
45	4	-0.9467×10^{-08}	0.2036×10^{-07}	0.3647×10^{-08}	-0.2942×10^{-08}
47	4	-0.1293×10^{-07}	0.2511×10^{-07}	-0.1741×10^{-09}	0.3373×10^{-08}
49	4	-0.1374×10^{-07}	0.3068×10^{-07}	-0.1172×10^{-08}	0.9215×10^{-08}
51	4	-0.1406×10^{-07}	0.2433×10^{-07}	0.1636×10^{-09}	0.2250×10^{-08}
53	4	-0.9025×10^{-08}	0.2112×10^{-07}	0.3625×10^{-08}	-0.9974×10^{-09}
55	4	-0.1262×10^{-07}	0.2008×10^{-07}	0.1129×10^{-09}	-0.1052×10^{-08}
57	4	-0.1736×10^{-07}	0.1678×10^{-07}	-0.5386×10^{-08}	-0.5801×10^{-08}
59	4	-0.1013×10^{-07}	0.2140×10^{-07}	0.3325×10^{-08}	0.4438×10^{-09}

Table 11: Recovered Coefficients for Block $m = 4$, $|l|_2 = 1$

		estimate		truth	
l	m	C_{lm}	S_{lm}	C_{lm}	S_{lm}
6	5	0.7037×10^{-07}	0.2277×10^{-07}	-0.2638×10^{-06}	-0.5362×10^{-06}
8	5	0.1283×10^{-06}	0.2931×10^{-06}	-0.1945×10^{-07}	0.8329×10^{-07}
10	5	0.3213×10^{-07}	0.9437×10^{-07}	-0.5876×10^{-07}	-0.4115×10^{-07}
12	5	0.9594×10^{-07}	0.9601×10^{-07}	0.4510×10^{-07}	0.8910×10^{-08}
14	5	0.6149×10^{-07}	0.5106×10^{-07}	0.2296×10^{-07}	-0.1503×10^{-07}
16	5	0.1843×10^{-07}	0.5881×10^{-07}	-0.1170×10^{-07}	0.1217×10^{-07}
18	5	0.2549×10^{-07}	0.4825×10^{-07}	0.3841×10^{-08}	0.1140×10^{-07}
20	5	0.1688×10^{-07}	0.1947×10^{-07}	-0.1798×10^{-08}	-0.1218×10^{-07}
22	5	0.1204×10^{-07}	0.2550×10^{-07}	-0.3324×10^{-08}	0.7321×10^{-09}
24	5	0.8765×10^{-08}	0.1440×10^{-07}	-0.4508×10^{-08}	-0.8155×10^{-08}
26	5	0.1709×10^{-07}	0.2139×10^{-07}	0.7388×10^{-08}	0.3360×10^{-08}
28	5	0.1603×10^{-07}	0.6439×10^{-08}	0.5653×10^{-08}	-0.1096×10^{-07}
30	5	0.8637×10^{-08}	0.6605×10^{-08}	0.3027×10^{-09}	-0.8291×10^{-08}
32	5	0.1024×10^{-07}	0.1300×10^{-07}	0.2999×10^{-08}	0.1008×10^{-09}
34	5	0.4313×10^{-08}	0.1409×10^{-07}	-0.2686×10^{-08}	0.2020×10^{-08}
36	5	0.1648×10^{-08}	0.1025×10^{-07}	-0.4502×10^{-08}	-0.2193×10^{-10}
38	5	-0.1346×10^{-08}	0.1746×10^{-07}	-0.6771×10^{-08}	0.7745×10^{-08}
40	5	0.1813×10^{-07}	0.6995×10^{-08}	0.1350×10^{-07}	-0.2944×10^{-08}
42	5	-0.5433×10^{-09}	-0.3098×10^{-09}	-0.6914×10^{-08}	-0.9063×10^{-08}
44	5	0.6143×10^{-08}	0.1020×10^{-07}	0.3318×10^{-08}	0.2380×10^{-08}
46	5	0.3217×10^{-09}	0.1520×10^{-08}	-0.4710×10^{-08}	-0.6417×10^{-08}
48	5	0.9098×10^{-08}	0.6334×10^{-08}	0.5787×10^{-08}	-0.2737×10^{-09}
50	5	0.2553×10^{-08}	0.7030×10^{-08}	-0.1680×10^{-08}	0.3931×10^{-09}
52	5	0.3543×10^{-08}	0.3762×10^{-08}	0.3971×10^{-09}	-0.2573×10^{-08}
54	5	0.4490×10^{-08}	0.3051×10^{-08}	0.1503×10^{-08}	-0.2284×10^{-08}
56	5	0.5396×10^{-08}	0.5867×10^{-08}	0.9243×10^{-09}	-0.8275×10^{-09}
58	5	0.5624×10^{-08}	0.2034×10^{-08}	0.3392×10^{-08}	-0.4546×10^{-08}
60	5	0.1537×10^{-08}	0.3130×10^{-08}	-0.2046×10^{-08}	-0.2401×10^{-08}

Table 12: Recovered Coefficients for Block $m = 5$, $|l|_2 = 0$

		estimate		truth	
l	m	C_{lm}	S_{lm}	C_{lm}	S_{lm}
5	5	0.5127×10^{-06}	-0.2042×10^{-06}	0.1733×10^{-06}	-0.6610×10^{-06}
7	5	0.1429×10^{-06}	0.3982×10^{-07}	0.1253×10^{-07}	0.1899×10^{-07}
9	5	0.4263×10^{-07}	-0.3675×10^{-07}	-0.2726×10^{-07}	-0.3387×10^{-07}
11	5	0.7550×10^{-07}	0.1392×10^{-07}	0.4477×10^{-07}	0.3494×10^{-07}
13	5	0.8485×10^{-07}	0.5233×10^{-07}	0.6588×10^{-07}	0.7450×10^{-07}
15	5	0.2214×10^{-07}	-0.8543×10^{-08}	0.4212×10^{-08}	0.6387×10^{-08}
17	5	-0.1935×10^{-08}	-0.3321×10^{-08}	-0.1595×10^{-07}	0.8627×10^{-08}
19	5	0.1755×10^{-07}	-0.1232×10^{-08}	0.7192×10^{-08}	0.8381×10^{-08}
21	5	0.1159×10^{-07}	-0.1488×10^{-07}	0.3017×10^{-08}	-0.6414×10^{-08}
23	5	0.8889×10^{-08}	0.1707×10^{-08}	0.1813×10^{-08}	0.9295×10^{-08}
25	5	-0.1498×10^{-08}	-0.9356×10^{-08}	-0.7896×10^{-08}	-0.2705×10^{-08}
27	5	0.2195×10^{-07}	0.3084×10^{-08}	0.1721×10^{-07}	0.8708×10^{-08}
29	5	0.3268×10^{-08}	-0.4251×10^{-08}	-0.2056×10^{-08}	0.1310×10^{-08}
31	5	0.2946×10^{-08}	-0.3015×10^{-08}	-0.1341×10^{-08}	0.2176×10^{-08}
33	5	0.3800×10^{-08}	0.1326×10^{-08}	-0.3341×10^{-09}	0.5819×10^{-08}
35	5	-0.7749×10^{-09}	-0.6035×10^{-08}	-0.4412×10^{-08}	-0.2658×10^{-08}
37	5	-0.2644×10^{-08}	0.3774×10^{-08}	-0.6016×10^{-08}	0.7904×10^{-08}
39	5	0.7722×10^{-08}	0.4435×10^{-08}	0.6153×10^{-08}	0.7278×10^{-08}
41	5	0.9249×10^{-08}	-0.4225×10^{-08}	0.5486×10^{-08}	-0.1461×10^{-08}
43	5	-0.9821×10^{-08}	-0.1264×10^{-08}	-0.1252×10^{-07}	0.2722×10^{-08}
45	5	0.5496×10^{-08}	-0.2271×10^{-08}	0.2959×10^{-08}	-0.1212×10^{-09}
47	5	0.2656×10^{-09}	-0.5855×10^{-08}	-0.1436×10^{-08}	-0.2918×10^{-08}
49	5	0.3687×10^{-08}	-0.2094×10^{-08}	0.9998×10^{-09}	0.3621×10^{-09}
51	5	-0.1589×10^{-08}	-0.4131×10^{-08}	-0.3731×10^{-08}	-0.2189×10^{-08}
53	5	0.1896×10^{-08}	-0.5368×10^{-08}	-0.9796×10^{-10}	-0.3444×10^{-08}
55	5	0.9494×10^{-08}	0.6484×10^{-08}	0.8351×10^{-08}	0.9581×10^{-08}
57	5	-0.1994×10^{-08}	0.3272×10^{-08}	-0.4272×10^{-08}	0.5538×10^{-08}
59	5	0.3510×10^{-08}	-0.1428×10^{-08}	0.1513×10^{-08}	0.9107×10^{-09}

Table 13: Recovered Coefficients for Block $m = 5$, $|l|_2 = 1$

		estimate		truth	
l	m	C_{lm}	S_{lm}	C_{lm}	S_{lm}
6	6	0.1750×10^{-06}	-0.7622×10^{-07}	0.6872×10^{-08}	-0.2371×10^{-06}
8	6	0.2833×10^{-07}	0.2032×10^{-06}	-0.6642×10^{-07}	0.3110×10^{-06}
10	6	0.1275×10^{-07}	-0.1049×10^{-06}	-0.4372×10^{-07}	-0.8351×10^{-07}
12	6	0.3468×10^{-07}	0.1090×10^{-07}	0.5968×10^{-08}	0.3544×10^{-07}
14	6	0.5246×10^{-08}	-0.1000×10^{-07}	-0.1341×10^{-07}	0.4073×10^{-08}
16	6	0.1428×10^{-07}	-0.5287×10^{-07}	0.1137×10^{-08}	-0.4556×10^{-07}
18	6	0.2102×10^{-07}	-0.2510×10^{-07}	0.1421×10^{-07}	-0.1700×10^{-07}
20	6	0.1826×10^{-07}	-0.6249×10^{-08}	0.1317×10^{-07}	-0.9172×10^{-09}
22	6	0.1649×10^{-07}	-0.7016×10^{-08}	0.1266×10^{-07}	-0.1379×10^{-08}
24	6	0.4380×10^{-08}	-0.3599×10^{-08}	0.1400×10^{-08}	0.4751×10^{-11}
26	6	0.1172×10^{-07}	-0.7606×10^{-08}	0.8964×10^{-08}	-0.3752×10^{-08}
28	6	0.6150×10^{-08}	0.1314×10^{-08}	0.3591×10^{-08}	0.5057×10^{-08}
30	6	0.5871×10^{-08}	0.2581×10^{-08}	0.3355×10^{-08}	0.6076×10^{-08}
32	6	0.1741×10^{-08}	-0.7688×10^{-08}	-0.1762×10^{-09}	-0.5283×10^{-08}
34	6	0.6993×10^{-08}	0.4661×10^{-08}	0.5561×10^{-08}	0.8176×10^{-08}
36	6	0.1488×10^{-07}	-0.3454×10^{-08}	0.1383×10^{-07}	-0.1517×10^{-08}
38	6	-0.1142×10^{-07}	0.1617×10^{-08}	-0.1371×10^{-07}	0.3657×10^{-08}
40	6	-0.5647×10^{-09}	0.1129×10^{-08}	-0.1484×10^{-08}	0.3410×10^{-08}
42	6	0.3408×10^{-08}	-0.4757×10^{-08}	0.2664×10^{-08}	-0.3197×10^{-08}
44	6	-0.5248×10^{-08}	0.3955×10^{-09}	-0.7911×10^{-08}	0.2485×10^{-08}
46	6	-0.3829×10^{-08}	-0.3263×10^{-08}	-0.4882×10^{-08}	-0.1506×10^{-08}
48	6	0.5185×10^{-08}	0.3618×10^{-08}	0.4229×10^{-08}	0.5803×10^{-08}
50	6	0.1357×10^{-08}	-0.1899×10^{-09}	0.4259×10^{-09}	0.1113×10^{-08}
52	6	-0.4011×10^{-08}	-0.3468×10^{-08}	-0.5492×10^{-08}	-0.1997×10^{-08}
54	6	0.4193×10^{-08}	-0.3914×10^{-08}	0.3399×10^{-08}	-0.2739×10^{-08}
56	6	-0.4150×10^{-08}	-0.5174×10^{-09}	-0.5610×10^{-08}	0.9118×10^{-09}
58	6	0.9002×10^{-10}	-0.1372×10^{-08}	-0.1102×10^{-08}	-0.2030×10^{-10}
60	6	-0.4797×10^{-08}	-0.1699×10^{-08}	-0.5000×10^{-08}	-0.3095×10^{-09}

Table 14: Recovered Coefficients for Block $m = 6$, $|l|_2 = 0$

		estimate		truth	
l	m	C_{lm}	S_{lm}	C_{lm}	S_{lm}
7	6	-0.1294×10^{-06}	0.2017×10^{-06}	-0.3607×10^{-06}	0.1518×10^{-06}
9	6	0.9954×10^{-07}	0.2821×10^{-06}	0.5770×10^{-07}	0.2106×10^{-06}
11	6	0.7660×10^{-08}	0.1356×10^{-06}	-0.9824×10^{-08}	0.3571×10^{-07}
13	6	-0.1714×10^{-07}	0.1070×10^{-06}	-0.2349×10^{-07}	0.2598×10^{-08}
15	6	0.1979×10^{-07}	0.6086×10^{-07}	0.2448×10^{-07}	-0.4019×10^{-07}
17	6	-0.2125×10^{-07}	0.5479×10^{-07}	-0.1682×10^{-07}	-0.3550×10^{-07}
19	6	-0.1073×10^{-07}	0.1011×10^{-06}	-0.3979×10^{-08}	0.2140×10^{-07}
21	6	-0.1110×10^{-07}	0.7648×10^{-07}	-0.3420×10^{-08}	0.7638×10^{-09}
23	6	-0.1717×10^{-07}	0.9139×10^{-07}	-0.9506×10^{-08}	0.2215×10^{-07}
25	6	-0.2945×10^{-08}	0.6887×10^{-07}	0.6582×10^{-08}	0.2377×10^{-08}
27	6	-0.3388×10^{-08}	0.6699×10^{-07}	0.5548×10^{-08}	0.4585×10^{-08}
29	6	-0.2295×10^{-08}	0.6364×10^{-07}	0.7066×10^{-08}	0.3580×10^{-08}
31	6	-0.1018×10^{-07}	0.6043×10^{-07}	-0.1459×10^{-08}	0.2522×10^{-08}
33	6	-0.9110×10^{-08}	0.5340×10^{-07}	-0.1414×10^{-11}	-0.1530×10^{-08}
35	6	-0.5891×10^{-08}	0.6033×10^{-07}	0.3154×10^{-08}	0.6401×10^{-08}
37	6	-0.9655×10^{-08}	0.5766×10^{-07}	-0.2523×10^{-08}	0.6194×10^{-08}
39	6	-0.1432×10^{-07}	0.5178×10^{-07}	-0.4754×10^{-08}	0.8801×10^{-09}
41	6	-0.8327×10^{-08}	0.5094×10^{-07}	0.5032×10^{-09}	0.1017×10^{-08}
43	6	0.5052×10^{-09}	0.4719×10^{-07}	0.9180×10^{-08}	-0.1126×10^{-08}
45	6	-0.1122×10^{-07}	0.4578×10^{-07}	-0.2392×10^{-08}	-0.2470×10^{-08}
47	6	-0.6049×10^{-08}	0.4613×10^{-07}	0.3306×10^{-08}	-0.7040×10^{-09}
49	6	-0.7116×10^{-08}	0.4899×10^{-07}	0.8487×10^{-09}	0.2003×10^{-08}
51	6	-0.6354×10^{-08}	0.4504×10^{-07}	0.1865×10^{-08}	-0.1430×10^{-08}
53	6	-0.5773×10^{-08}	0.4538×10^{-07}	0.3644×10^{-08}	-0.2797×10^{-09}
55	6	-0.6518×10^{-08}	0.4507×10^{-07}	0.1263×10^{-08}	-0.5922×10^{-10}
57	6	-0.7728×10^{-08}	0.4444×10^{-07}	0.1513×10^{-08}	-0.1098×10^{-08}
59	6	-0.1423×10^{-07}	0.4395×10^{-07}	-0.6645×10^{-08}	-0.1370×10^{-08}

Table 15: Recovered Coefficients for Block $m = 6$, $|l|_2 = 1$

		estimate		truth	
l	m	C_{lm}	S_{lm}	C_{lm}	S_{lm}
8	7	-0.5801×10^{-07}	-0.6969×10^{-07}	0.6962×10^{-07}	0.7323×10^{-07}
10	7	-0.5507×10^{-07}	-0.8564×10^{-07}	0.2090×10^{-07}	-0.2644×10^{-08}
12	7	-0.6541×10^{-07}	-0.3413×10^{-07}	-0.2024×10^{-07}	0.2704×10^{-07}
14	7	-0.9888×10^{-08}	-0.4046×10^{-07}	0.2767×10^{-07}	0.1725×10^{-09}
16	7	-0.3292×10^{-07}	-0.4382×10^{-07}	-0.9166×10^{-08}	-0.1529×10^{-07}
18	7	-0.1201×10^{-07}	-0.2220×10^{-07}	0.7629×10^{-08}	0.2093×10^{-08}
20	7	-0.2827×10^{-07}	-0.1905×10^{-07}	-0.1340×10^{-07}	0.6783×10^{-09}
22	7	-0.6457×10^{-08}	-0.1075×10^{-07}	0.7758×10^{-08}	0.5242×10^{-08}
24	7	-0.1349×10^{-07}	-0.9185×10^{-08}	-0.2038×10^{-08}	0.4077×10^{-08}
26	7	-0.1199×10^{-07}	-0.1719×10^{-07}	-0.2803×10^{-08}	-0.5208×10^{-08}
28	7	-0.9597×10^{-08}	-0.7304×10^{-08}	-0.6703×10^{-09}	0.2921×10^{-08}
30	7	-0.7250×10^{-09}	-0.8703×10^{-08}	0.7415×10^{-08}	0.6068×10^{-09}
32	7	-0.8996×10^{-08}	-0.7833×10^{-08}	-0.2750×10^{-08}	0.2504×10^{-09}
34	7	-0.6862×10^{-08}	-0.8441×10^{-08}	-0.3106×10^{-09}	-0.1337×10^{-08}
36	7	-0.6353×10^{-08}	-0.1048×10^{-08}	-0.4350×10^{-09}	0.5864×10^{-08}
38	7	-0.5638×10^{-08}	-0.1354×10^{-07}	-0.1142×10^{-08}	-0.8848×10^{-08}
40	7	-0.6942×10^{-08}	-0.7329×10^{-08}	-0.2567×10^{-08}	-0.1286×10^{-08}
42	7	-0.1611×10^{-08}	-0.1123×10^{-07}	0.2737×10^{-08}	-0.6817×10^{-08}
44	7	0.2337×10^{-08}	0.3946×10^{-08}	0.7088×10^{-08}	0.9518×10^{-08}
46	7	-0.2386×10^{-09}	-0.1580×10^{-07}	0.3778×10^{-08}	-0.1278×10^{-07}
48	7	-0.6055×10^{-08}	-0.4999×10^{-08}	-0.2541×10^{-08}	0.7060×10^{-10}
50	7	-0.6774×10^{-09}	-0.1839×10^{-09}	0.3055×10^{-08}	0.4305×10^{-08}
52	7	-0.6316×10^{-08}	-0.4045×10^{-08}	-0.3350×10^{-08}	-0.1222×10^{-08}
54	7	-0.1410×10^{-08}	-0.6386×10^{-08}	0.1933×10^{-08}	-0.1875×10^{-08}
56	7	-0.1567×10^{-08}	-0.3518×10^{-08}	0.1196×10^{-08}	-0.3526×10^{-09}
58	7	-0.8121×10^{-08}	0.8855×10^{-09}	-0.5674×10^{-08}	0.4590×10^{-08}
60	7	-0.2759×10^{-08}	-0.4326×10^{-08}	0.4289×10^{-09}	-0.1701×10^{-08}

Table 16: Recovered Coefficients for Block $m = 7$, $|l|_2 = 0$

		estimate		truth	
l	m	C_{lm}	S_{lm}	C_{lm}	S_{lm}
7	7	0.3174×10^{-06}	-0.1031×10^{-07}	0.5054×10^{-08}	0.2149×10^{-07}
9	7	0.6037×10^{-07}	-0.3307×10^{-07}	-0.1028×10^{-06}	-0.1003×10^{-06}
11	7	0.9204×10^{-07}	-0.3849×10^{-07}	0.1774×10^{-07}	-0.9378×10^{-07}
13	7	0.4081×10^{-07}	0.1979×10^{-07}	-0.2396×10^{-08}	-0.1288×10^{-07}
15	7	0.7950×10^{-07}	0.3236×10^{-07}	0.5528×10^{-07}	0.1095×10^{-07}
17	7	0.4959×10^{-07}	0.4568×10^{-08}	0.3206×10^{-07}	-0.1247×10^{-07}
19	7	0.2330×10^{-07}	0.8919×10^{-08}	0.7307×10^{-08}	-0.4410×10^{-08}
21	7	0.5310×10^{-08}	0.1941×10^{-07}	-0.7609×10^{-08}	0.9642×10^{-08}
23	7	0.8454×10^{-08}	0.1487×10^{-07}	-0.3268×10^{-08}	0.6396×10^{-08}
25	7	0.1312×10^{-07}	-0.3381×10^{-08}	0.3819×10^{-08}	-0.1182×10^{-07}
27	7	0.4428×10^{-09}	0.5157×10^{-08}	-0.8214×10^{-08}	-0.8199×10^{-09}
29	7	0.5419×10^{-08}	-0.2392×10^{-09}	-0.1806×10^{-08}	-0.6346×10^{-08}
31	7	0.8683×10^{-08}	0.3587×10^{-08}	0.1717×10^{-08}	-0.1433×10^{-08}
33	7	-0.1024×10^{-08}	0.4270×10^{-08}	-0.7097×10^{-08}	-0.1650×10^{-09}
35	7	0.3182×10^{-08}	0.5859×10^{-08}	-0.2234×10^{-08}	0.2247×10^{-08}
37	7	0.1084×10^{-07}	0.1032×10^{-07}	0.6409×10^{-08}	0.6383×10^{-08}
39	7	0.6102×10^{-08}	-0.2286×10^{-08}	0.1708×10^{-08}	-0.5238×10^{-08}
41	7	0.4090×10^{-08}	0.4649×10^{-08}	0.3510×10^{-09}	0.1675×10^{-08}
43	7	0.1473×10^{-08}	0.2375×10^{-08}	-0.2575×10^{-08}	0.5244×10^{-09}
45	7	0.3355×10^{-08}	0.5511×10^{-08}	-0.8100×10^{-09}	0.1684×10^{-08}
47	7	0.2207×10^{-08}	-0.5454×10^{-08}	-0.1802×10^{-08}	-0.7127×10^{-08}
49	7	0.2491×10^{-08}	0.2323×10^{-08}	-0.2902×10^{-09}	0.2029×10^{-09}
51	7	0.3007×10^{-08}	0.6889×10^{-08}	-0.5111×10^{-09}	0.4632×10^{-08}
53	7	0.2650×10^{-08}	-0.5344×10^{-08}	0.2163×10^{-09}	-0.8169×10^{-08}
55	7	0.5141×10^{-08}	0.3833×10^{-08}	0.2451×10^{-08}	0.2340×10^{-08}
57	7	0.1385×10^{-08}	0.3299×10^{-08}	-0.1808×10^{-08}	0.1690×10^{-08}
59	7	0.2542×10^{-09}	0.5026×10^{-08}	-0.1681×10^{-08}	0.2735×10^{-08}

Table 17: Recovered Coefficients for Block $m = 7$, $|l|_2 = 1$

		estimate		truth	
l	m	C_{lm}	S_{lm}	C_{lm}	S_{lm}
8	8	0.2016×10^{-06}	-0.3392×10^{-06}	-0.1190×10^{-06}	0.1093×10^{-06}
10	8	0.1427×10^{-06}	-0.2123×10^{-06}	0.4874×10^{-07}	-0.7202×10^{-07}
12	8	0.3999×10^{-07}	-0.6142×10^{-07}	-0.1986×10^{-07}	0.2862×10^{-07}
14	8	0.6291×10^{-08}	-0.6646×10^{-07}	-0.3502×10^{-07}	-0.9040×10^{-08}
16	8	-0.1185×10^{-07}	-0.3751×10^{-07}	-0.3917×10^{-07}	0.3830×10^{-08}
18	8	0.5125×10^{-07}	-0.2834×10^{-07}	0.3543×10^{-07}	0.3494×10^{-08}
20	8	0.1794×10^{-07}	-0.1104×10^{-07}	0.4059×10^{-08}	0.1485×10^{-07}
22	8	-0.2004×10^{-07}	-0.1722×10^{-07}	-0.3188×10^{-07}	0.2914×10^{-08}
24	8	0.1932×10^{-07}	-0.2081×10^{-07}	0.1259×10^{-07}	-0.4507×10^{-08}
26	8	0.7610×10^{-08}	-0.1681×10^{-07}	0.9028×10^{-09}	-0.3295×10^{-08}
28	8	0.6911×10^{-08}	-0.1509×10^{-07}	0.1503×10^{-08}	-0.2171×10^{-08}
30	8	0.3667×10^{-08}	0.2371×10^{-09}	0.4713×10^{-10}	0.1067×10^{-07}
32	8	0.1242×10^{-07}	-0.2447×10^{-08}	0.9457×10^{-08}	0.7227×10^{-08}
34	8	-0.7679×10^{-08}	-0.5526×10^{-08}	-0.1150×10^{-07}	0.2212×10^{-08}
36	8	0.3052×10^{-08}	-0.1028×10^{-07}	0.9438×10^{-10}	-0.3564×10^{-08}
38	8	0.5463×10^{-08}	-0.5407×10^{-08}	0.3777×10^{-08}	0.1863×10^{-08}
40	8	0.7907×10^{-08}	-0.2545×10^{-08}	0.5908×10^{-08}	0.2552×10^{-08}
42	8	0.4186×10^{-08}	-0.8110×10^{-08}	0.2908×10^{-08}	-0.2444×10^{-08}
44	8	-0.6108×10^{-08}	-0.5257×10^{-08}	-0.8194×10^{-08}	-0.1681×10^{-09}
46	8	0.5875×10^{-09}	-0.1010×10^{-08}	-0.3281×10^{-09}	0.3699×10^{-08}
48	8	0.3773×10^{-08}	-0.2395×10^{-08}	0.2099×10^{-08}	0.2050×10^{-08}
50	8	-0.3182×10^{-08}	-0.6258×10^{-08}	-0.4874×10^{-08}	-0.2563×10^{-08}
52	8	0.1505×10^{-08}	-0.3795×10^{-08}	0.2233×10^{-09}	-0.3470×10^{-09}
54	8	0.2067×10^{-08}	-0.5294×10^{-08}	0.9532×10^{-09}	-0.1832×10^{-08}
56	8	-0.7950×10^{-09}	-0.9549×10^{-08}	-0.1446×10^{-08}	-0.6491×10^{-08}
58	8	0.2954×10^{-08}	0.1545×10^{-08}	0.2019×10^{-08}	0.4413×10^{-08}
60	8	0.4263×10^{-08}	-0.2996×10^{-08}	0.3292×10^{-08}	0.4599×10^{-10}

Table 18: Recovered Coefficients for Block $m = 8$, $|l|_2 = 0$

		estimate		truth	
l	m	C_{lm}	S_{lm}	C_{lm}	S_{lm}
9	8	0.1354×10^{-06}	0.8727×10^{-07}	0.1945×10^{-06}	0.1198×10^{-08}
11	8	0.5108×10^{-07}	0.1144×10^{-06}	0.2039×10^{-07}	0.4441×10^{-07}
13	8	0.3535×10^{-07}	0.7167×10^{-07}	-0.1550×10^{-07}	-0.1247×10^{-08}
15	8	0.1693×10^{-07}	0.8951×10^{-07}	-0.3655×10^{-07}	0.2511×10^{-07}
17	8	0.7765×10^{-07}	0.6086×10^{-07}	0.3382×10^{-07}	-0.2060×10^{-08}
19	8	0.7431×10^{-07}	0.5934×10^{-07}	0.2951×10^{-07}	0.8912×10^{-09}
21	8	0.4120×10^{-07}	0.5995×10^{-07}	-0.3108×10^{-08}	0.4808×10^{-08}
23	8	0.3925×10^{-07}	0.5055×10^{-07}	-0.4129×10^{-09}	-0.1493×10^{-08}
25	8	0.5047×10^{-07}	0.4850×10^{-07}	0.1091×10^{-07}	-0.3497×10^{-09}
27	8	0.4188×10^{-07}	0.3256×10^{-07}	0.4165×10^{-08}	-0.1484×10^{-07}
29	8	0.2832×10^{-07}	0.5283×10^{-07}	-0.8659×10^{-08}	0.9225×10^{-08}
31	8	0.3586×10^{-07}	0.4371×10^{-07}	0.1069×10^{-08}	0.2498×10^{-09}
33	8	0.3606×10^{-07}	0.4980×10^{-07}	0.1207×10^{-08}	0.8409×10^{-08}
35	8	0.3399×10^{-07}	0.4302×10^{-07}	0.2106×10^{-08}	0.2764×10^{-08}
37	8	0.2682×10^{-07}	0.3519×10^{-07}	-0.5473×10^{-08}	-0.3821×10^{-08}
39	8	0.3203×10^{-07}	0.4737×10^{-07}	0.7851×10^{-09}	0.9794×10^{-08}
41	8	0.2598×10^{-07}	0.3361×10^{-07}	-0.5399×10^{-08}	-0.4456×10^{-08}
43	8	0.2715×10^{-07}	0.3644×10^{-07}	-0.3541×10^{-08}	-0.4985×10^{-10}
45	8	0.2475×10^{-07}	0.3787×10^{-07}	-0.4246×10^{-08}	0.1926×10^{-08}
47	8	0.3319×10^{-07}	0.3689×10^{-07}	0.4612×10^{-08}	0.7766×10^{-09}
49	8	0.2909×10^{-07}	0.3791×10^{-07}	-0.8153×10^{-10}	0.2294×10^{-08}
51	8	0.2861×10^{-07}	0.3775×10^{-07}	0.8215×10^{-09}	0.3070×10^{-08}
53	8	0.2742×10^{-07}	0.3515×10^{-07}	-0.7927×10^{-09}	0.1264×10^{-09}
55	8	0.2413×10^{-07}	0.3447×10^{-07}	-0.4466×10^{-08}	-0.4961×10^{-09}
57	8	0.2902×10^{-07}	0.3960×10^{-07}	0.1596×10^{-08}	0.6478×10^{-08}
59	8	0.2953×10^{-07}	0.3451×10^{-07}	0.1766×10^{-08}	-0.9429×10^{-09}

Table 19: Recovered Coefficients for Block $m = 8$, $|l|_2 = 1$

		estimate		truth	
l	m	C_{lm}	S_{lm}	C_{lm}	S_{lm}
10	9	-0.1531×10^{-06}	-0.3231×10^{-07}	0.1243×10^{-06}	-0.4088×10^{-07}
12	9	-0.1415×10^{-06}	0.1643×10^{-07}	0.3980×10^{-07}	0.3063×10^{-07}
14	9	-0.1058×10^{-06}	0.1591×10^{-07}	0.1821×10^{-07}	0.2687×10^{-07}
16	9	-0.1099×10^{-06}	-0.5081×10^{-07}	-0.2389×10^{-07}	-0.5027×10^{-07}
18	9	-0.8810×10^{-07}	0.1652×10^{-07}	-0.2129×10^{-07}	0.2512×10^{-07}
20	9	-0.4250×10^{-07}	-0.4277×10^{-08}	0.1320×10^{-07}	0.5617×10^{-09}
22	9	-0.4004×10^{-07}	0.8716×10^{-08}	0.4872×10^{-08}	0.1229×10^{-07}
24	9	-0.4846×10^{-07}	-0.2460×10^{-07}	-0.1182×10^{-07}	-0.2214×10^{-07}
26	9	-0.4289×10^{-07}	0.1558×10^{-08}	-0.9284×10^{-08}	0.4153×10^{-08}
28	9	-0.2075×10^{-07}	-0.5122×10^{-08}	0.8193×10^{-08}	-0.4057×10^{-08}
30	9	-0.3196×10^{-07}	-0.5596×10^{-08}	-0.7258×10^{-08}	-0.3901×10^{-08}
32	9	-0.2041×10^{-07}	-0.3481×10^{-08}	0.2354×10^{-08}	-0.1813×10^{-08}
34	9	-0.2003×10^{-07}	-0.8035×10^{-09}	0.4458×10^{-09}	0.8343×10^{-09}
36	9	-0.1757×10^{-07}	-0.1722×10^{-08}	0.1012×10^{-08}	-0.1510×10^{-09}
38	9	-0.1060×10^{-07}	-0.3810×10^{-08}	0.6977×10^{-08}	-0.1801×10^{-08}
40	9	-0.1492×10^{-07}	0.1750×10^{-09}	-0.1622×10^{-09}	0.1263×10^{-08}
42	9	-0.1648×10^{-07}	0.1060×10^{-08}	-0.1354×10^{-08}	0.1937×10^{-08}
44	9	-0.1347×10^{-07}	-0.9001×10^{-08}	0.2005×10^{-09}	-0.7535×10^{-08}
46	9	-0.7349×10^{-08}	-0.5857×10^{-09}	0.5190×10^{-08}	0.1447×10^{-08}
48	9	-0.1586×10^{-07}	0.2641×10^{-08}	-0.3948×10^{-08}	0.3988×10^{-08}
50	9	-0.1370×10^{-07}	0.4798×10^{-09}	-0.2317×10^{-08}	0.9108×10^{-09}
52	9	-0.1316×10^{-07}	-0.4716×10^{-08}	-0.2667×10^{-08}	-0.3721×10^{-08}
54	9	-0.8838×10^{-08}	0.4068×10^{-08}	0.1330×10^{-08}	0.6034×10^{-08}
56	9	-0.7253×10^{-08}	0.2354×10^{-08}	0.2965×10^{-08}	0.3267×10^{-08}
58	9	-0.1243×10^{-07}	-0.4833×10^{-08}	-0.3562×10^{-08}	-0.3847×10^{-08}
60	9	-0.7154×10^{-08}	0.7376×10^{-09}	0.2488×10^{-08}	0.2052×10^{-08}

Table 20: Recovered Coefficients for Block $m = 9$, $|l|_2 = 0$

		estimate		truth	
l	m	C_{lm}	S_{lm}	C_{lm}	S_{lm}
9	9	0.2161×10^{-06}	0.1167×10^{-06}	-0.4490×10^{-07}	0.8300×10^{-07}
11	9	0.9118×10^{-07}	0.4504×10^{-07}	-0.3117×10^{-07}	0.5650×10^{-07}
13	9	0.6566×10^{-07}	0.3984×10^{-07}	-0.3652×10^{-08}	0.5511×10^{-07}
15	9	0.5580×10^{-07}	0.2834×10^{-07}	0.1097×10^{-07}	0.3753×10^{-07}
17	9	0.3260×10^{-07}	-0.3917×10^{-07}	0.7388×10^{-10}	-0.3587×10^{-07}
19	9	0.3127×10^{-07}	-0.5876×10^{-08}	0.7484×10^{-08}	-0.3321×10^{-08}
21	9	0.3447×10^{-07}	0.1064×10^{-07}	0.1455×10^{-07}	0.1543×10^{-07}
23	9	0.1844×10^{-07}	-0.1380×10^{-07}	0.8397×10^{-09}	-0.1206×10^{-07}
25	9	-0.1195×10^{-07}	0.6443×10^{-08}	-0.2786×10^{-07}	0.1184×10^{-07}
27	9	0.1224×10^{-07}	0.1297×10^{-07}	0.4291×10^{-09}	0.1673×10^{-07}
29	9	0.1120×10^{-07}	0.4577×10^{-09}	-0.4921×10^{-09}	0.3591×10^{-08}
31	9	0.7488×10^{-08}	-0.5687×10^{-09}	-0.1704×10^{-08}	0.2351×10^{-08}
33	9	0.7192×10^{-08}	-0.5837×10^{-09}	-0.1606×10^{-08}	0.1999×10^{-08}
35	9	0.7294×10^{-08}	-0.2835×10^{-08}	-0.3823×10^{-09}	-0.8356×10^{-09}
37	9	0.7441×10^{-08}	-0.6238×10^{-08}	0.5915×10^{-09}	-0.4685×10^{-08}
39	9	0.1418×10^{-07}	0.4807×10^{-08}	0.7844×10^{-08}	0.7154×10^{-08}
41	9	-0.3601×10^{-09}	0.2978×10^{-08}	-0.6638×10^{-08}	0.4913×10^{-08}
43	9	0.5809×10^{-08}	-0.8692×10^{-08}	0.6125×10^{-09}	-0.8150×10^{-08}
45	9	0.1007×10^{-07}	-0.6726×10^{-08}	0.5668×10^{-08}	-0.4822×10^{-08}
47	9	0.3694×10^{-08}	0.2529×10^{-08}	-0.1809×10^{-08}	0.4123×10^{-08}
49	9	0.3780×10^{-08}	0.5580×10^{-08}	-0.2210×10^{-09}	0.6961×10^{-08}
51	9	0.5860×10^{-08}	-0.3246×10^{-08}	0.2005×10^{-08}	-0.2567×10^{-08}
53	9	0.6105×10^{-08}	-0.3452×10^{-08}	0.2767×10^{-08}	-0.1838×10^{-08}
55	9	0.4237×10^{-08}	0.2124×10^{-08}	0.4647×10^{-09}	0.2930×10^{-08}
57	9	0.5303×10^{-08}	-0.2800×10^{-08}	0.1317×10^{-08}	-0.2636×10^{-08}
59	9	0.2607×10^{-08}	-0.6082×10^{-09}	-0.3646×10^{-09}	0.1065×10^{-08}

Table 21: Recovered Coefficients for Block $m = 9$, $|l|_2 = 1$

		estimate		truth	
l	m	C_{lm}	S_{lm}	C_{lm}	S_{lm}
10	10	-0.5140×10^{-06}	-0.4307×10^{-07}	0.1075×10^{-06}	-0.2786×10^{-07}
12	10	-0.2473×10^{-06}	-0.1140×10^{-07}	0.2920×10^{-08}	0.3278×10^{-07}
14	10	-0.1262×10^{-06}	-0.3844×10^{-07}	0.1650×10^{-07}	-0.4170×10^{-08}
16	10	-0.8863×10^{-07}	-0.2367×10^{-07}	0.1315×10^{-08}	0.5816×10^{-08}
18	10	-0.3985×10^{-07}	-0.2389×10^{-07}	0.2249×10^{-07}	0.5368×10^{-09}
20	10	-0.6424×10^{-07}	-0.2814×10^{-07}	-0.2261×10^{-07}	-0.6292×10^{-08}
22	10	-0.3040×10^{-07}	0.1949×10^{-08}	0.2076×10^{-08}	0.2270×10^{-07}
24	10	-0.1668×10^{-07}	0.6901×10^{-08}	0.7879×10^{-08}	0.2529×10^{-07}
26	10	-0.2793×10^{-07}	-0.2574×10^{-07}	-0.1040×10^{-07}	-0.1149×10^{-07}
28	10	-0.2393×10^{-07}	-0.1958×10^{-08}	-0.8553×10^{-08}	0.1151×10^{-07}
30	10	-0.1347×10^{-07}	-0.1563×10^{-07}	-0.1655×10^{-08}	-0.4794×10^{-08}
32	10	-0.9087×10^{-08}	-0.1613×10^{-07}	0.1360×10^{-08}	-0.6172×10^{-08}
34	10	-0.1675×10^{-07}	-0.1073×10^{-07}	-0.8343×10^{-08}	-0.1238×10^{-08}
36	10	-0.8031×10^{-08}	-0.3227×10^{-08}	-0.2170×10^{-09}	0.5186×10^{-08}
38	10	-0.9255×10^{-08}	-0.1178×10^{-07}	-0.3025×10^{-08}	-0.4598×10^{-08}
40	10	-0.1060×10^{-07}	0.1348×10^{-08}	-0.4826×10^{-08}	0.8558×10^{-08}
42	10	-0.9558×10^{-09}	-0.3201×10^{-08}	0.4033×10^{-08}	0.3632×10^{-08}
44	10	-0.8301×10^{-08}	-0.9874×10^{-08}	-0.3711×10^{-08}	-0.4245×10^{-08}
46	10	-0.6224×10^{-09}	-0.5392×10^{-08}	0.3573×10^{-08}	0.4634×10^{-09}
48	10	-0.3753×10^{-08}	-0.1804×10^{-08}	-0.4231×10^{-09}	0.3661×10^{-08}
50	10	-0.7997×10^{-08}	-0.4131×10^{-08}	-0.4087×10^{-08}	0.7728×10^{-09}
52	10	-0.3065×10^{-08}	-0.5195×10^{-08}	0.1736×10^{-09}	0.7139×10^{-10}
54	10	-0.2656×10^{-09}	-0.3731×10^{-08}	0.1743×10^{-08}	0.1307×10^{-08}
56	10	-0.5989×10^{-08}	-0.4236×10^{-08}	-0.3497×10^{-08}	-0.2255×10^{-09}
58	10	-0.3760×10^{-08}	-0.7944×10^{-08}	-0.8522×10^{-09}	-0.4618×10^{-08}
60	10	-0.3664×10^{-08}	-0.5742×10^{-08}	-0.1824×10^{-08}	-0.1196×10^{-08}

Table 22: Recovered Coefficients for Block $m = 10$, $|l|_2 = 0$

		estimate		truth	
l	m	C_{lm}	S_{lm}	C_{lm}	S_{lm}
11	10	0.3627×10^{-07}	0.5296×10^{-07}	-0.4870×10^{-07}	-0.1692×10^{-07}
13	10	0.8194×10^{-07}	0.2467×10^{-07}	0.3043×10^{-07}	-0.4290×10^{-07}
15	10	0.5272×10^{-07}	0.5619×10^{-07}	0.5619×10^{-08}	0.6209×10^{-08}
17	10	0.4956×10^{-07}	0.5642×10^{-07}	0.7784×10^{-08}	0.1316×10^{-07}
19	10	0.3049×10^{-07}	0.3325×10^{-07}	-0.1068×10^{-07}	-0.7629×10^{-08}
21	10	0.2775×10^{-07}	0.3662×10^{-07}	-0.7907×10^{-08}	0.6094×10^{-10}
23	10	0.4146×10^{-07}	0.3367×10^{-07}	0.8725×10^{-08}	-0.1901×10^{-08}
25	10	0.3967×10^{-07}	0.2854×10^{-07}	0.8381×10^{-08}	-0.6219×10^{-08}
27	10	0.1951×10^{-07}	0.3215×10^{-07}	-0.1019×10^{-07}	0.2050×10^{-08}
29	10	0.3267×10^{-07}	0.3211×10^{-07}	0.5527×10^{-08}	0.1588×10^{-08}
31	10	0.2386×10^{-07}	0.2500×10^{-07}	-0.2927×10^{-08}	-0.3669×10^{-08}
33	10	0.2167×10^{-07}	0.2401×10^{-07}	-0.4557×10^{-08}	-0.3459×10^{-08}
35	10	0.2075×10^{-07}	0.3120×10^{-07}	-0.3516×10^{-08}	0.4851×10^{-08}
37	10	0.2389×10^{-07}	0.2981×10^{-07}	-0.3048×10^{-10}	0.3140×10^{-08}
39	10	0.2051×10^{-07}	0.2972×10^{-07}	-0.2746×10^{-08}	0.4983×10^{-08}
41	10	0.2519×10^{-07}	0.2577×10^{-07}	0.3415×10^{-08}	-0.2164×10^{-09}
43	10	0.1964×10^{-07}	0.2702×10^{-07}	-0.3208×10^{-08}	0.1770×10^{-08}
45	10	0.2347×10^{-07}	0.2397×10^{-07}	0.2470×10^{-08}	-0.2523×10^{-09}
47	10	0.2321×10^{-07}	0.2615×10^{-07}	0.1688×10^{-08}	0.1998×10^{-08}
49	10	0.1524×10^{-07}	0.2509×10^{-07}	-0.6413×10^{-08}	0.6391×10^{-09}
51	10	0.2268×10^{-07}	0.2000×10^{-07}	0.2505×10^{-08}	-0.4520×10^{-08}
53	10	0.2870×10^{-07}	0.2261×10^{-07}	0.8869×10^{-08}	-0.1494×10^{-08}
55	10	0.1950×10^{-07}	0.2777×10^{-07}	-0.1480×10^{-08}	0.4015×10^{-08}
57	10	0.1788×10^{-07}	0.2602×10^{-07}	-0.2301×10^{-08}	0.2124×10^{-08}
59	10	0.2292×10^{-07}	0.1963×10^{-07}	0.2990×10^{-08}	-0.4309×10^{-08}

Table 23: Recovered Coefficients for Block $m = 10$, $|l|_2 = 1$

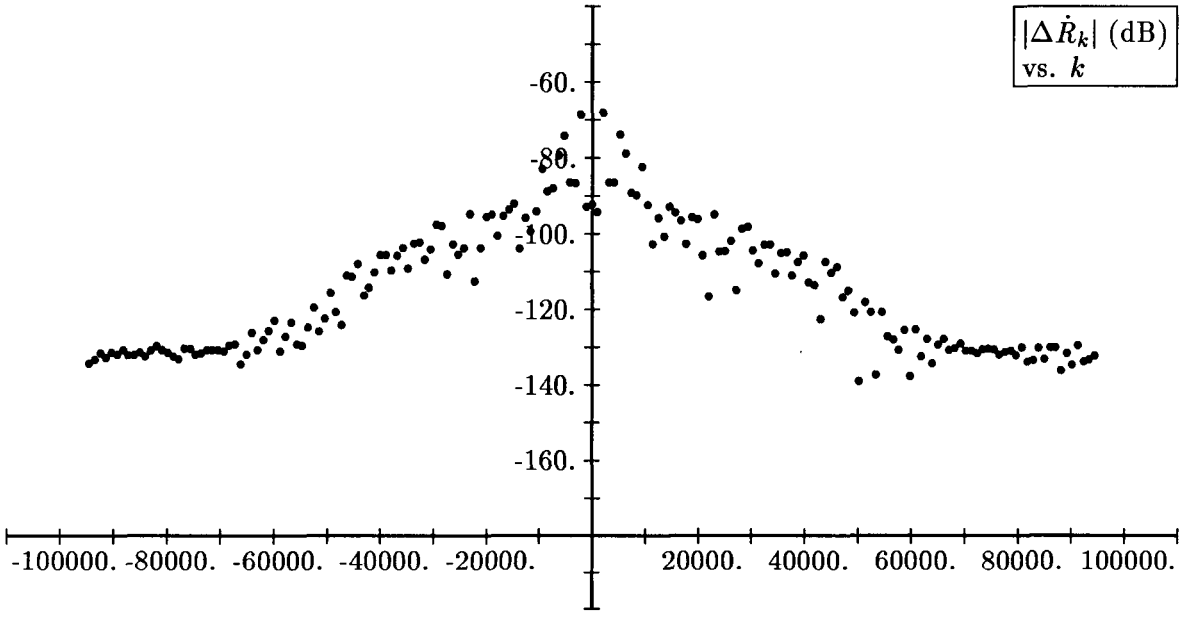

Figure 3: Observed SST Range Rate Perturbation Spectral Amplitude: $m = 1,\ |l|_2 = 0$

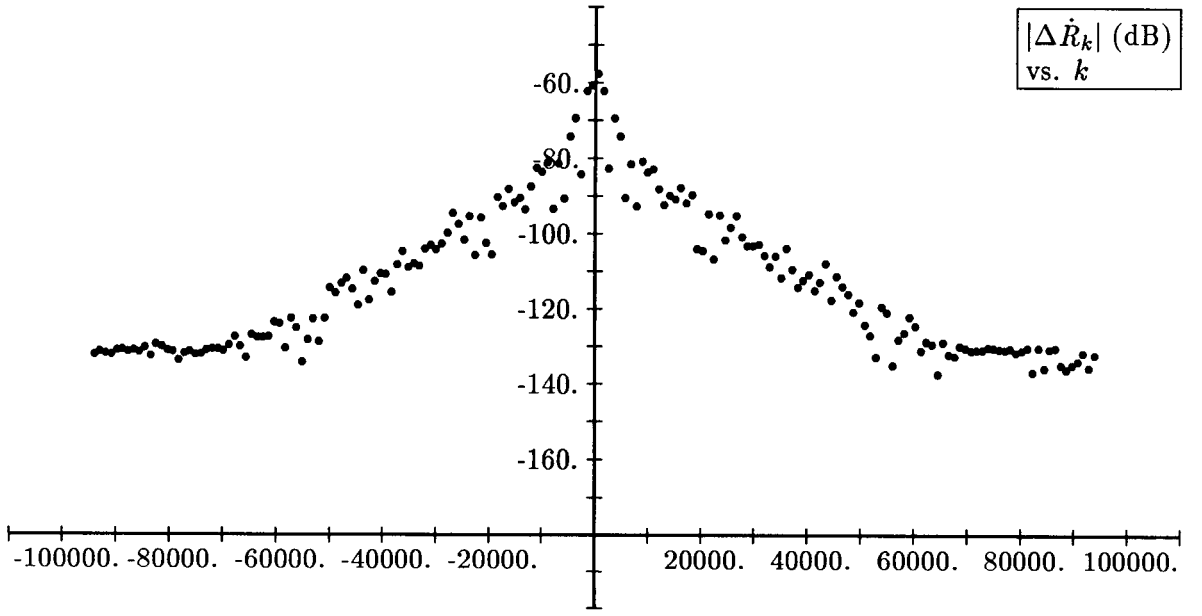

Figure 4: Observed SST Range Rate Perturbation Spectral Amplitude: $m = 1$, $|l|_2 = 1$

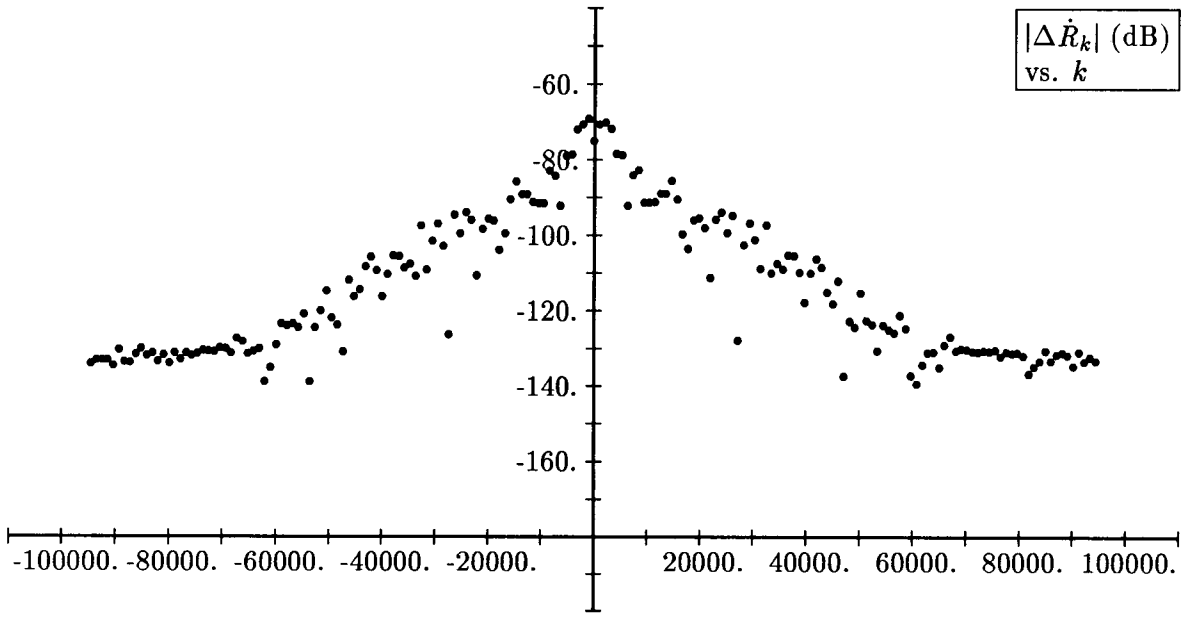

Figure 5: Observed SST Range Rate Perturbation Spectral Amplitude: $m = 2,\ |l|_2 = 0$

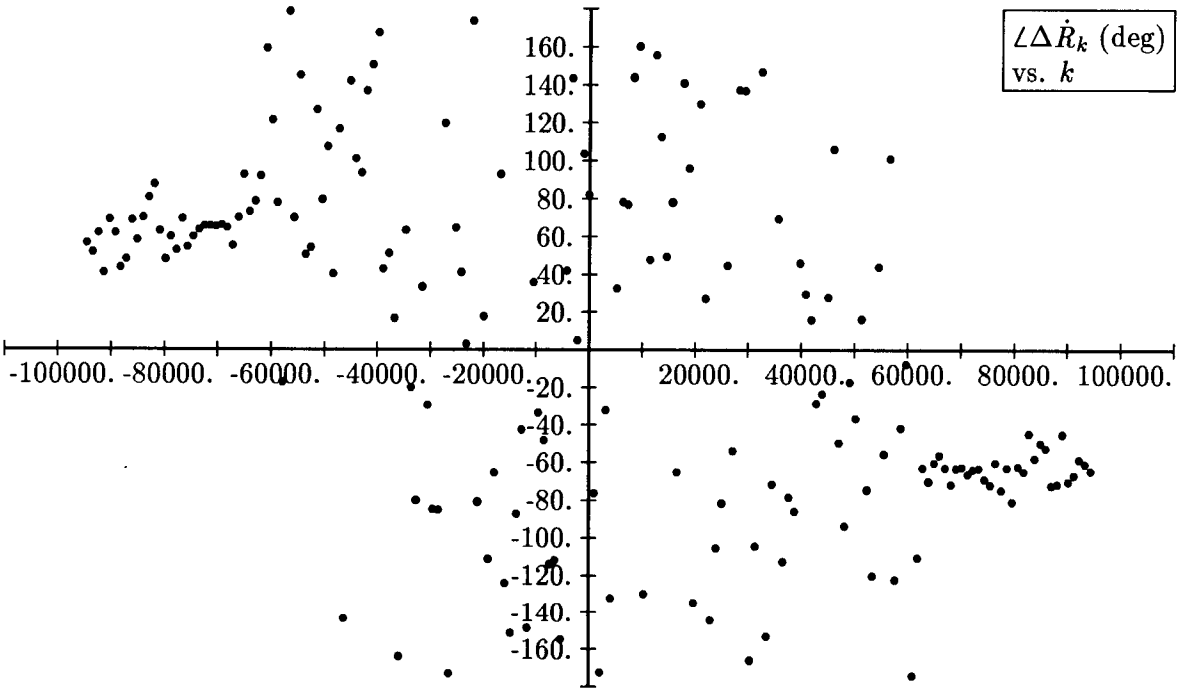

Figure 6: Observed SST Range Rate Perturbation Spectral Phase: $m = 2,\ |l|_2 = 0$

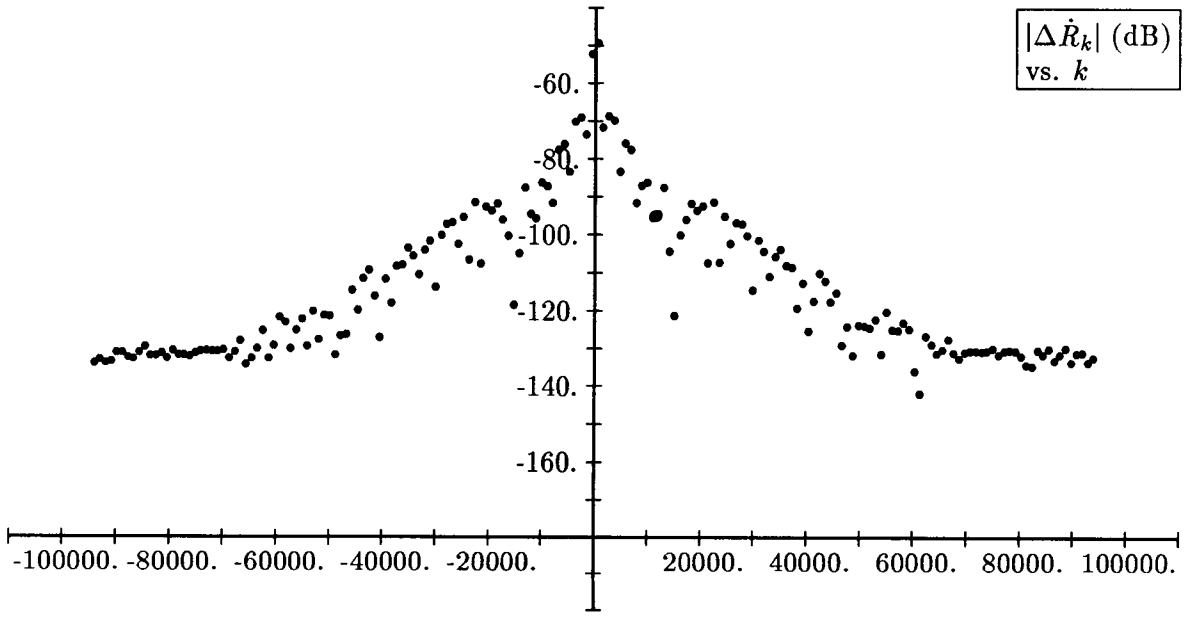

Figure 7: Observed SST Range Rate Perturbation Spectral Amplitude: $m = 2$, $|l|_2 = 1$

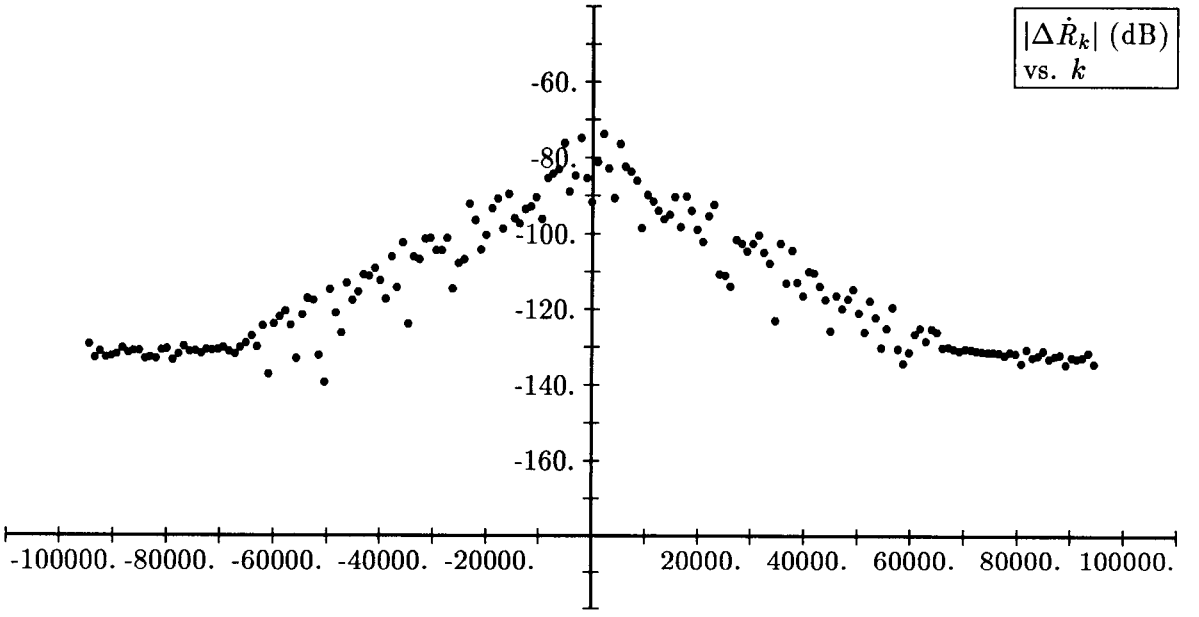

Figure 8: Observed SST Range Rate Perturbation Spectral Amplitude: $m = 3,\ |l|_2 = 0$

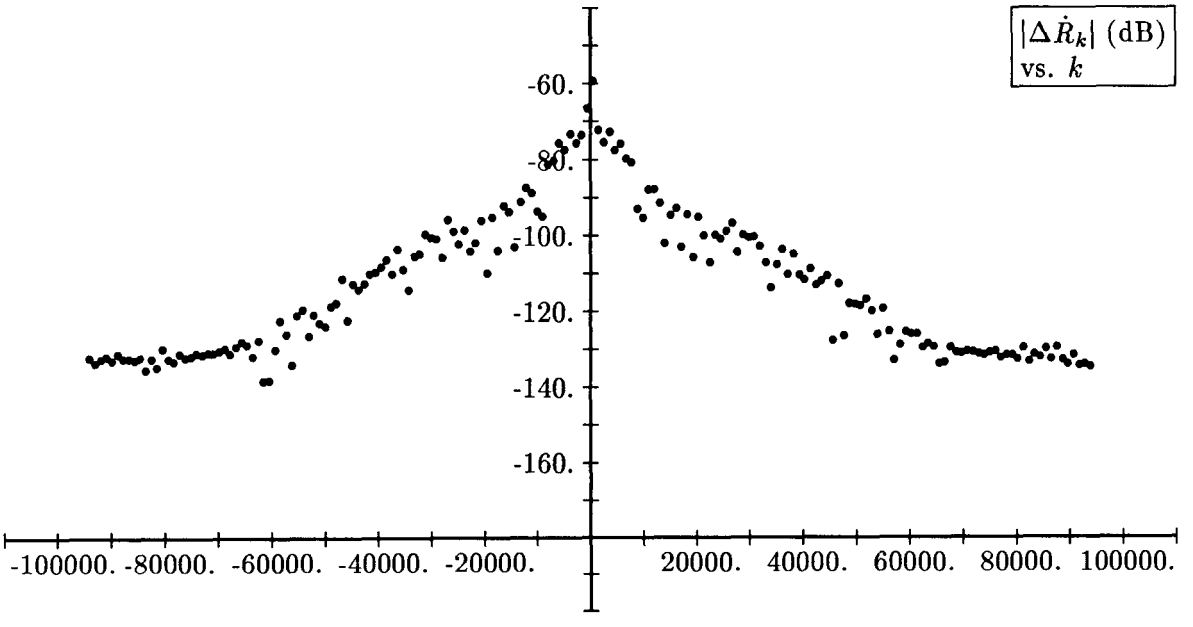

Figure 9: Observed SST Range Rate Perturbation Spectral Amplitude: $m = 3$, $|l|_2 = 1$

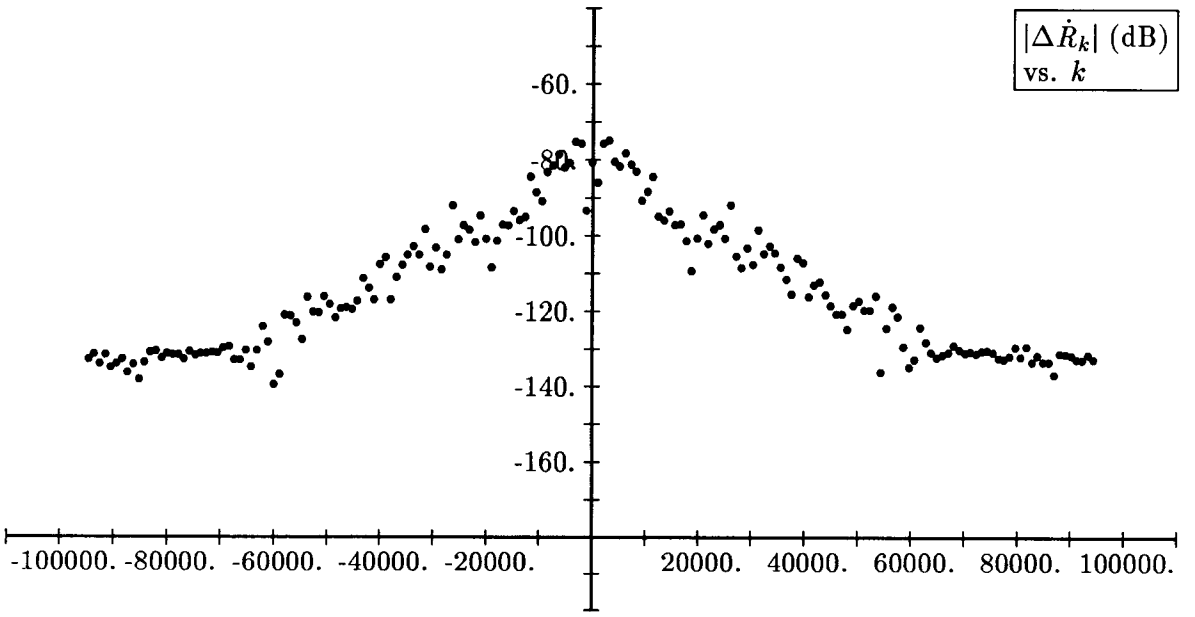

Figure 10: Observed SST Range Rate Perturbation Spectral Amplitude: $m = 4$, $|l|_2 = 0$

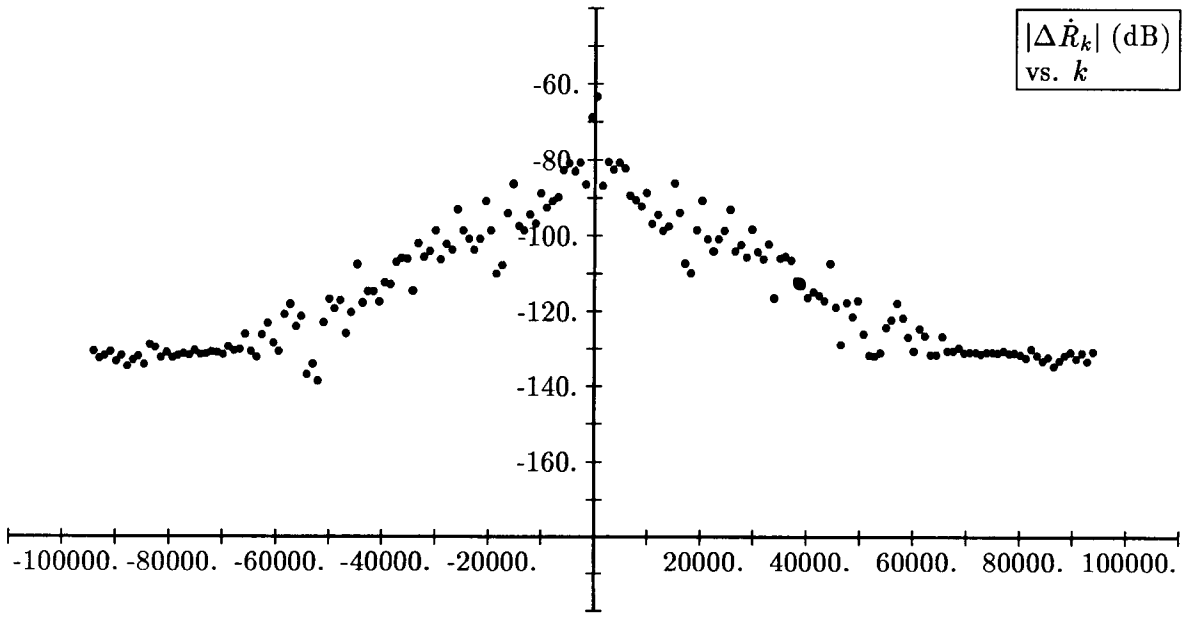

Figure 11: Observed SST Range Rate Perturbation Spectral Amplitude: $m = 4,\ |l|_2 = 1$

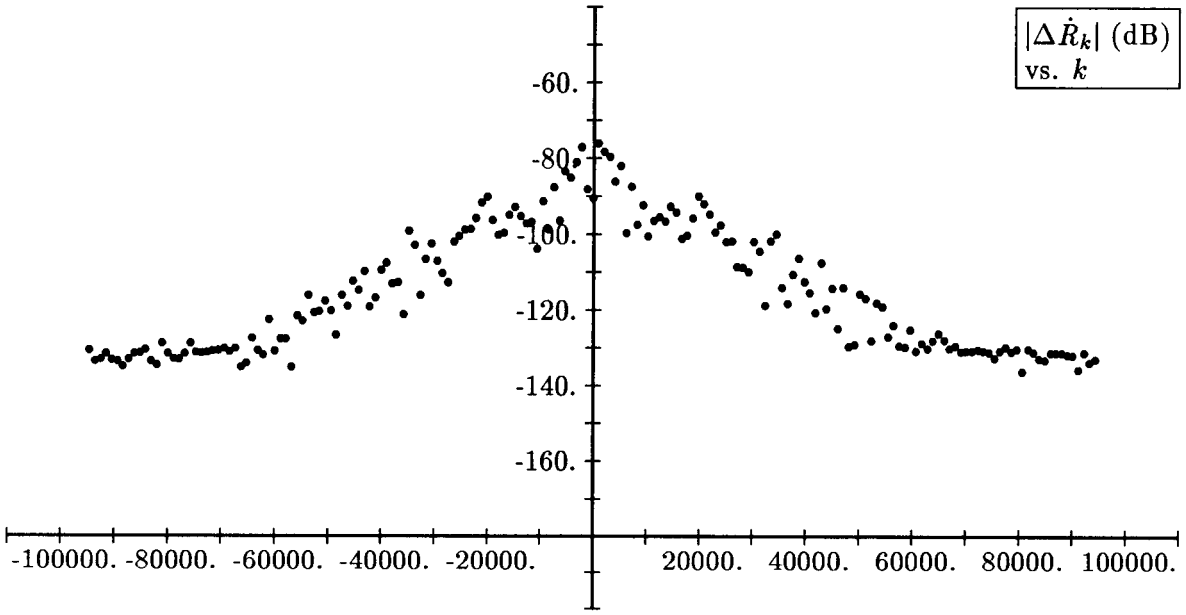

Figure 12: Observed SST Range Rate Perturbation Spectral Amplitude: $m = 5,\ |l|_2 = 0$

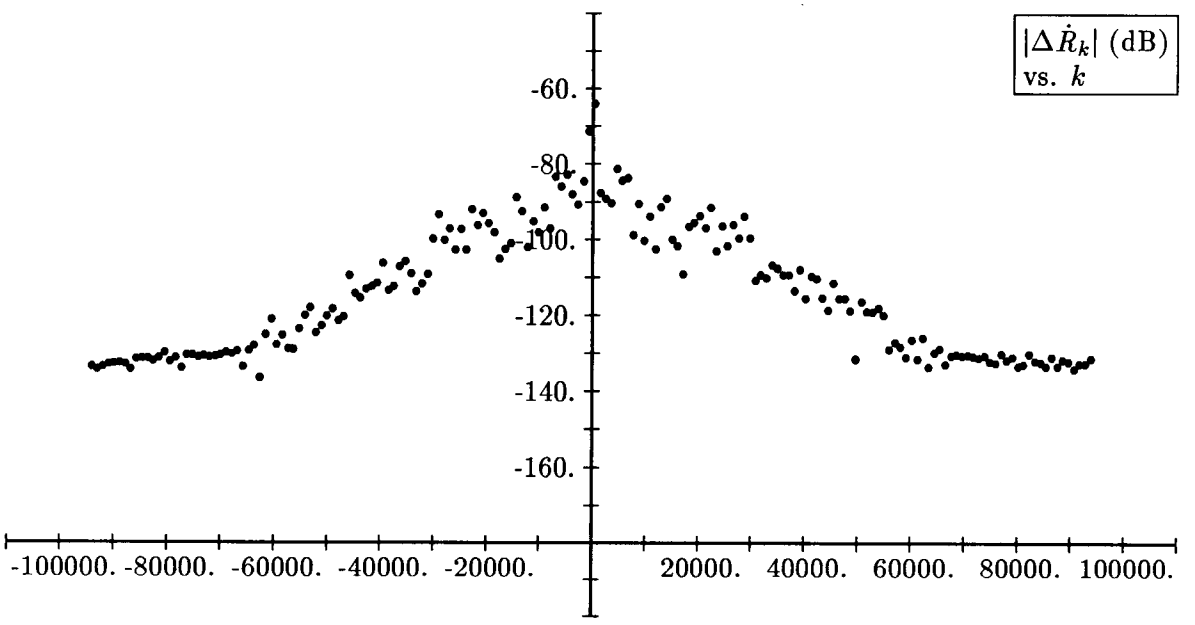

Figure 13: Observed SST Range Rate Perturbation Spectral Amplitude: $m = 5,\ |l|_2 = 1$

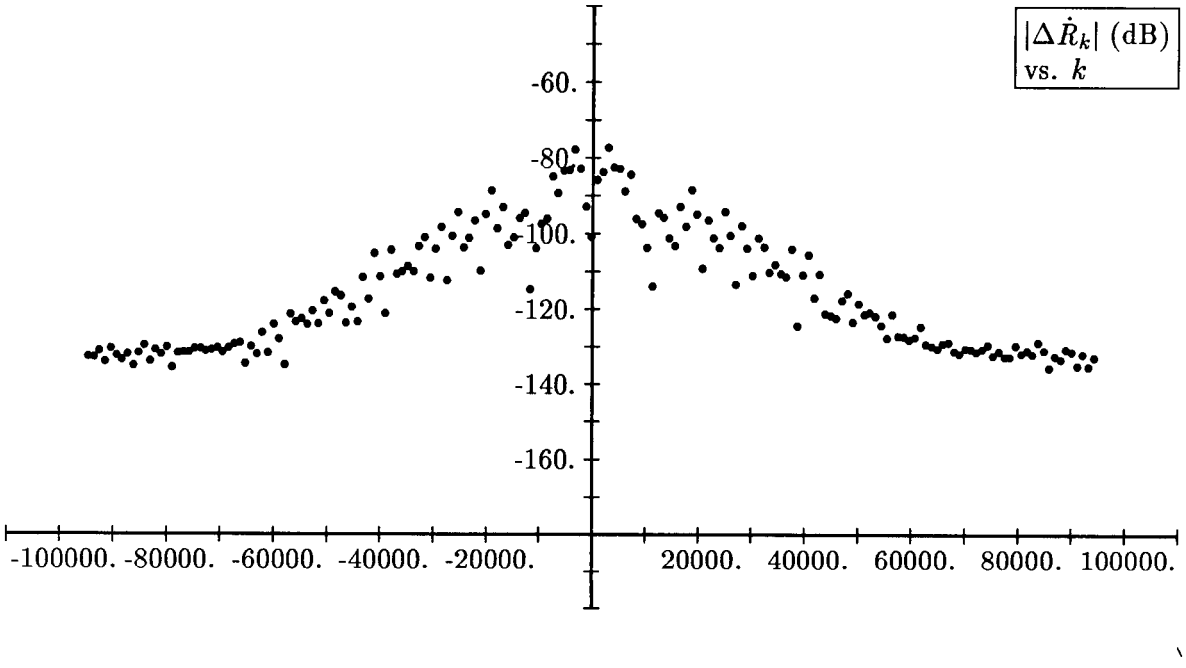

Figure 14: Observed SST Range Rate Perturbation Spectral Amplitude: $m = 6,\ |l|_2 = 0$

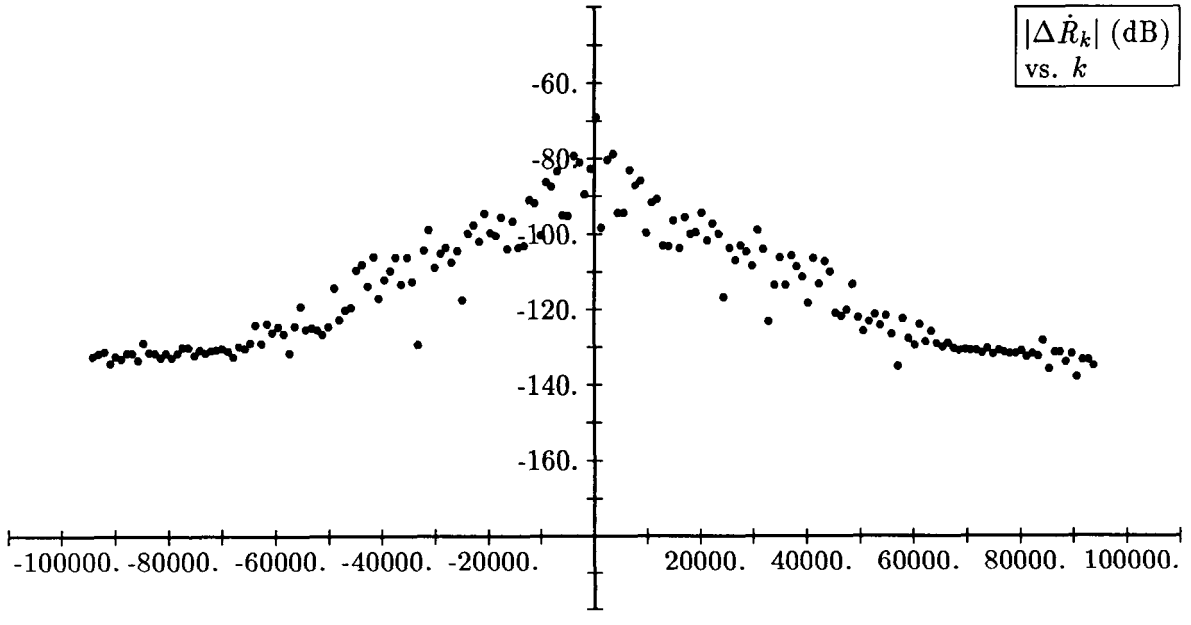

Figure 15: Observed SST Range Rate Perturbation Spectral Amplitude: $m = 6$, $|l|_2 = 1$

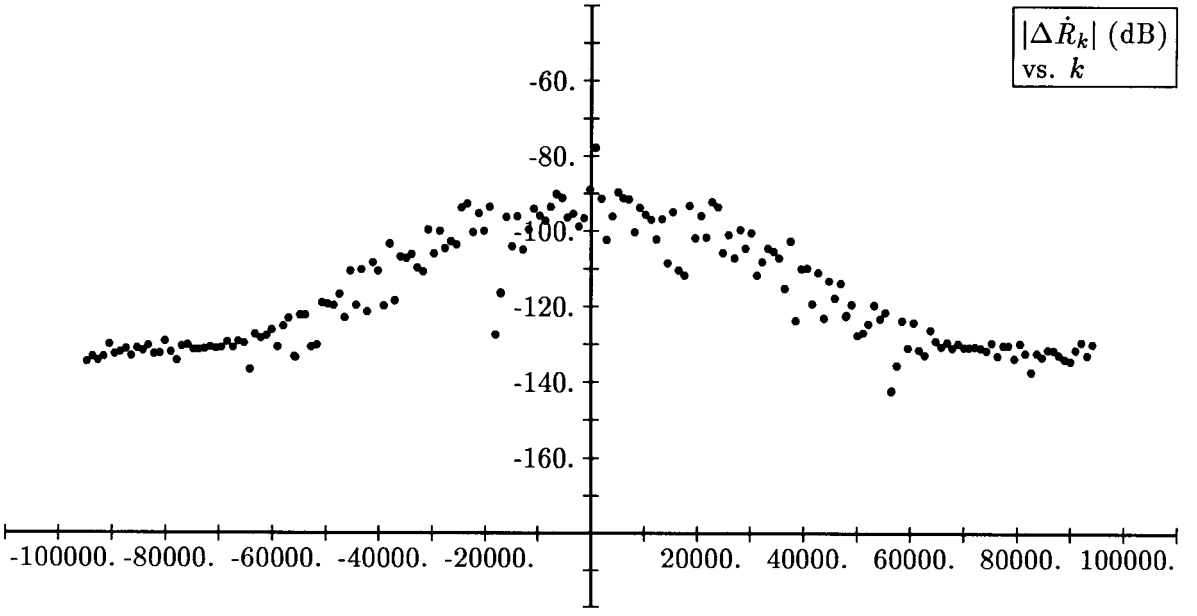

Figure 16: Observed SST Range Rate Perturbation Spectral Amplitude: $m = 7,\ |l|_2 = 0$

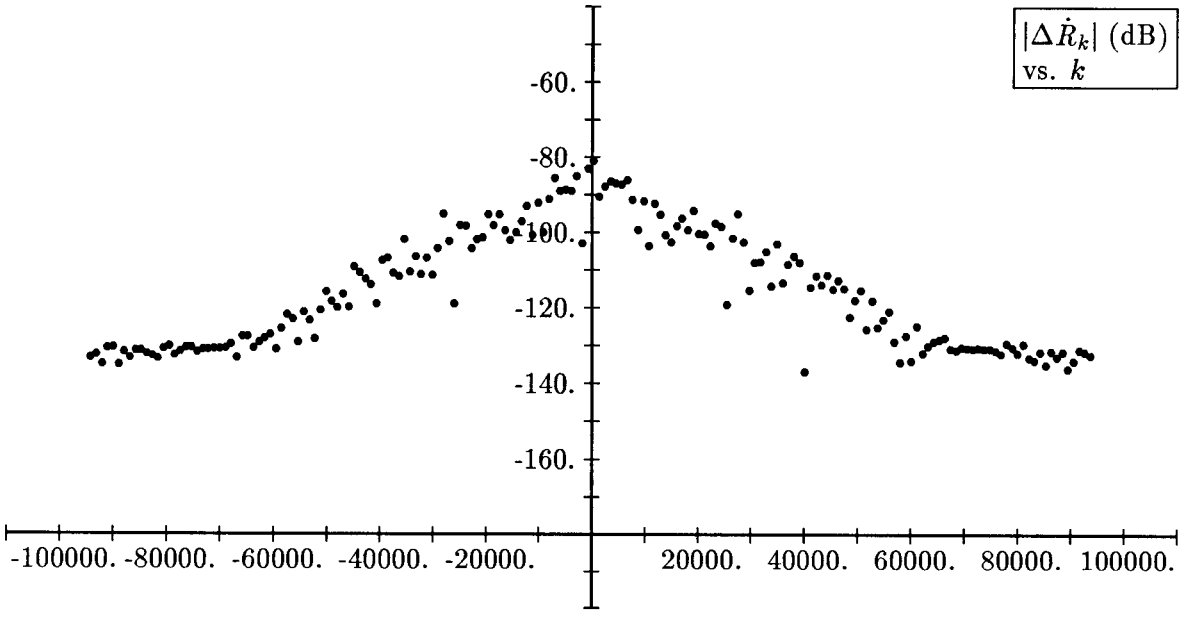

Figure 17: Observed SST Range Rate Perturbation Spectral Amplitude: $m = 7,\ |l|_2 = 1$

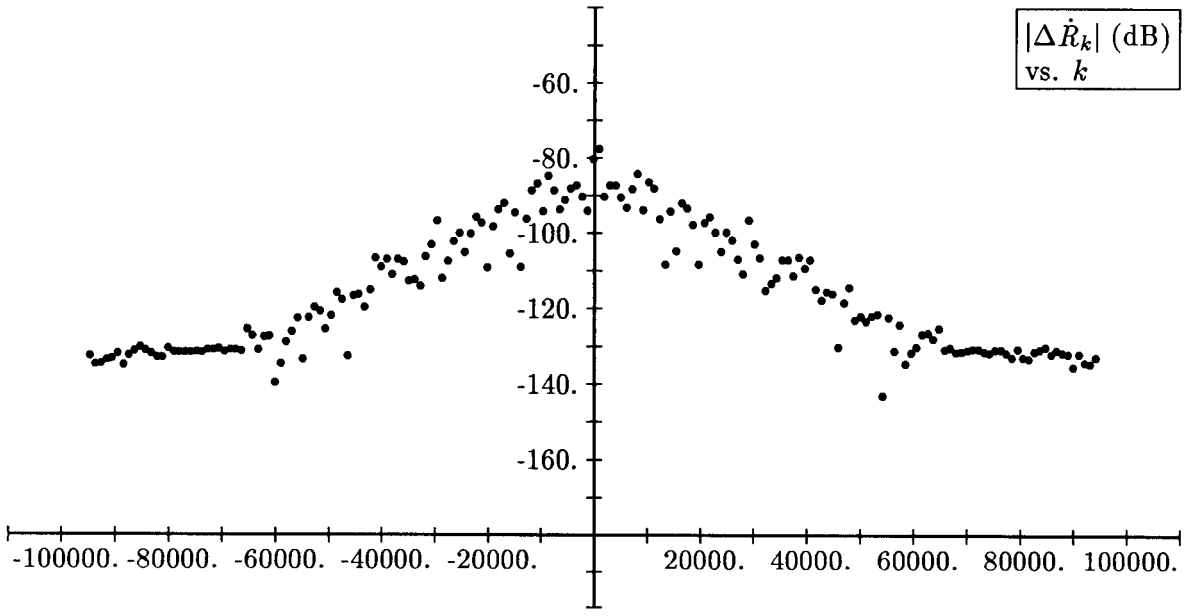

Figure 18: Observed SST Range Rate Perturbation Spectral Amplitude: $m = 8,\ |l|_2 = 0$

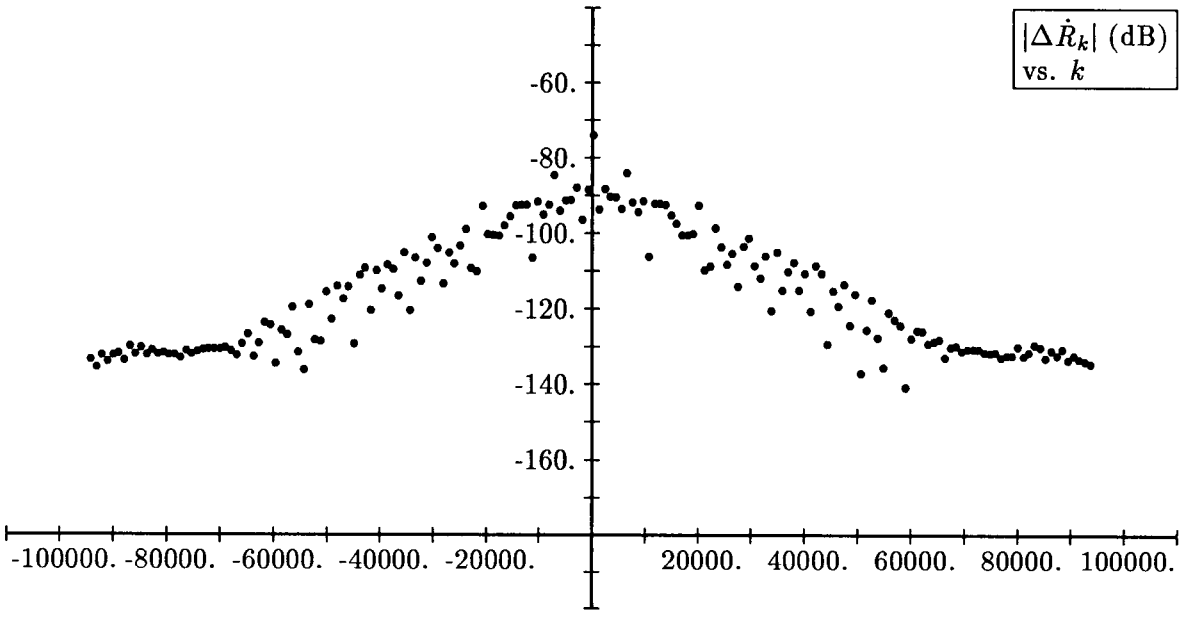

Figure 19: Observed SST Range Rate Perturbation Spectral Amplitude: $m = 8$, $|l|_2 = 1$

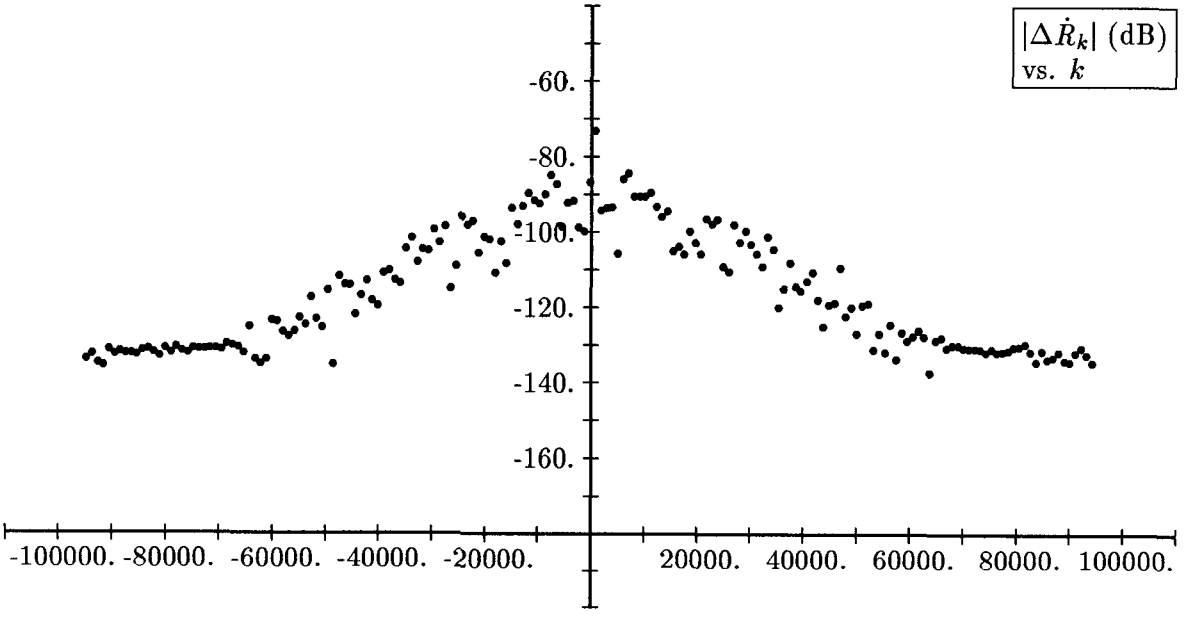

Figure 20: Observed SST Range Rate Perturbation Spectral Amplitude: $m = 9,\ |l|_2 = 0$

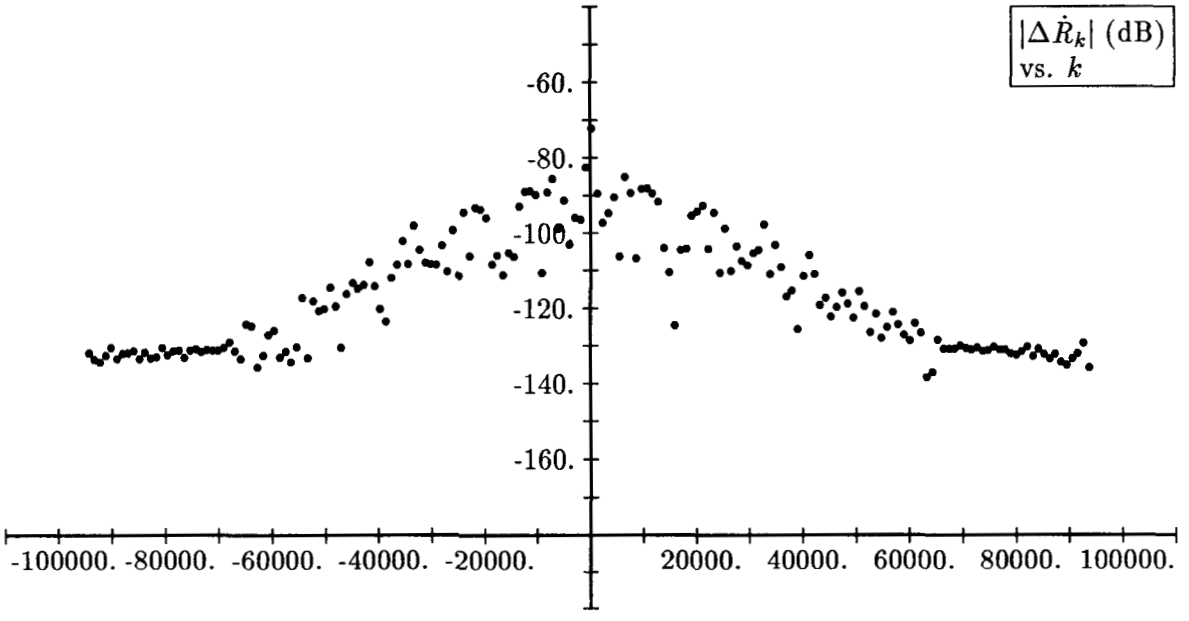

Figure 21: Observed SST Range Rate Perturbation Spectral Amplitude: $m = 9,\ |l|_2 = 1$

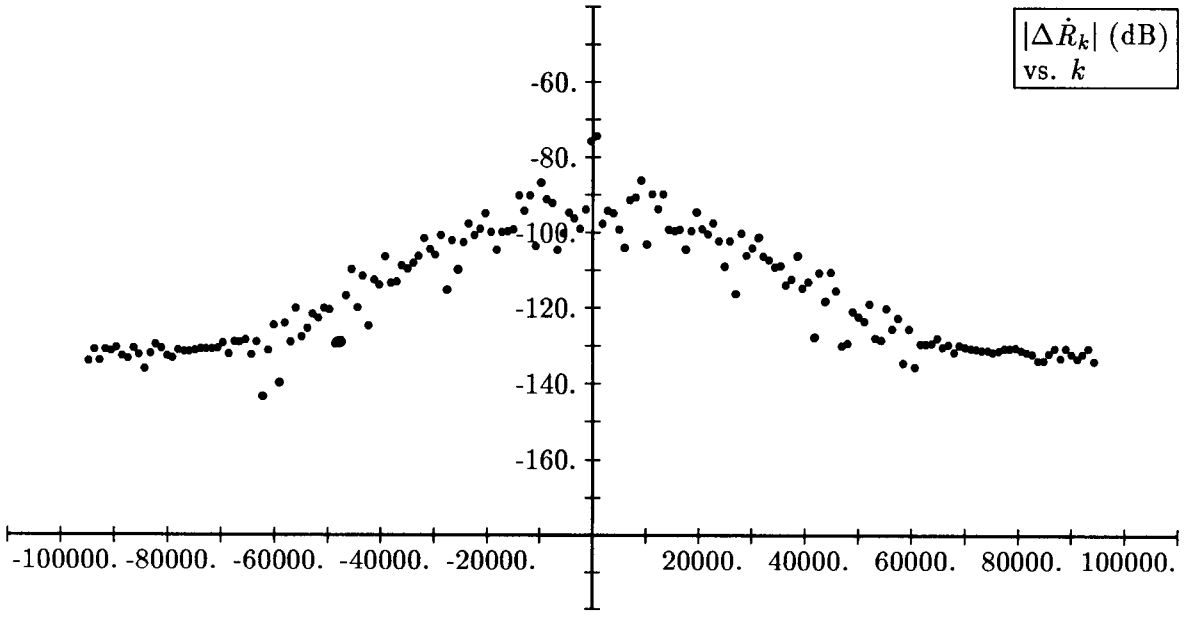

Figure 22: Observed SST Range Rate Perturbation Spectral Amplitude: $m = 10$, $|l|_2 = 0$

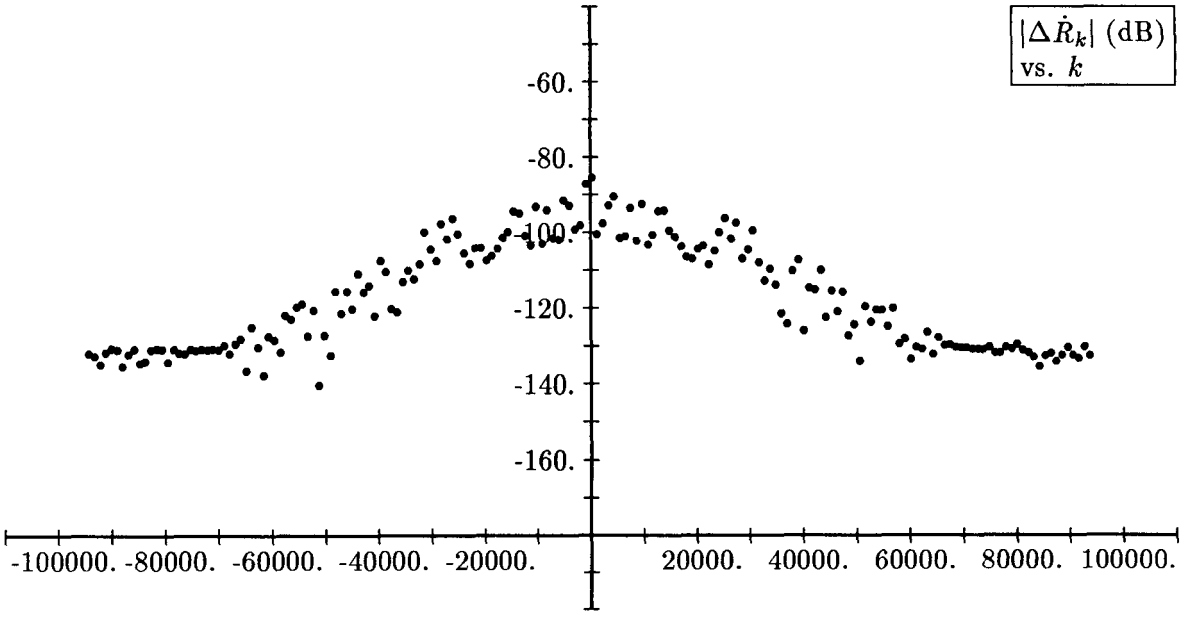

Figure 23: Observed SST Range Rate Perturbation Spectral Amplitude: $m = 10$, $|l|_2 = 1$

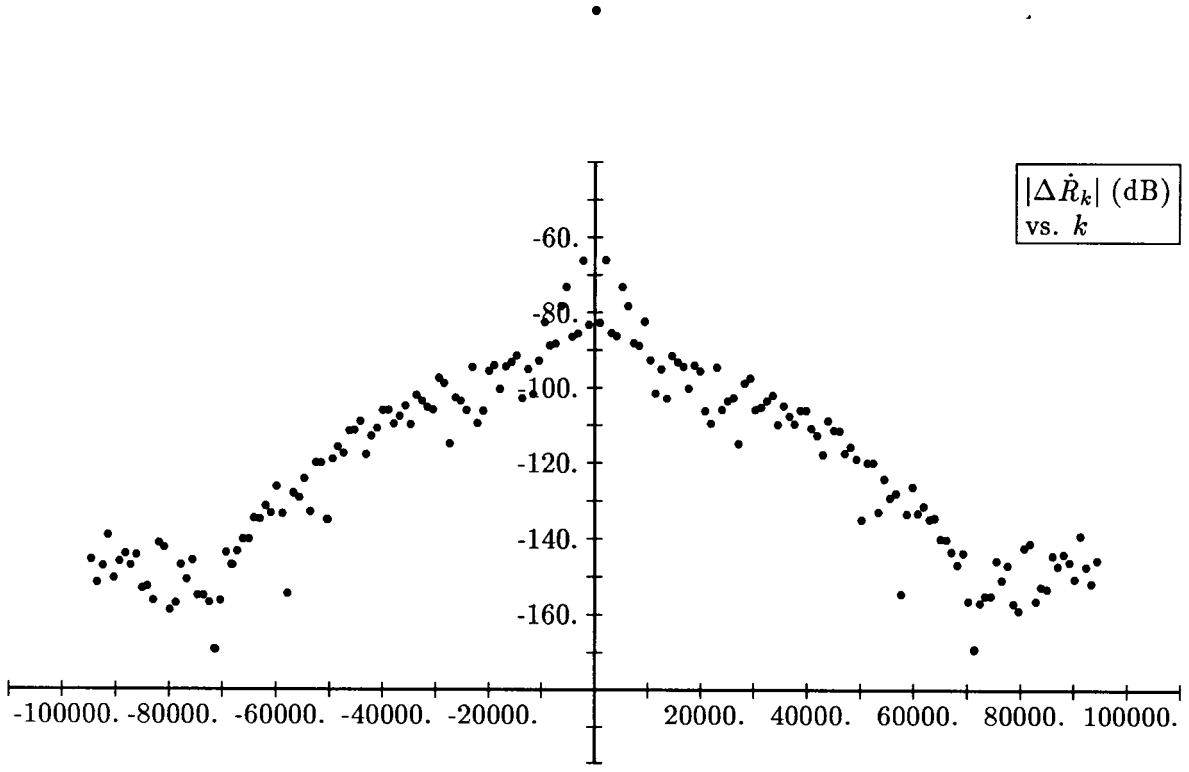

Figure 24: Predicted SST Range Rate Perturbation Spectral Amplitude: $m = 1,\ |l|_2 = 0$

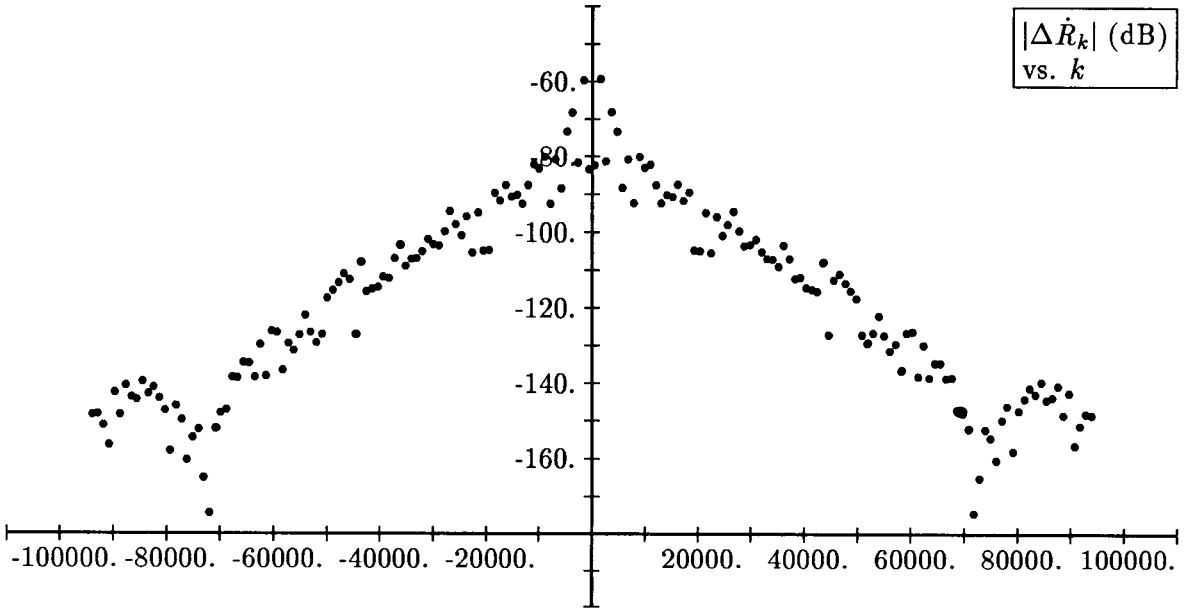

Figure 25: Predicted SST Range Rate Perturbation Spectral Amplitude: $m = 1,\ |l|_2 = 1$

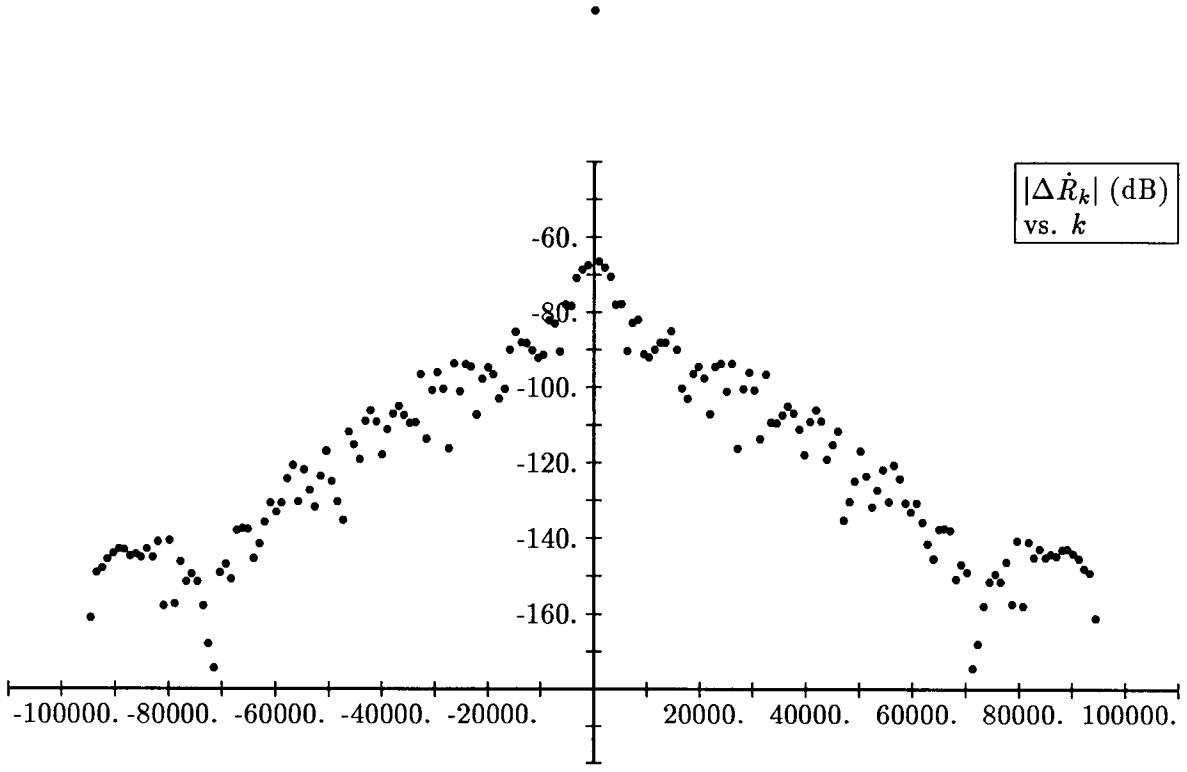

Figure 26: Predicted SST Range Rate Perturbation Spectral Amplitude: $m = 2,\ |l|_2 = 0$

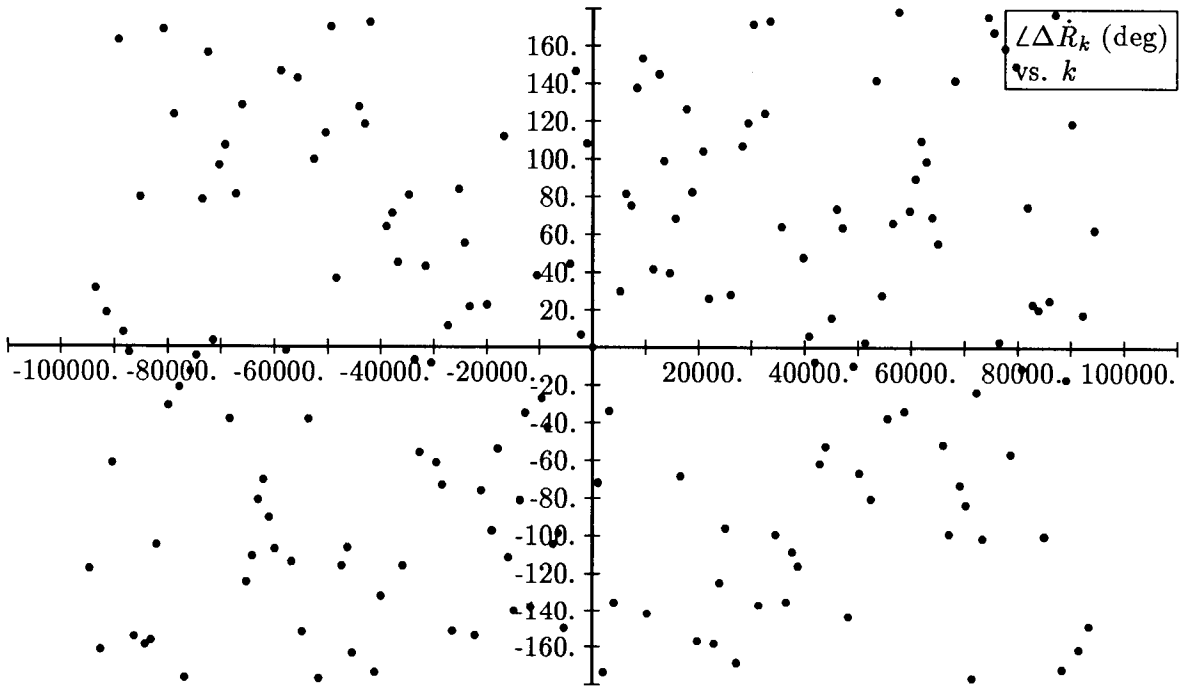

Figure 27: Predicted SST Range Rate Perturbation Spectral Phase: $m = 2,\ |l|_2 = 0$

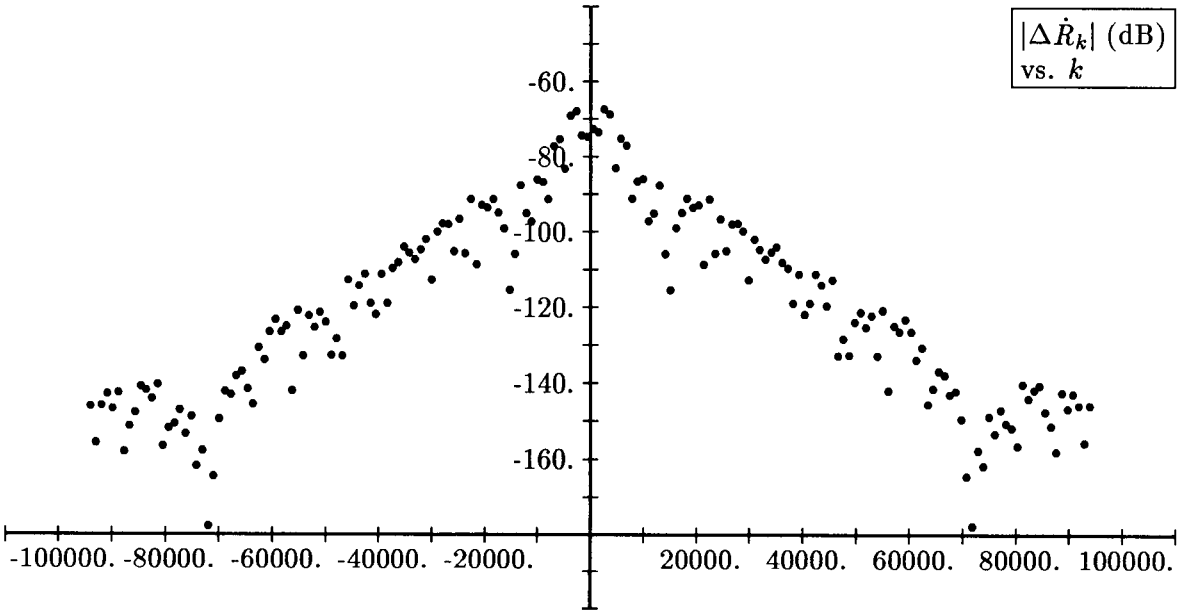

Figure 28: Predicted SST Range Rate Perturbation Spectral Amplitude: $m = 2,\ |l|_2 = 1$

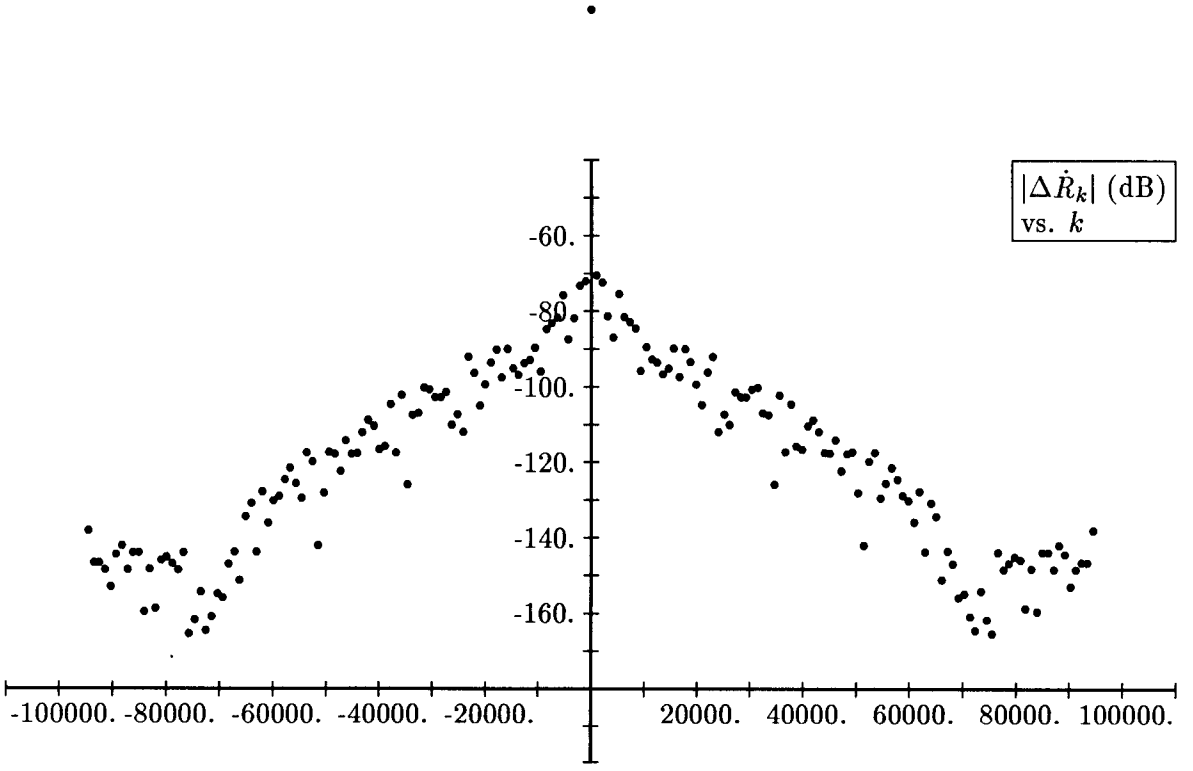

Figure 29: Predicted SST Range Rate Perturbation Spectral Amplitude: $m = 3,\ |l|_2 = 0$

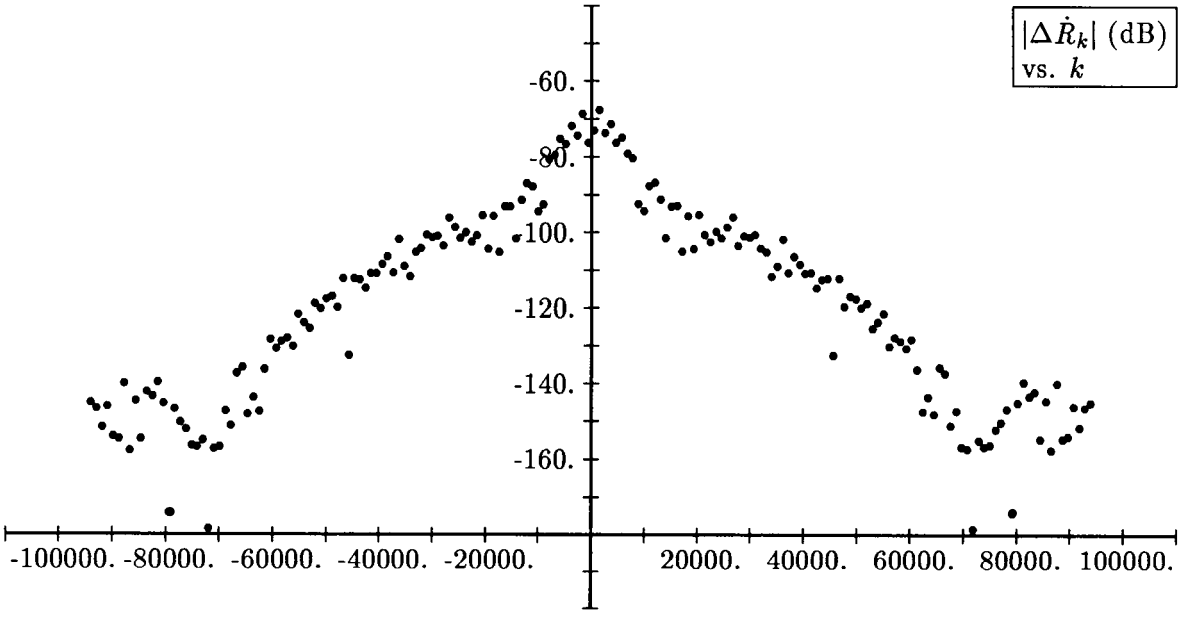

Figure 30: Predicted SST Range Rate Perturbation Spectral Amplitude: $m = 3,\ |l|_2 = 1$

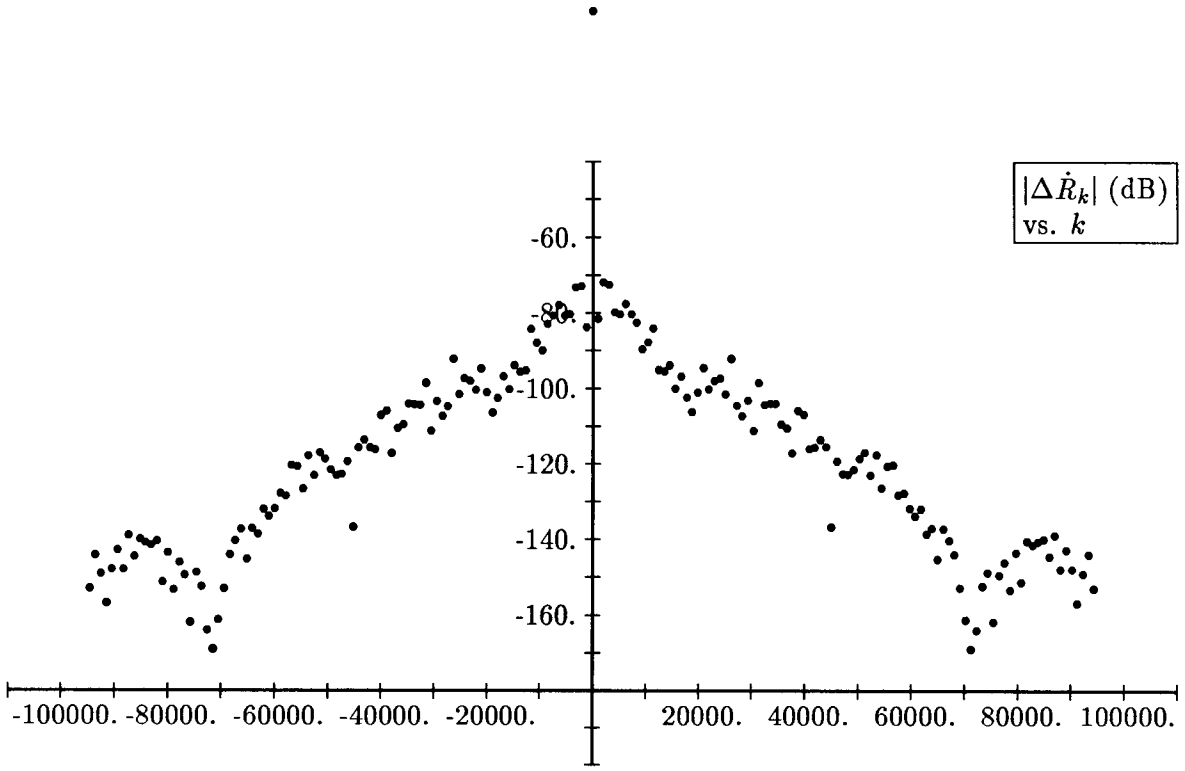

Figure 31: Predicted SST Range Rate Perturbation Spectral Amplitude: $m = 4,\ |l|_2 = 0$

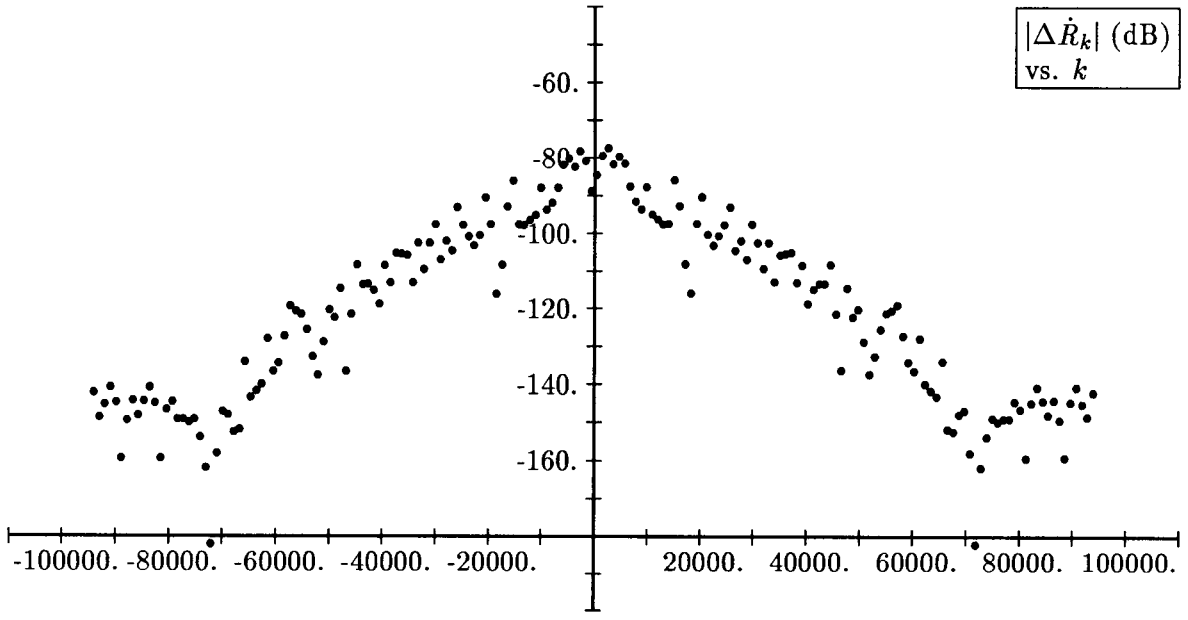

Figure 32: Predicted SST Range Rate Perturbation Spectral Amplitude: $m = 4,\ |l|_2 = 1$

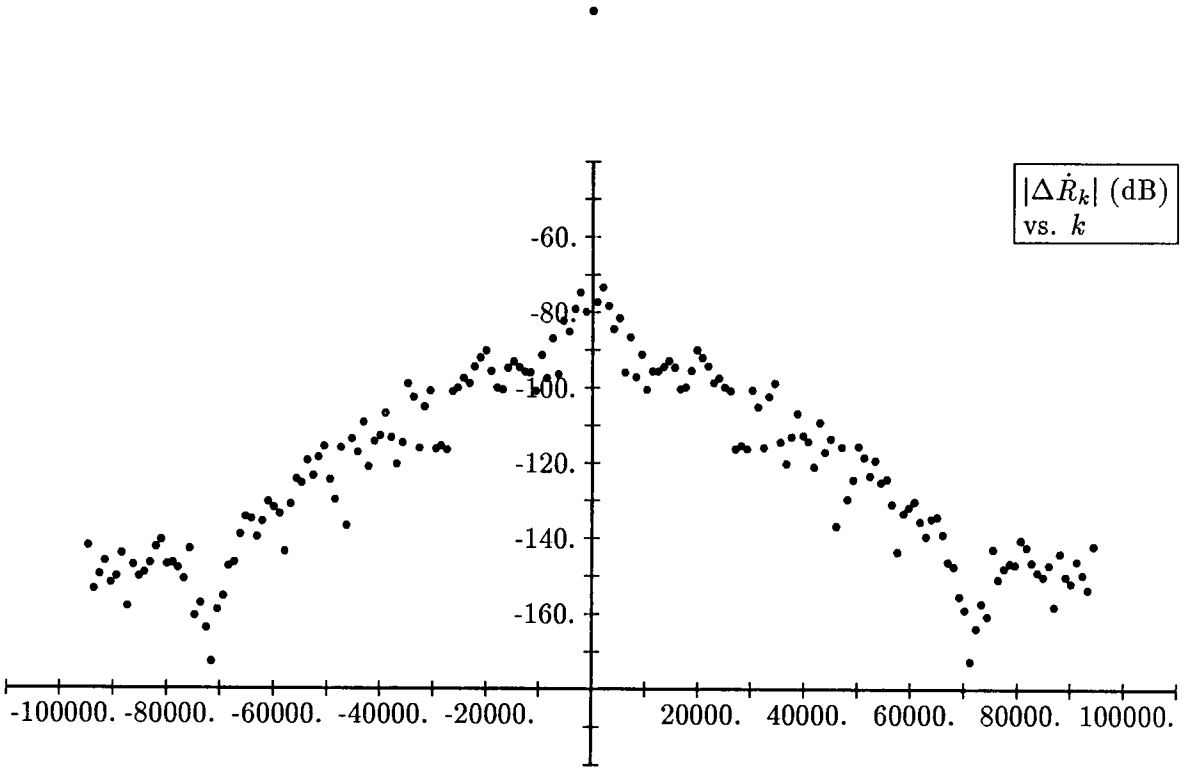

Figure 33: Predicted SST Range Rate Perturbation Spectral Amplitude: $m = 5,\ |l|_2 = 0$

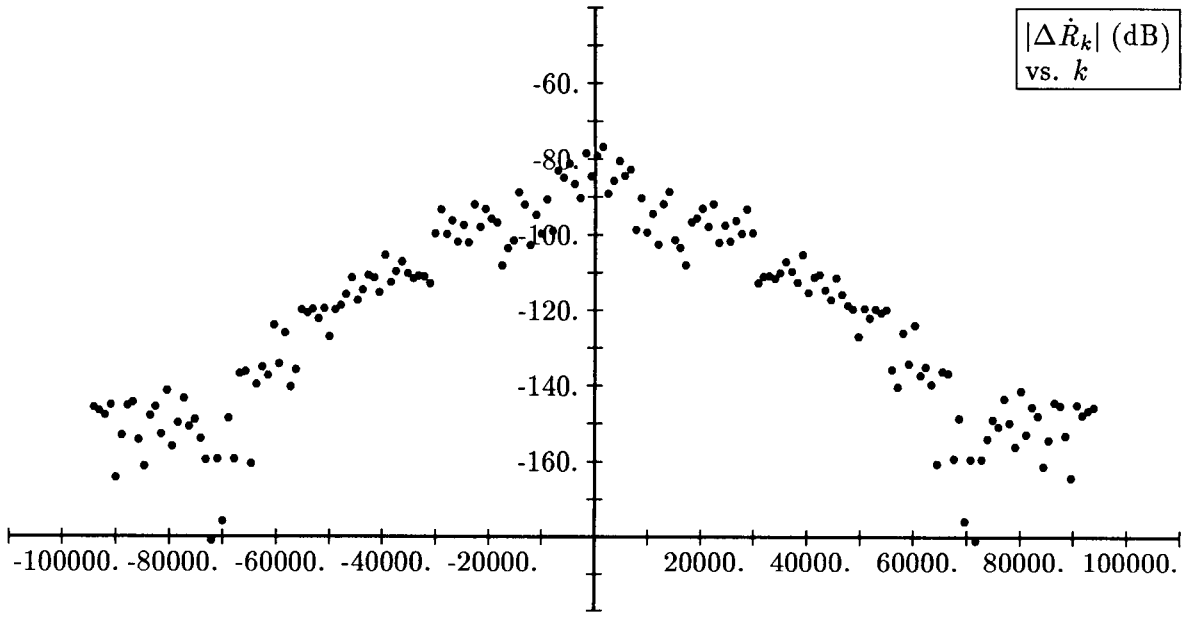

Figure 34: Predicted SST Range Rate Perturbation Spectral Amplitude: $m = 5,\ |l|_2 = 1$

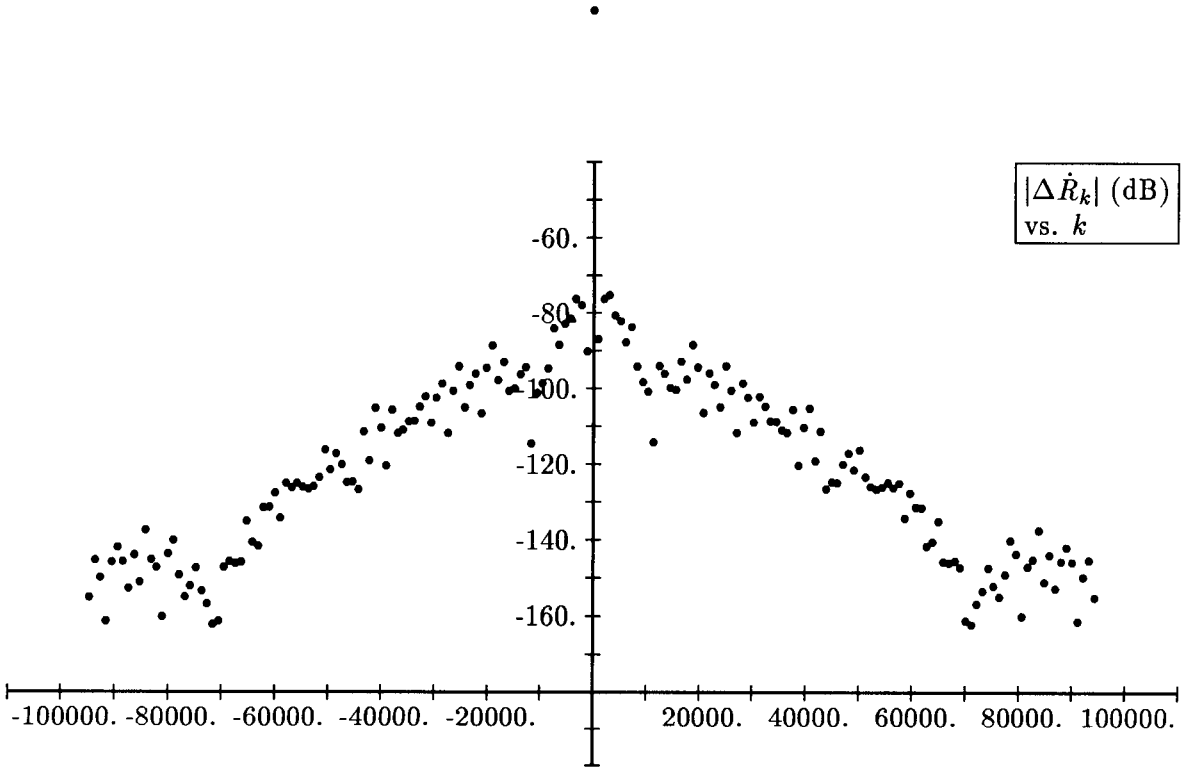

Figure 35: Predicted SST Range Rate Perturbation Spectral Amplitude: $m = 6,\ |l|_2 = 0$

C-2

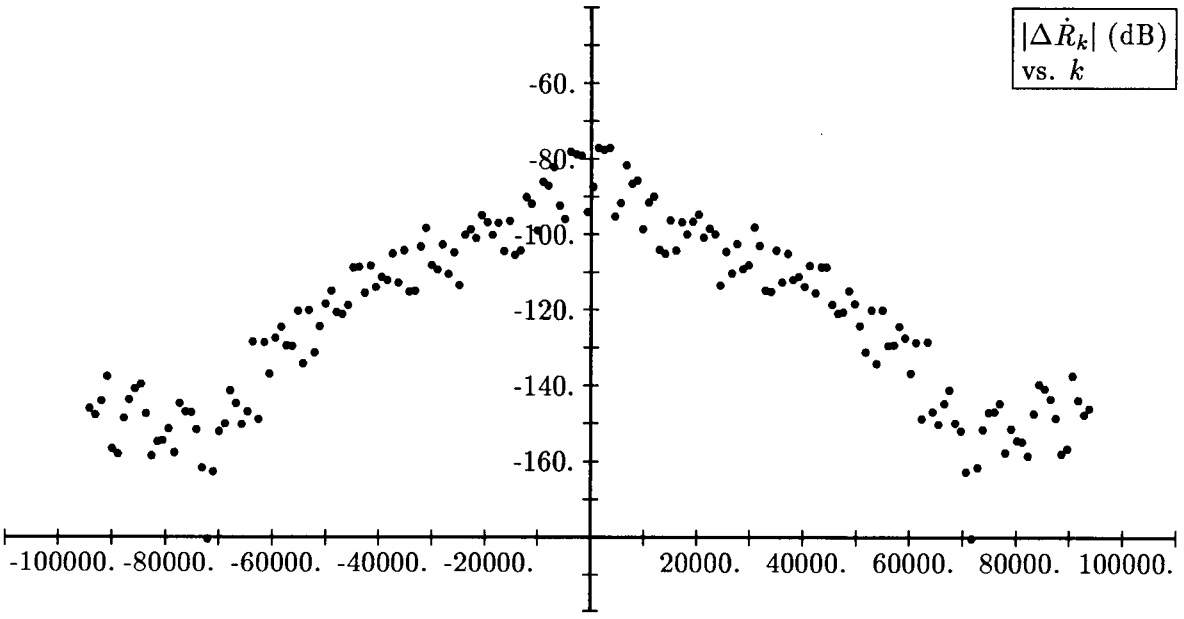

Figure 36: Predicted SST Range Rate Perturbation Spectral Amplitude: $m = 6$, $|l|_2 = 1$

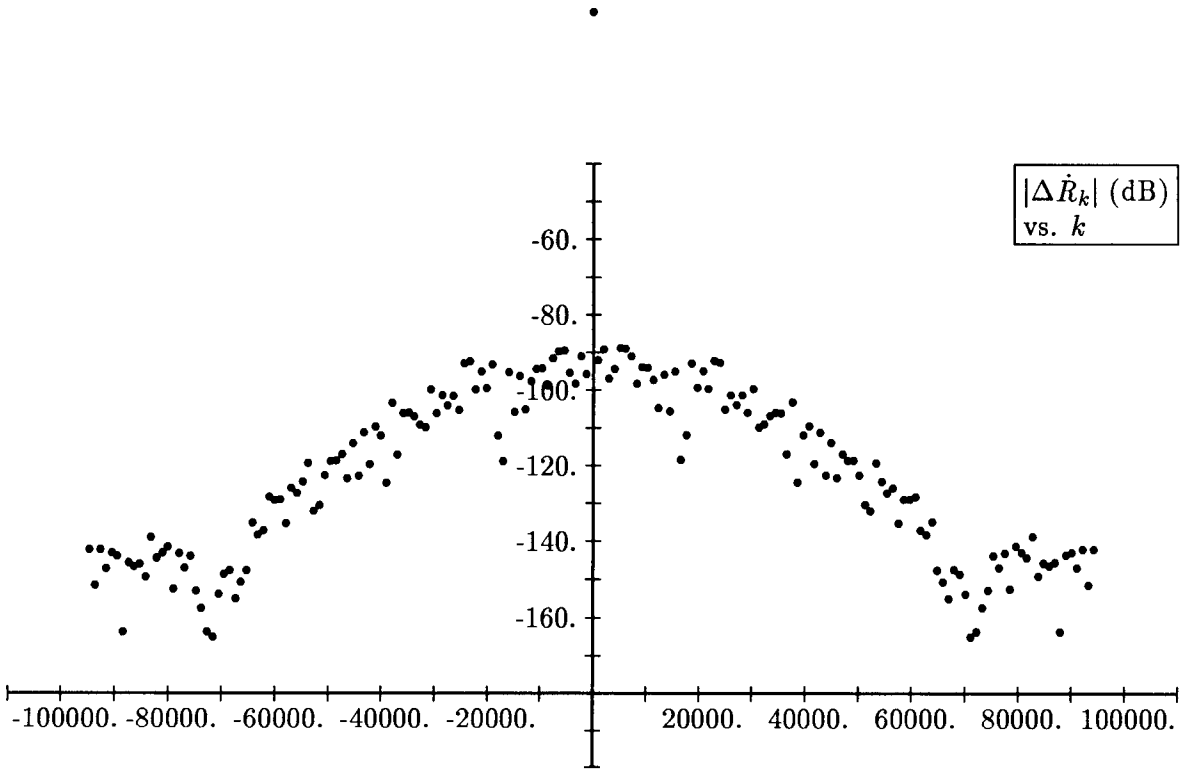

Figure 37: Predicted SST Range Rate Perturbation Spectral Amplitude: $m = 7,\ |l|_2 = 0$

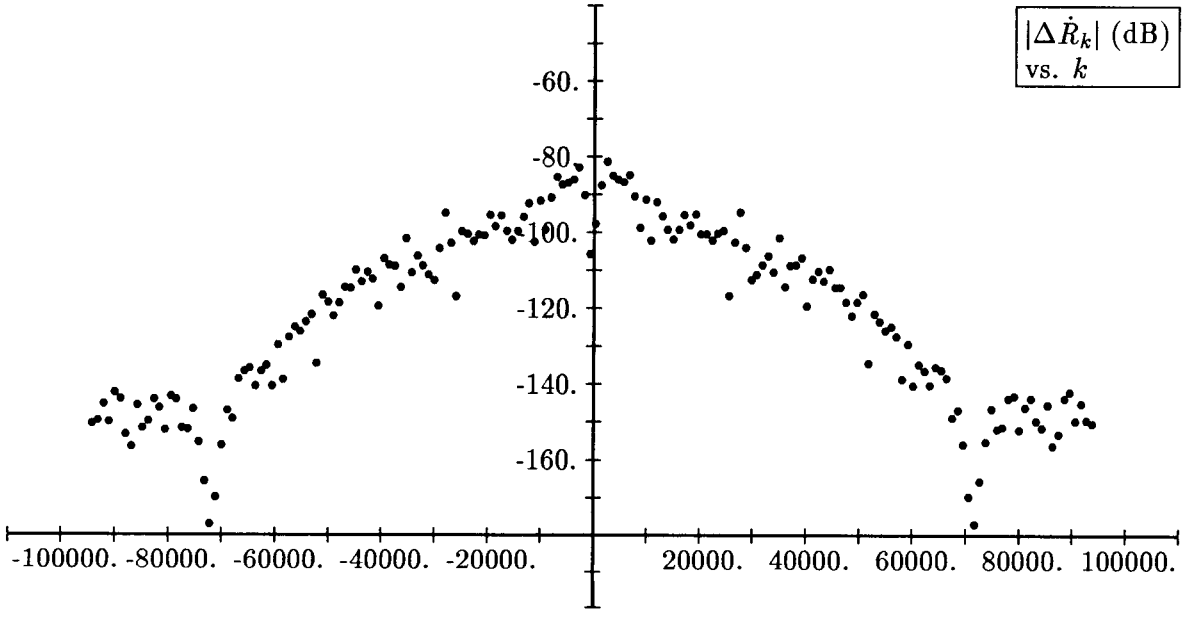

Figure 38: Predicted SST Range Rate Perturbation Spectral Amplitude: $m = 7,\ |l|_2 = 1$

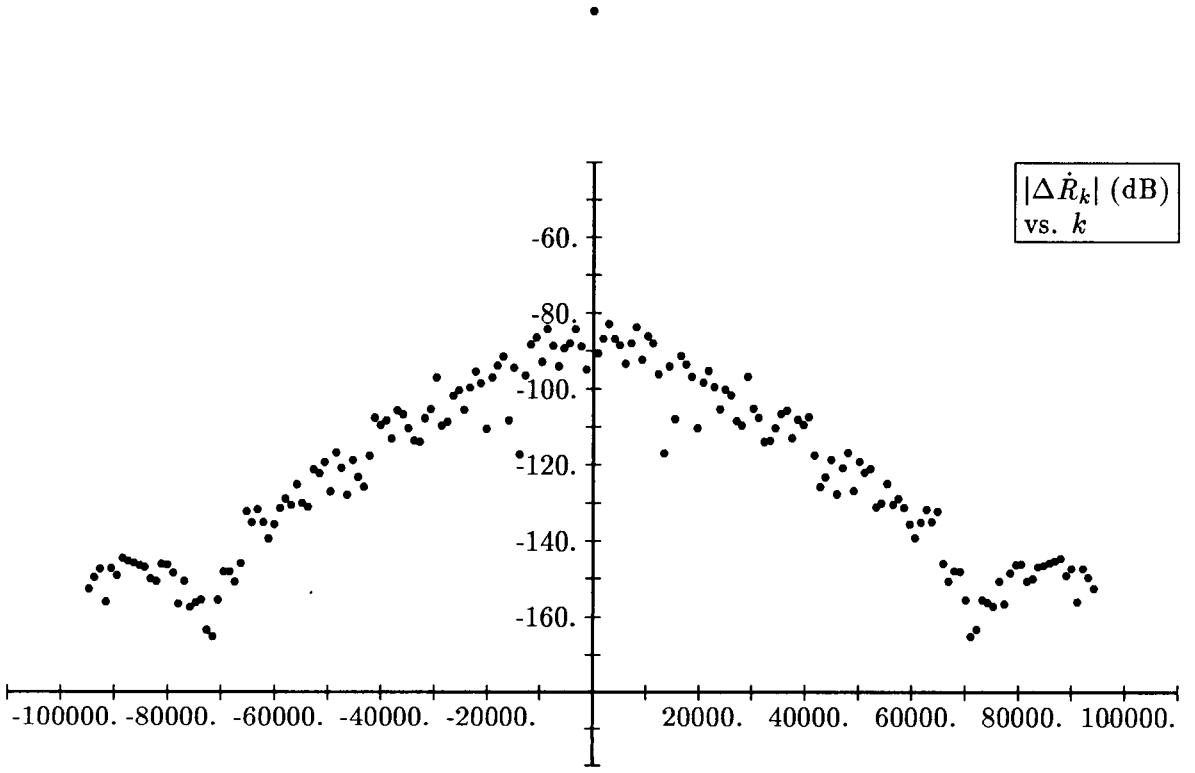

Figure 39: Predicted SST Range Rate Perturbation Spectral Amplitude: $m = 8,\ |l|_2 = 0$

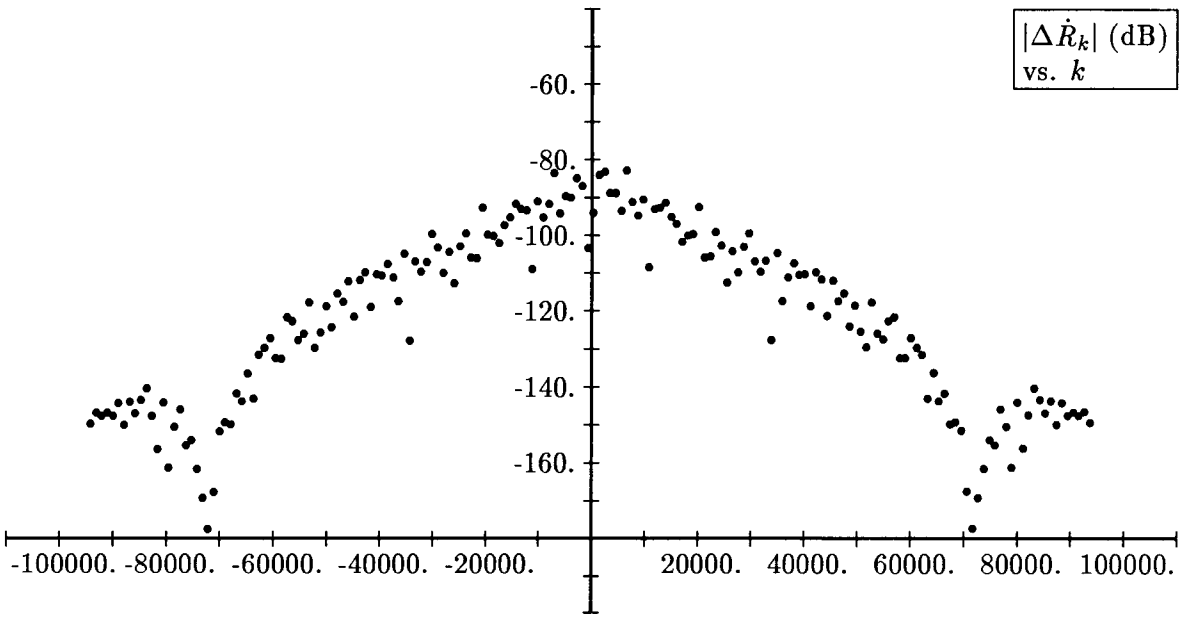

Figure 40: Predicted SST Range Rate Perturbation Spectral Amplitude: $m = 8$, $|l|_2 = 1$

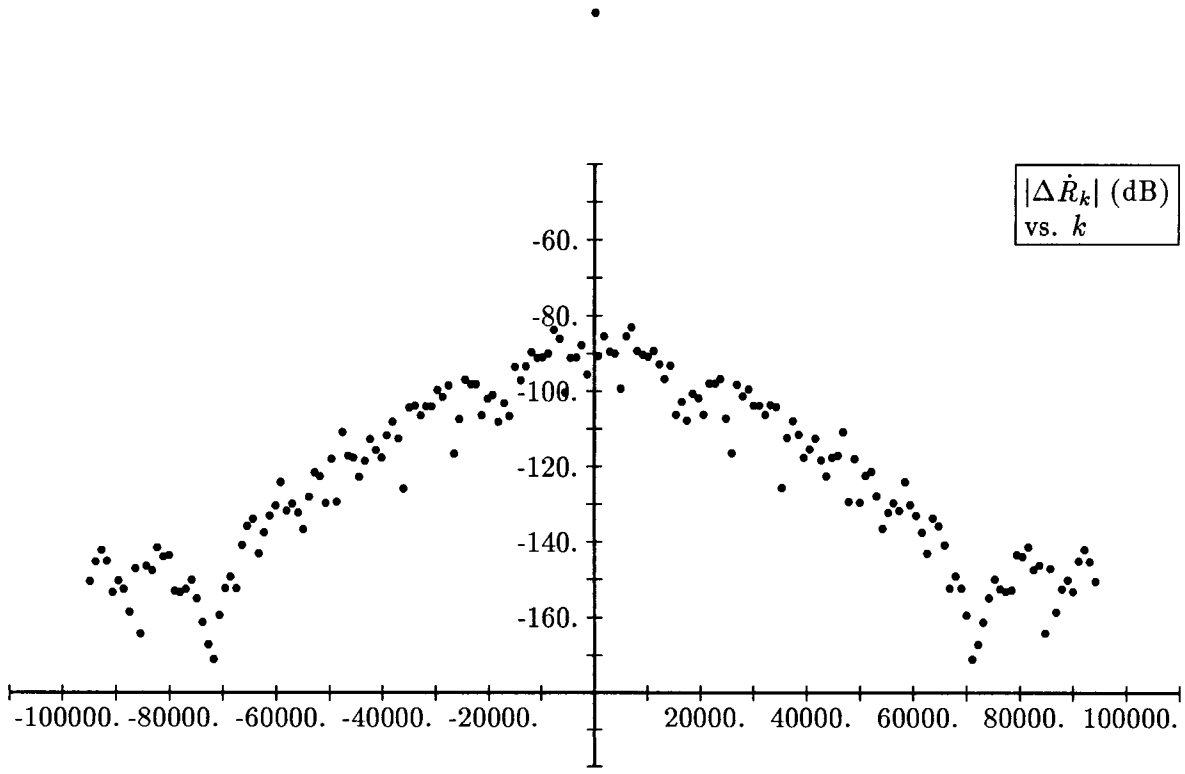

Figure 41: Predicted SST Range Rate Perturbation Spectral Amplitude: $m = 9,\ |l|_2 = 0$

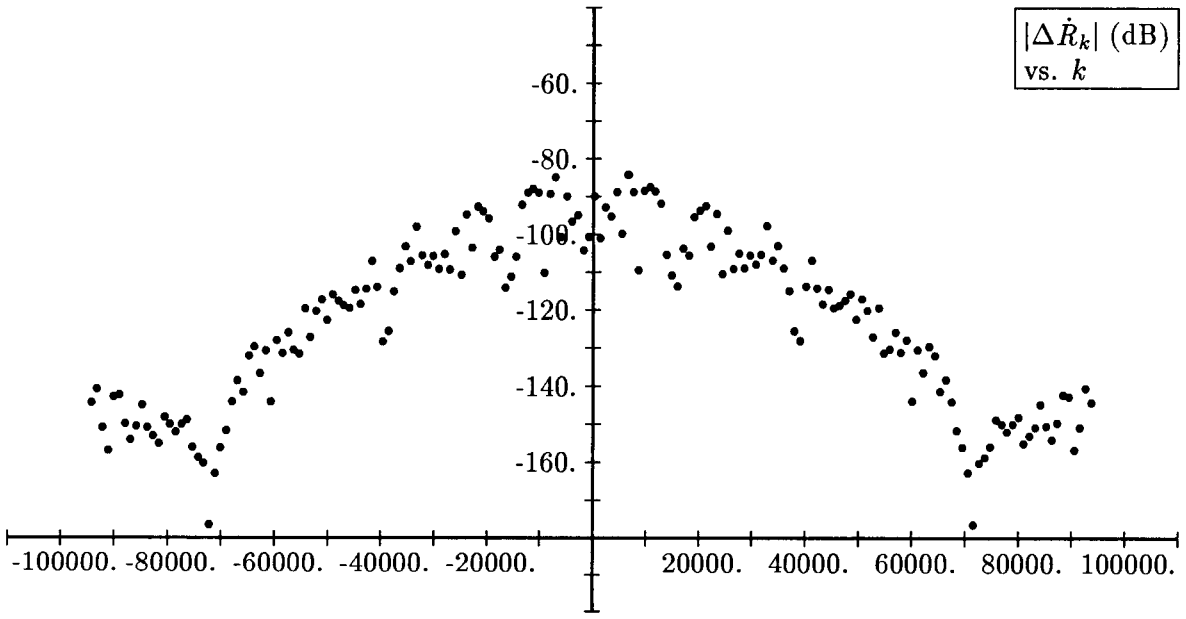

Figure 42: Predicted SST Range Rate Perturbation Spectral Amplitude: $m = 9,\ |l|_2 = 1$

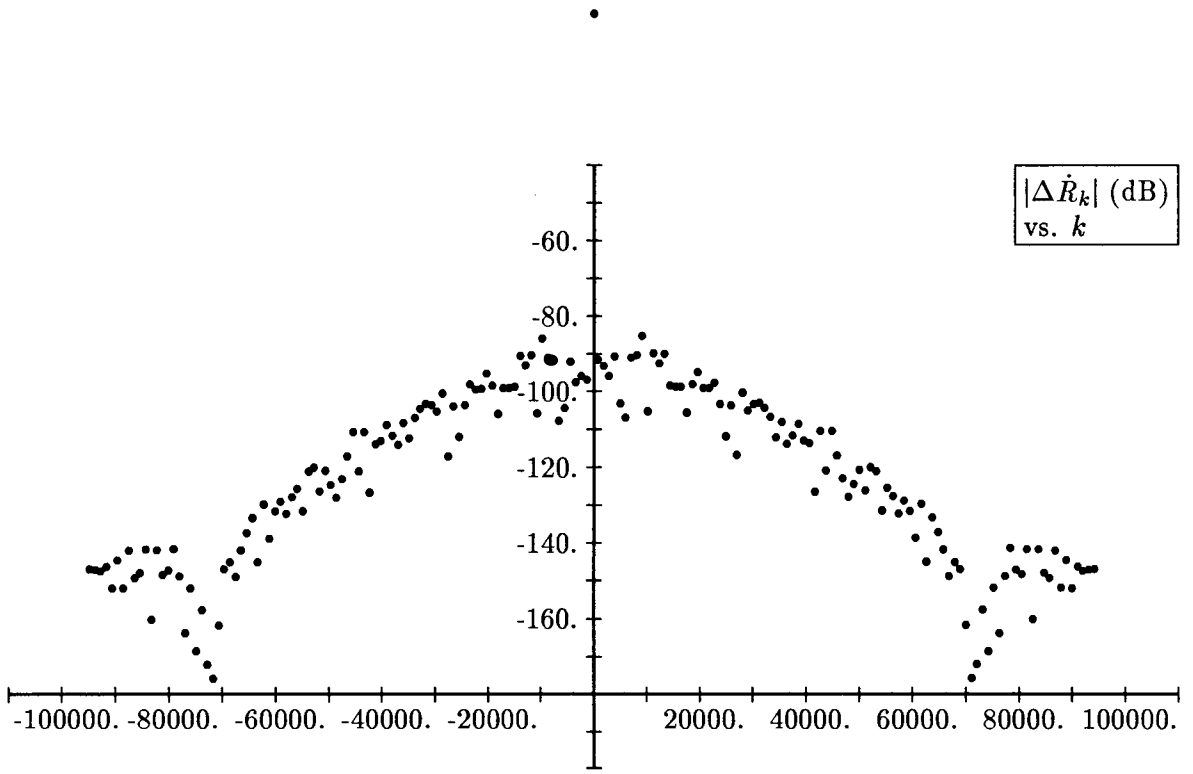

Figure 43: Predicted SST Range Rate Perturbation Spectral Amplitude: $m = 10$, $|l|_2 = 0$

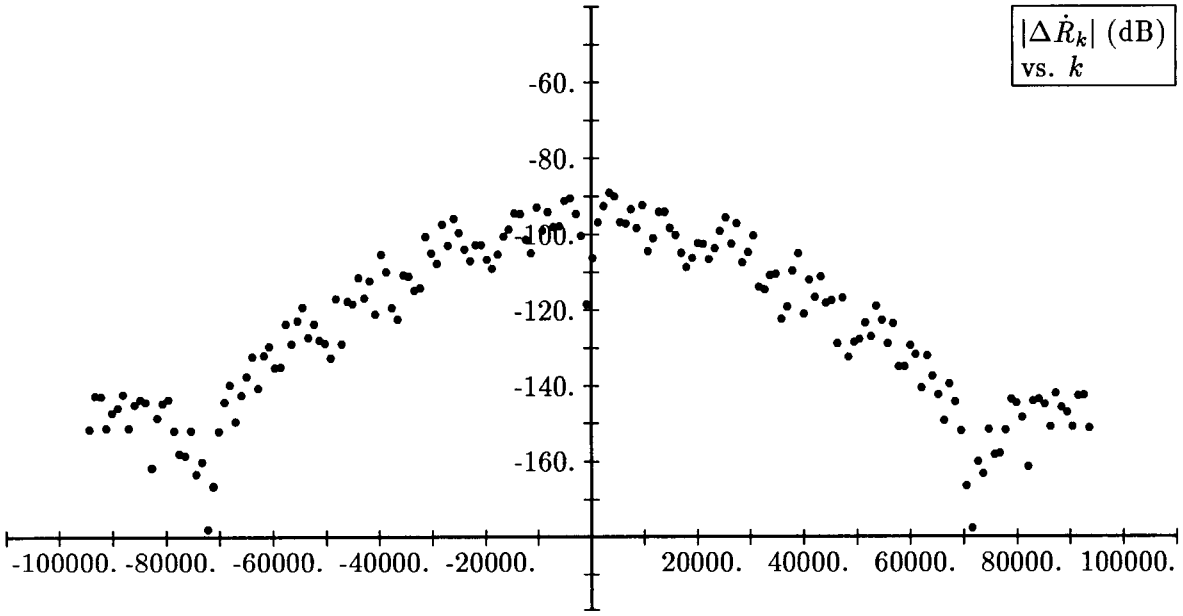

Figure 44: Predicted SST Range Rate Perturbation Spectral Amplitude: $m = 10$, $|l|_2 = 1$